Modeling and Control of Magnetic Shape Memory Alloys using Port-Hamiltonian Framework.

Nandish Calchand

▶ **To cite this version:**

Nandish Calchand. Modeling and Control of Magnetic Shape Memory Alloys using Port-Hamiltonian Framework.. Engineering Sciences [physics]. Université de Franche-Comté, 2014. English. NNT : . tel-01141978

HAL Id: tel-01141978
https://hal.science/tel-01141978v1

Submitted on 14 Apr 2015

HAL is a multi-disciplinary open access archive for the deposit and dissemination of scientific research documents, whether they are published or not. The documents may come from teaching and research institutions in France or abroad, or from public or private research centers.

L'archive ouverte pluridisciplinaire **HAL**, est destinée au dépôt et à la diffusion de documents scientifiques de niveau recherche, publiés ou non, émanant des établissements d'enseignement et de recherche français ou étrangers, des laboratoires publics ou privés.

SPIM

Thèse de Doctorat

école doctorale **sciences pour l'ingénieur et microtechniques**

UFC UNIVERSITÉ DE FRANCHE-COMTÉ

Modeling and Control of Magnetic Shape Memory Alloys using Port-Hamiltonian Framework

NANDISH R CALCHAND

SPIM

Thèse de Doctorat

UFC

école doctorale **sciences pour l'ingénieur et microtechniques**

UNIVERSITÉ DE FRANCHE-COMTÉ

N° | X | X | X

THÈSE présentée par

NANDISH R CALCHAND

pour obtenir le

Grade de Docteur de
l'Université de Franche-Comté

Spécialité : **Automatique**

Modeling and Control of Magnetic Shape Memory Alloys using Port-Hamiltonian Framework

Soutenue publiquement le 12 June 2014 devant le Jury composé de :

LAURENT LEFÈVRE	Rapporteur	Professeur des Universités, INP DE GRENOBLE
BETTY LEMAIRE-SEMAIL	Rapporteur	Professeur des Universités, Université Lille 1
BERNHARD MASCHKE	Membre	Professeur des Universités, Université Lyon 1
WILFRID MARQUIS-FAVRE	Membre	Professeur des Universités, INSA Lyon
YANN LE GORREC	Directeur de thèse	Professeur des Universités, ENSMM, Besançon
ARNAUD HUBERT	Co-Directeur de thèse	Maître de Conférence, Université de Franche-Comté, Besançon

Acknowledgements

A PhD thesis is never an easy endeavor. Particularly this one would have been impossible without my 2 supervisors-Professor Yann Le Gorrec and Mr Arnaud Hubert. I thank them with all my heart for bearing with me when I was being stubborn, for encouraging me when I lost hope, for guiding me when I was clueless and more importantly for treating me as a friend and sometimes almost as a son. They first of all deserve all my gratitude.

Secondly, I wish to thank the lovely people whom I have had the pleasure of meeting during the course of my PhD years. Some became good friends, others mere acquaintances but they all helped to make life easier. Worth mentioning among them are Baptiste Véron and Hectór Ramirez. Baptiste for a myriad of things (being my chauffeur, teaching me how to swim, bringing my keys when I would forget them, encourage me when I was hopeless) among which the most important is how a good human being should be. And Hectór for showing me how a human being should not be (Hectór if you ever read this, I love you). Also, I would like to thank Amélie Cot, Naresh Marturi and Margot Billot for tolerating my singing in the office.

Thirdly, I would like to thank all the people of AS2M department for their welcome and constant warmth and friendship throughout my stay. Particularly I would like to thank Mr Michael Gauthier for his help during the last months of the thesis. Also, I would like to thank the CNRS and the french taxpayers without whose money this thesis would have been impossible.

Last but not least, I thank my parents for always pushing me to aspire for more. At great sacrifice to themselves they gave my brother and me a good education and they made sure we never miss anything. This thesis is theirs as much as it is mine.

Résumé

Dans cette thèse on s'intéresse à la modélisation et la commande d'un système micro-mécatronique à base de matériau actif appelé Alliage à Mémoire de Forme Magnétique (AMFM). La principale propriété de ce matériau est sa déformation sous l'action d'un champ magnétique ou d'une contrainte, avec des plages importantes de déformation le rendant intéressant d'un point de vue applicatif par rapport à ses homologues tels que les actionneurs piézoélectriques. Le matériau étant fortement dissipatif et hystérétique, une fois déformé par une stimulation externe, il ne revient pas à sa position initiale. C'est la raison pour laquelle il est principalement utilisé dans des configurations de type *push-pull*. Comme pour tout matériau actif, les champs d'application des AMFM sont très divers et on peut en particulier les utiliser comme actionneurs pour des déplacements à l'échelle millimétrique. Comme ils réagissent à la fois à une contrainte et à une déformation, ils peuvent être utilisés comme capteur de force, capteur de position et pour mesurer des champs magnétiques. Etant fortement dissipatifs, ils peuvent aussi être utilisés comme amortisseur pour le contrôle de vibrations. Enfin il peuvent être utilisés comme transformateurs d'énergie dans le cadre de problématiques de récupération d'énergie. Pour toutes ces applications, il est nécessaire d'avoir un modèle précis du comportement dynamique du matériau pour pouvoir l'utiliser de manière optimale.

Etant donnés leur aspect multiphysique, leur structure cristalline complexe, leur caractère irréversible et non linéaire, la modélisation de ces matériaux reste un sujet de recherche ouvert. Dans la littérature, des modèles basés sur la thermodynamique irréversibles sont proposés. Ces modèles arrivent à prédire le comportement du matériau en mode quasi-statique. Malheureusement pour être précis et fiable comme actionneur il faut prendre en compte la dynamique. C'est dans ce domaine que cette thèse apporte toute sa contribution.

Une première partie de la thèse porte sur l'amélioration d'un modèle préexistant du MSMA et de l'actionneur. Ce modèle inspiré d'une approche mécanicienne, repose sur un choix exhaustif des variables d'état et l'utilisation de contraintes algébriques associées à l'utilisation de multiplicateurs de Lagrange. L'approche Hamiltonienne généralisé proposé dans cette thèse a permis de réduire le nombre d'état et un changement approprié de

variables a permis de projeter la solution sur un espace réduit aboutissant à un modèle sans contrainte algébrique et de dimension réduite. La cohérence thermodynamique et des problèmes de causalité liés au choix des variables manipulées (manipulables) et à l'aspect électro-magnéto-mécanique du système nous ont poussé à reprendre entièrement le modèle proposé.

La deuxième partie du travail a donc consisté à utiliser le formalisme de Hamiltonien à ports basé sur la thermodynamique pour proposer un modèle thermodynamiquement cohérent liant la dynamique du matériau et son énergie interne, en incluant les problématiques d'hystérésis par l'ajout de variables internes. Ce modèle est ensuite connecté au circuit électrique de l'actionneur par le biais des variables de port d'interaction, et ce de manière naturelle dans le cadre des systèmes Hamiltonien à ports, la partie électrique de l'actionneur étant modélisé de manière minimale. Ce modèle a été validé en simulation et confronté aux résultats expérimentaux issus de l'actionneur mis en oeuvre dans le cadre de la thèse.

La troisième partie de la thèse porte sur une première approche de commande de l'actionneur par le biais de techniques de type IDA-PBC. Pour cela nous nous sommes inspirés de la commande des systèmes de type *lévitation magnétique* qui présentent un couplage électro-magnétique assez similaire aux MSMA. L'originalité consiste en la prise en compte l'hystérésis lors de la commande par passivation. Une première loi de commande est proposée et ouvre de nombreuses perspectives pour la commande des matériaux actifs hystérétiques.

Contents

1 Introduction **1**
- 1.1 Introduction . . . 1
- 1.2 Overview of Magnetic Shape Memory Alloys . . . 4
- 1.3 Unified Energy Modelling . . . 7
- 1.4 Hysteresis . . . 13
- 1.5 Objective of thesis and Outline of Manuscript . . . 15

2 A naive model **17**
- 2.1 Introduction . . . 17
- 2.2 Description of actuator . . . 18
- 2.3 Modeling-Classical Hamiltonian Approach . . . 19
  - 2.3.1 The electrical subsystem . . . 20
  - 2.3.2 The MSMA subsystem . . . 21
  - 2.3.3 The mechanical subsystem . . . 22
  - 2.3.4 Energy of the Actuator . . . 22
  - 2.3.5 Hamilton Equations . . . 22
- 2.4 The Port-Hamiltonian Approach . . . 25
  - 2.4.1 The electrical subsystem . . . 26
  - 2.4.2 The MSMA+Load Subsystem . . . 29
  - 2.4.3 Interconnection of system I and system II . . . 30
  - 2.4.4 Model Reduction . . . 31
- 2.5 Discussion . . . 33

3 MSMA: An energy conversion device **35**
- 3.1 Introduction . . . 36
- 3.2 Magnetism . . . 36
  - 3.2.1 Magnetization . . . 37
- 3.3 Physics of the MSMA . . . 39
  - 3.3.1 Motion of Magnetic Wall . . . 40
  - 3.3.2 Rotation of Magnetization vector . . . 41
  - 3.3.3 Strain Mechanism . . . 41
- 3.4 Distributed Parameter Modelling of MSMA . . . 42
  - 3.4.1 Representative Volume . . . 43

3.4.2 Thermodynamics of MSMA . . . 44
3.4.3 Magnetization of MSMA . . . 46
3.4.4 Magnetic Energy . . . 47
3.4.5 Mechanical Energy . . . 50
3.4.6 Gibbs Free Energy . . . 51
3.5 Lumped Parameters Modelling of MSMA . . . 52
3.5.1 Terminal Variables . . . 52
3.5.2 Reluctances . . . 55
3.5.3 MSMA Actuator lumped Parameters . . . 56
3.5.4 Energy Considerations . . . 59
3.6 Discussion . . . 66

4 Bond Graph Modeling 69
4.1 Introduction . . . 69
4.2 Network Modelling . . . 70
4.3 Energy flow in Bond Graph . . . 71
4.3.1 The inductive element . . . 72
4.3.2 The capacitive element . . . 73
4.3.3 The resistive element . . . 73
4.4 Bond Graphs . . . 74
4.4.1 Junctions . . . 74
4.4.2 Transformers and Gyrators . . . 76
4.4.3 Causality . . . 77
4.4.4 Bond Graph Examples . . . 80
4.5 MSMA Actuator Bond Graph . . . 83
4.5.1 Electric/Magnetic Subsystem Bond Graph . . . 83
4.5.2 Mechanical subsystem Bond Graph . . . 85
4.5.3 MSMA subsystem Bond Graph . . . 87
4.5.4 Hysteresis in MSMA . . . 90
4.6 Discussion . . . 95

5 Experimental Validation and Control 97
5.1 Introduction . . . 97
5.2 Experimental Setup . . . 97
5.3 Control Perspectives . . . 103
5.3.1 Passivity Based Control . . . 103
5.3.2 IDA-PBC Technique . . . 105
5.3.3 Magnetic Levitation Example . . . 107
5.3.4 Control of MSMA Actuator . . . 113
5.4 Discussion . . . 117

6 Conclusion 119

A Linear Graph Theory in Brief **123**
A.1 Linear Graphs 123
A.2 Trees and links 124
A.3 Loop Set and Cut Set 124
A.4 State-Space formulation of Linear Graph Network 127

B Magnetism theory in Brief **129**
B.1 Magnetic Work 129
B.1.1 Magnetics in vacuum 129
B.1.2 Magnetization in matter 131
B.2 Magnetic Circuits 131
B.2.1 MMF, reluctance and scalar magnetic potential 131
B.2.2 Application to a simple magnetic circuit 133

C Thermodynamic theory in brief **135**
C.1 The First law of Thermodynamics 135
C.2 The Second law of Thermodynamics 136
C.3 Energy and Work. 137
C.4 Maximum Work 138
C.5 Equilibrium and Stability 138
C.6 Irreversible thermodynamics 140

List of Figures

1.1 The Scale of Things (Image: US Department of Energy). . . . 2
1.2 Energy Density of MSMA compared to other active materials 5
1.3 Sensor (left), Material (middle) and Actuator (right) from Adaptamat. . . . 5
1.4 Push-Pull Actuator built in 2008 based on paper by Gauthier et al. [17]. . . . 6
1.5 Phase and Variant Transformation . . . 7
1.6 Mass-Spring and its network structure. . . . 9
1.7 Mass Spring Damper System. . . . 11
1.8 Bond Graph and Linear Graph of spring damper system. . . . 12
1.9 Typical hyster B-H curve which occurs in ferromagnetic materials. . . . 13
1.10 Elementary hysteron and the hysteresis operator. . . . 14

2.1 MSMA Actuator . . . 18
2.2 Actuation Mechanism. . . . 19
2.3 Energy repartition . . . 20
2.4 MSMA electrical subsystem . . . 20
2.5 Expression for hysteresis. π^z is same as π^f . . . 25
2.6 MSMA electrical subsystem . . . 26
2.7 Linear graph of MSMA actuator . . . 27
2.8 Tree and Co-Tree of Actuator. $u_{L_{FE}}$ . . . 28
2.9 Addition of Lagrange Multiplier. Loop sets should contain only one link (dashed) and cut sets should have only one tree branch. . . . 28

3.1 Deformation with different applies stress [38]. . . . 39
3.2 Crystallographic Change . . . 40
3.3 Relative Magnetization Response as reported by Heczko et al. [27]. . . . 41
3.4 Representative volume. The direction of the magnetization vector in α is in the same direction as H_0. . . . 44
3.5 Twinning mechanism. Formation of domain walls and rotation of magnetization vector. . . . 45

3.6 Variation of α, θ with applied H_0 47
3.7 Magnetization for different values of z. Dotted line shows a possible magnetization curve of the material as z changes. Solid lines show magnetization at constant z. 48
3.8 Energy and Co-energy for Magnetic part of MSMA. 49
3.9 53
3.10 Magnetic Circuit with 2 different magnetic materials embedded in the core. The cross-sectional length is D. 55
3.11 Reluctance model of the MSMA Actuator 56
3.12 MSMA in Air Gap 57
3.13 Constitutive Equations between total magnetic flux λ and i for the actuator. The curves are shown for the different values of z. 60
3.14 Comparaison of constitutive equations taking into account change in length of air-gap, w, as well as change in length of MSMA, l. Dashed lines show the constitutive equations when the changes in length are taken into consideration while Solid lines show the equations when the changes are assumed negligible. 61
3.15 Variable Space. 62
3.16 Driving force f^{mag} derived from co-energy, W^*_{mag}. 65
3.17 Driving force f^{mag} derived from energy, W_{mag}. 66

4.1 The four-element quadrangle 74
4.2 0-junction and 1-junction. In both cases, $\sum_i^n e_i f_i = 0$. 75
4.3 Bond Graph of RLC circuit. 75
4.4 Two-port devices. 77
4.5 Causal Stroke. 78
4.6 Effort and flow Sources. 78
4.7 Integral (top) and Derivative Causality of "I" and "C" elements. 78
4.8 Both can only take one of these allowed causalities. 79
4.9 Resistive element can take both causalities. 79
4.10 Causality assignment for voltage input and current input. . . 79
4.11 Mechanical System Bond Graph. 80
4.12 DC Motor and its Bond Graph. 81
4.13 Non-Linear Example. 82
4.14 Schematic diagram showing the subsystems of the actuator with the arrows showing the power exchanging ports. 83
4.15 Electric susbsystem Bond Graph. 84
4.16 Bond graph model of reluctance circuit 85
4.17 Mechanical subsystem and its Bond Graph. 86
4.18 The Bond Graph of the MSMA. The "IC" field and the transformer "TF" act as energy converting ports. 88

4.19 Energy is stored in the MSMA by the rotation of magnetisation vector θ and the change in size of α. 88
4.20 Complete Bond Graph without hysteresis details. 89
4.21 A typical hysteresis curve for MSMA. 91
4.22 Basic Hysteretic elements. 91
4.23 Constitutive Equation for Damper (R-element). 92
4.24 Simulation of one hysteron to show it has the same shape (approximate) as experimental curves. 93
4.25 Bond Graph for multiple hysterons. 94

5.1 Block diagram of the experimental test bench. 98
5.2 Electromagnet used to generate magnetic field. 99
5.3 Mechanical structure. 99
5.4 Assembled electric circuit and mechanical structure to make a crude actuator. 100
5.5 Response of actuator to different stresses with an applied sinusoidal input. 101
5.6 Hysteresis of actuator between current and position. 101
5.7 Preisach Model with different number of hysterons to model experimental curve. N is the number of hysterons. 102
5.8 Illustration of the preisach plane 102
5.9 Movement of Preisach plane 102
5.10 Example of a mechanical passive system. 104
5.11 Magnetic Levitation System 107
5.12 Open Loop and Closed loop of H_d.Desired Position=0.05 . . . 111
5.13 Postion Control and Control voltage when the designed control law is applied. 111
5.14 Postion Control and Control voltage when damping is added to the sytem. 112

A.1 Two terminal lumped element and its associated linear graph. 123
A.2 Linear graph example. 124
A.3 The tree is on the left whereas the remaining branches added to the tree are called links are on the right. 124
A.4 A loop set(left) contains only 1 link whereas a cut set(right) cuts only 1 tree branch. 125

B.1 Solenoid with and without material 130
B.2 Magnetic Circuit. 133

C.1 Laws of Thermodynamics 137

List of Tables

2.1 Generalized Coordinates and Momentum for electrical part . 21
2.2 Generalized Coordinates and Momentum for MSMA 21
2.3 Generalized Coordinates and Momentum for Load 22

3.1 Values used for simulation 59
3.2 Energy Relation 64

5.1 Identified Values 107

Chapter 1

Introduction

Contents

1.1	Introduction	1
1.2	Overview of Magnetic Shape Memory Alloys	4
1.3	Unified Energy Modelling	7
1.4	Hysteresis	13
1.5	Objective of thesis and Outline of Manuscript	15

1.1 Introduction

Advances in technology has reached such a level that previously unimaginable tasks are becoming possible. Manipulation of DNA, manufacturing of 3-D transistors, targeted delivered of drugs to infected cells and monitoring of health with lab-on-chip technology among others are fast becoming standards largely due to miniaturisation. Miniaturisation has played a considerable role in improving technology and almost everyday new products are introduced in the market. From medicine to household equipments and cosmetics, there is some measure of micro- and nanotechnology in our everyday life. As these sizes are very unintuitive, Figure 1.1 helps to show how the micro world and the nano world scale in relation to things that we perceive.

At the nanoscale, nanotechnology is helping to considerably improve many technology and industry sectors such as information technology, energy, environmental science, medicine, food safety and transportation among others. It has been developing at an astounding pace since the last 20 years. At such a scale, scientists are able to tailor the structure and properties of materials to make them stronger, lighter, more reactive, and more conductive among many other traits. Furthermore, the electrical and magnetic characteristics are fundamentally different than their bulk counterpart. This has given rise to a number of applications such as nanoscale transistors which are

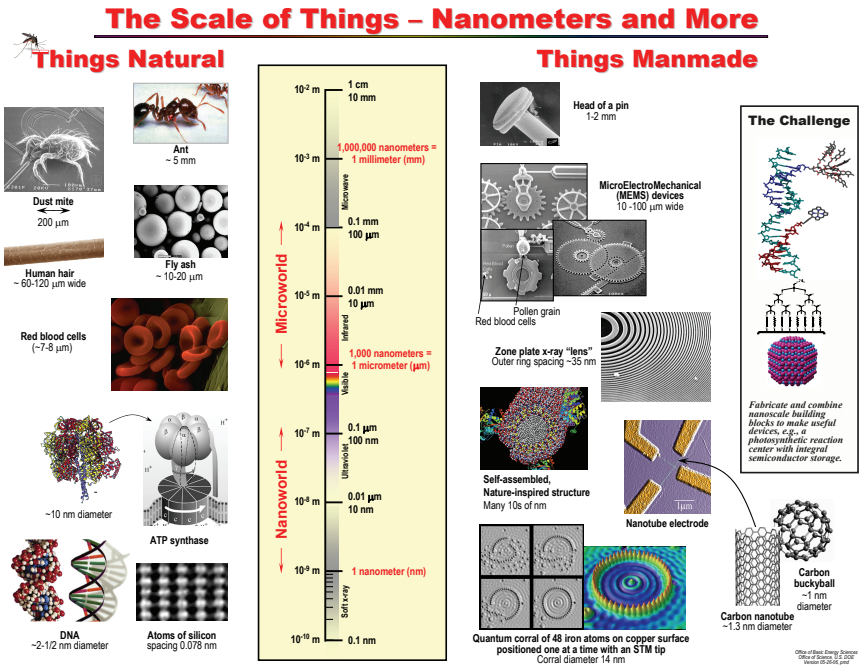

Figure 1.1: The Scale of Things (Image: US Department of Energy).

faster, more powerful and increasingly energy efficient. Displays for TVs, laptops, phones and digital cameras now include nanostructured polymer films known as organic light-emitting diodes, or OLEDS, which have considerably improved the viewing angles, the weight as well as the energy efficiency and the lifetimes. A host of other applications are being engineered and researched everyday.

Just a few orders of magnitude of above the nanoscale lies the microscale. Unlike the nanoscale, characteristics at this scale are not fundamentally different from those in the macro world. Nonetheless due to devices of this size being lighter, faster, more energy efficient, easier to integrate into systems and cost less to produce, they are also having an astounding success. The range of applications for such devices are numerous. Micro-electro-mechanical-systems (MEMS) which in a single package contains the necessary mechanical and electronic components to make transducers have found their uses in a variety of fields. In the automotive industry, it is used in the airbag systems, vehicle security and active suspensions to name a few. In the consumer domain, video projectors, phones, cameras or ink-jet printers all embark one or two MEMS such as accelerometers, gyroscopes or DLP (Digital Light Projector).

Apart from MEMS, in the micro world there is lots of application which involve micro assembly and micro manipulation. Microrobotics [1], a term used to define micro manipulation of objects with characteristic dimensions

in the millimetre to the micrometer range as well as the design and fabrication of robotic structures in a similar size range (micro robots), has been gaining momentum these last few years.

Examples of micro manipulation are the characterisation of biological cells and/or organic tissue. This is important in the domain of genetics where new DNA material has to be inserted in the cell. Mechanical characterisation to measure forces on cells is also done through micro manipulation. This is important in the development of tools for robotic surgery as forces requires to open a tissue, or carry out a microinjection are mostly in the micro newton range. Other uses of micro manipulation is to assemble parts called micro assembly.

Microassembly circumvents the limitations of the traditional way MEMS are built. To build MEMS, usually a silicon wafer is used on which lithography and etching are applied to create the appropriate parts. The major limitation is that as the micro fabrication process is planar, 3-D structures are impossible to achieve. With micro assembly this limitation can be circumvented and a whole new lot of applications can be developed.

To this end, sensors and actuators which can work at these scales are needed. Unfortunately to manipulate the small or micro, we need actuators of that size and who can work in that range.

Smart Materials, materials who reacts to a stimulus by either changing shape, colour, permittivity or permeability can be used for such purposes.

These materials are used in a variety of diverse fields ranging from automobile to sports. They are used as sensors and actuators. Often, they have the ability to 'self-sense', i.e the material in addition to being an actuator, it performs as a sensor as well. This is due to the strong coupling between the transduction mechanism. For example, a material which produces a strain when a voltage is applied can also produce a voltage when an external factor changes its shape. These effects are usually called the *direct* effect and, its opposite the *converse* effect. Being able to sense and actuate at the same time, obviously gives smart materials an added advantage over traditional actuators and sensors[71]. There are a varieties of these smart materials and they work on different transduction principles. Some of the most common are

- *Piezomaterials*[10] are very popular smart materials used as sensor and actuators. A mechanical change such as an elongation is observed when a voltage is applied to it. And when the material is compressed or extended, a voltage is developed across it.

- *Magnetostrictive* materials [11] will produce an induced mechanical strain when subjected to a magnetic field. The property that changes is the permeability of the material. Hence on application of a mechanical deformation, the material will change its permeability which can be measured with a coil.

- *Ionic Polymers* or *Electroactive polymers* [21] will deform on application of a voltage. They are able to develop a large deformation while sustaining a large force.

- *Shape Memory Alloys* [70] reacts to temperature. It will undergo phase transformations which will change its shape. It deforms to its 'martensitic' condition at low temperature and regains its original shape in its 'austenite' condition when heated (high temperature).

- *Magnetic Shape Memory Alloys* (MSMA) [7] is also one such very promising material akin in some ways to Shape Memory Alloys (SMA). It also deforms on application of heat but has the added advantage that it deforms under the action of a magnetic field.

1.2 Overview of Magnetic Shape Memory Alloys

Magnetic Shape Memory Alloys (MSMA) are a relatively new class of material. Like *Shape Memory Alloys*, they deform under the action of a stress and in addition they are also responsive to a magnetic field. The most common magnetic shape memory material that has been intensively investigated is an alloy of Ni-Mn-Ga. A great amount of research interest has been generated by this material due to its ability to produce large strains-upto 10%.

Compared to other other materials (see Fig. 1.2), MSMA work at a lower frequency than piezoelectric or magnetostrictive devices but have a higher deformation. Conversely, they have a higher operating frequency than classical Shape Memory Alloys but a lower deformation. Being placed roughly in the middle of the table, opens up a large amount of potential applications for MSMA such as sensors, actuators, energy harvesting, motion/vibration control etc. In Fig. 1.3, the material is shown along with a sensor and an actuator commercialised by a Finnish company named Adaptamat Ltd.

Each of the aforementioned application require that the MSMA operate either in the actuation or sensing mode. In actuation mode, on application of a magnetic field, an elongation occurs which can be used to do work. Conversely in sensing mode, on compression/elongation of the material, a change in magnetization is observed. By measuring the change in magnetisation, the change in length can be deduced. The coil in the sensor of Fig. 1.3 is used for such a purpose.

Apart from Adaptamat, a very basic actuator has been developed in Gauthier et al. [17] whereas a sensing device is described in Sarawate [63]. An example of the actuator built by Gauthier et al. [17] during his PhD thesis is shown in Fig. 1.4. It is a push-pull actuator which uses two MSM elements in an antagonistic manner to move a positioning stage. A detail description and the workings of this actuator as well as its design can be found in Gauthier et al. [17].

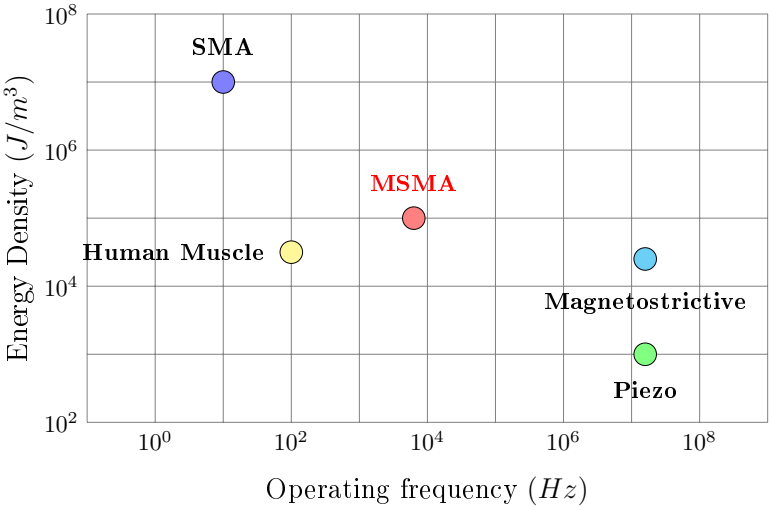

Figure 1.2: Energy Density of MSMA compared to other active materials

Figure 1.3: Sensor (left), Material (middle) and Actuator (right) from Adaptamat.

MSMA are able to exhibit such large deformation due to a change in crystallographic arrangement of the martensitic variant. The material exists in 2 main phases-the high temperature phase which is called austenite and the low temperature phase which is called martensite. Figure 1.5 shows the different conditions under which the phases exist and within the martensitic phase how the different variants occur. The figure shows that all variants have 2 axis, a long axis ,a, and a short axis, c. These axis point in different directions for each variant. Depending on the external inputs such as stress or magnetic field, a sample of the material can entirely consist of one variant only or a mixture of variants. This changing of configuration due to an external stimulus is the process responsible for the macroscopic change.

Unfortunately this macroscopic change is quite complex in nature. This limits the development and the widespread use of this material. The material

(a) Lab Prototype.

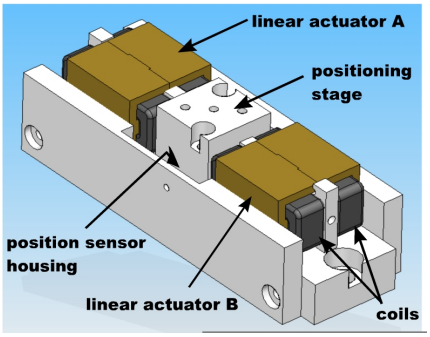

(b) CAD Image.

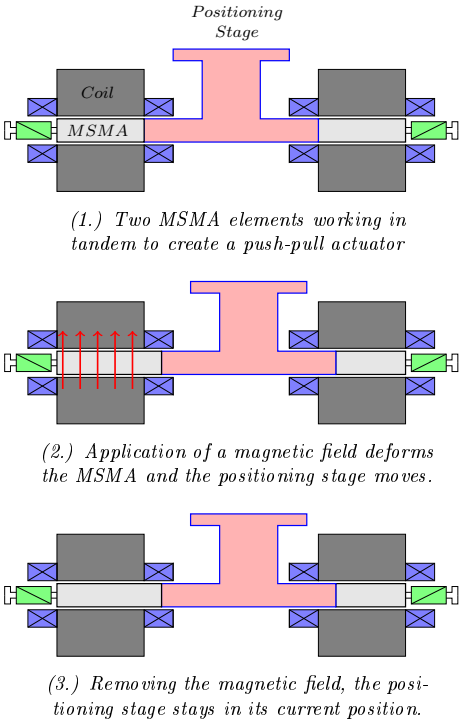

(c) Workings of Push-Pull Actuator.

Figure 1.4: Push-Pull Actuator built in 2008 based on paper by Gauthier et al. [17].

has a non-linear hysteretic behaviour. Furthermore for an actuator to be able to operate with precision, the deformation of material needs to be controlled.

Since its discovery by Ullakko [75] most of the research carried on Magnetic Shape Memory alloys has been centered around its modelling. Irreversible thermodynamics has been extensively used to predict the behaviour of the material [28, 37, 41, 36]. A variational approach has been used in Wang and Steinmann [78] which is very similar to the thermodynamics approach. Unfortunately, these subsequent models have not been used to design the associated control system.

In the few works that have attempted [61, 62] to design a control law for the material, the physics of the material has not been taken into consideration. Notably most of them use a linear dynamics model in series with a non linear hysteretic behaviour. The hysteresis is modelled and then inverted to linearise the plant. Then control strategies such as PI, PID or adaptive control [60]. are applied to them. The linear model identified can either be a first or a second order model. Usually, a second order model is used as the material is pre-stressed by a load. The thermodynamics or variational model usually developed are almost never used to control the material.

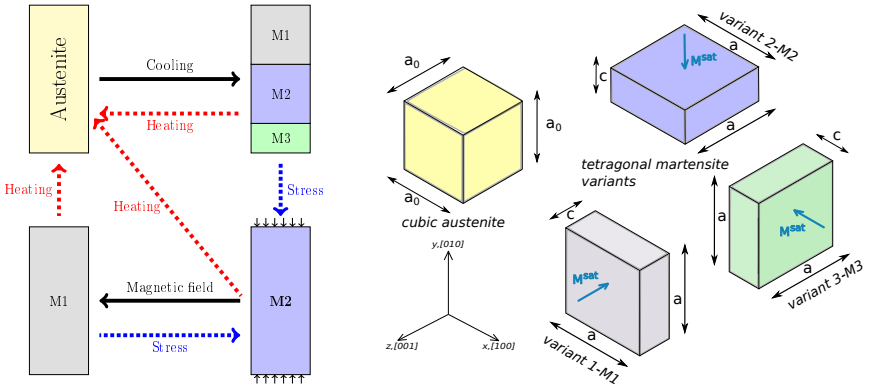

(a) Austenitic-Martensitic Transformation (b) Crystallographic Structure

Figure 1.5: Phase and Variant Transformation

To be able to take into account the physics of the material for the design of control law, a unified energy modelling seems most appropriate as the MSMA and any actuator based on it is highly multi physics. Since energy is a common denominator in all domains, an energetic approach has many advantages. Firstly physical system can be viewed as simpler subsystems which exchange energy among themselves and the environment [31]. Secondly energy being a scalar, different energies from different domains can be combined by simply adding them up. Lastly, the role of energy and interconnections between subsystems provide the basis for various control strategies [49, 5]. And finally they obey the laws of thermodynamics which is not the case for phenomenological models.

1.3 Unified Energy Modelling

To harness the full power of Magnetic Shape Memory alloys as actuator, control of the deformation is essential. Furthermore using a black box model or a linear model of the system does not allow us to use the full potential of the material as the physics of the material is obscured by approximations and linearization.

One way to overcome such limitations is to an energy framework as they are neither restricted by the domain of application nor by linearity. The port-Hamiltonian framework is an energy framework which has been rapidly developing and is an ongoing subject of research since many years now. The port-Hamiltonian framework combines Hamilton's equations of motion from analytical mechanics with *network* theory prevalent in electrical engineering [64].

The port-Hamiltonian framework first and foremost models a system in

a particular fashion i.e in terms of *energy* and *co-energy* variables. Energy is the ability to do work while co-energy is its complement. For example, in a spring with a linear constitutive equation (the relation between the force, F, and its displacement, x, is linear), we have, taking the stiffness of the spring to be k:

$$F = kx$$

The energy E_s is then given by

$$E_s(x) = \int F\,dx = \int_0^x kx\,dx = \frac{1}{2}kx^2$$

whereas its co-energy E_s' is

$$E_s^*(F) = \int x\,dF = \int_0^F \frac{F}{k}\,dF = \frac{1}{2}\frac{F^2}{k}$$

We see that the the energy $E_s(x)$ is in terms of x, the energy variable and $E_s^*(F)$ in terms of F-the co-energy variable.

After formulating a port Hamiltonian model we then have a host of techniques such as *IDA-PBC* and *energy shaping* [51] at our disposal to control it. Since thermodynamics which is the science of energy is extensively used to model MSMA, it is natural that control strategies based on port Hamiltonian framework is a natural extension.

The main advantage of port-Hamiltonian systems as compared to the classic state space model is the appearance of the *structure* matrix (how elements are connected to each other-the topology or network structure of the system) explicitly.

Classical dynamical systems are usually written in the form

$$\dot{x} = f(x, u)$$

or in the linear case

$$\begin{aligned}\dot{x} =& Ax + Bu\\ y =& Cx + Du\end{aligned}$$

where x is the state variable matrix and u the input. In the port-Hamiltonian framework, the system is of the form

$$\begin{aligned}\dot{x} =& (\mathcal{J} - \mathcal{R})\frac{\partial \mathcal{H}}{\partial x} + gu\\ y =& g^T u\end{aligned} \tag{1.1}$$

where

- $\mathcal{J}$ is the interconnection matrix (skew-symmetric matrix, $J = -J^T$). It represents the connections between the elements of the system and defines its structure.

- $\mathcal{R}$ is the dissipation matrix (diagonal matrix, symmetric and, in physical systems semi-positive definite $R = R^T \geq 0$).
- g the port connection of the system to the outside world. It transmits energy to/from the system through the port variables u and y.
- $\mathcal{H}(x)$ is the Hamiltonian of the system (usually the total stored energy of the system).

Also, J, R and g can be functions of the state variables where they are represented as $J(x)$, $R(x)$ and $g(x)$. From (1.1), rate of change of the Hamiltonian which gives the power of the system is given by

$$\frac{d\mathcal{H}}{dt} = -\frac{\partial^T \mathcal{H}}{\partial x}\mathcal{R}\frac{\partial \mathcal{H}}{\partial x} + u^T y \leq u^T y \tag{1.2}$$

which yields a passive system if $\mathcal{R} \geq 0$. $\mathcal{J}$ disappears in the power balance equation above due to its skew-symmetric nature.

We will now illustrate by means of an example, the port-Hamiltonian representation.

Example

Consider a mass-spring system as in Figure 1.6 in which a mass m is interconnected with a spring of stiffness k. Choosing as state variables x, the

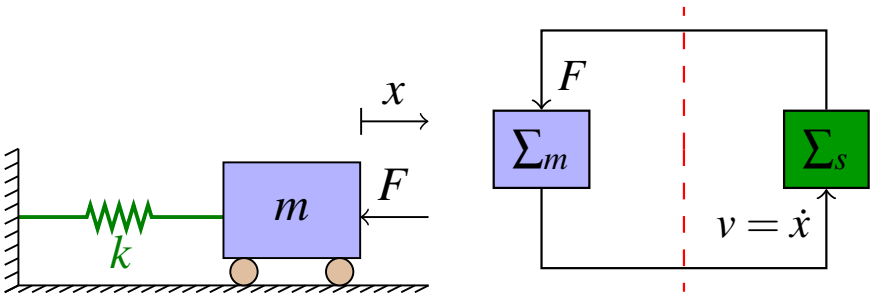

(a) Mass-Spring System.

(b) Network Representation of Mass-Spring System.

Figure 1.6: Mass-Spring and its network structure.

spring deformation, and p, the momentum of the mass, we can model the two elements-mass and spring separately as follows:

$$\sum_m : \begin{cases} \dot{p} = F \\ y = \dfrac{p}{m} \end{cases} \quad (= v) \qquad \sum_s : \begin{cases} \dot{x} = v \\ y = -kx \end{cases} \quad (= F) \tag{1.3}$$

in which $\sum_m$ is the mass model and $\sum_s$ is the spring model. In (1.3), F is the force applied to the mass by the spring and it is the output of subsystem $\sum_s$ while v is the mass speed, the output of system $\sum_m$.

As shown in Figure 1.6b, the interconnection is in feedback. The mass integrates the force F to determine its speed while the speed v is integrated by the spring to calculate its deformation. This kind of behaviour is very general in dealing with *physics* of the systems. The only way systems can be connected is through feedback i.e there is a mutual influence between interacting systems and this interaction can be revealed by analysing the kind of information exchanged.

As will be seen in the chapter on Bond Graphs, this exchange of information occurs through *effort* and *flow* variables. In this example, the effort is the force F while the flow is the velocity v. Their product is power $F.v$. What happens is that one system takes in the effort F, in this case the mass and imposes the velocity v while the converse occurs in the spring-it takes in the velocity v and imposes the force F. Hence interconnection results in an exchange of power between the subsystems through ports. This become more obvious if the energy of the subsystems is considered.

The kinetic energy E_k of the mass and the potential energy of the spring E_p is given by

$$E_k(p) = \frac{p^2}{2m} \qquad E_p(x) = \frac{1}{2}kx^2 \tag{1.4}$$

The variables p and x which are called state variables in classical system theory are in the port-Hamiltonian framework called *energy variables*. The time rate of change of the energies is then given by:

$$\frac{dE_k}{dt} = \frac{p}{m} \cdot \dot{p} = v.F = P \qquad \frac{dE_p}{dt} = (kx).\dot{x} = -F.v = -P \tag{1.5}$$

where P is the power. The 2 relations in (1.5) expresses the well-known physical property of spring-mass system, a continuous conversion between kinetic and potential energy which results in the oscillatory behaviour of the system. This interaction is succinctly captured by the port-Hamiltonian framework in its structure matrix J. The port-Hamiltonian formulation for the mass-spring system is:

$$\underbrace{\frac{d}{dt}\begin{bmatrix} x \\ p \end{bmatrix}}_{\text{Energy Variables}} = \underbrace{\begin{bmatrix} 0 & 1 \\ -1 & 0 \end{bmatrix}}_{\mathcal{J}} \underbrace{\begin{pmatrix} \frac{\partial \mathcal{H}}{\partial x} = kx = F \\ \frac{\partial \mathcal{H}}{\partial p} = v \end{pmatrix}}_{\text{Co-Energy Variables}} + \underbrace{\begin{bmatrix} 0 \\ 1 \end{bmatrix}}_{input} F$$

$$y = \begin{bmatrix} 1 & 0 \end{bmatrix} \begin{pmatrix} \frac{\partial \mathcal{H}}{\partial x} \\ \frac{\partial \mathcal{H}}{\partial p} \end{pmatrix} \tag{1.6}$$

where $\mathcal{H}$ is the total stored energy of the system:

$$\mathcal{H}(p, x) = \frac{1}{2}\frac{p^2}{m} + \frac{1}{2}kx^2 \tag{1.7}$$

From (1.10) and (1.7), it is seen that to write the port Hamiltonian formulation, $\mathcal{H}$ need not be necessarily quadratic in the energy variables. For other energy functions which yield non-linear constitutive equations between effort and integrated flow or integrated flow and effort, it can just be as easily integrated into the formulation.

As for the power balance equation it is given by:

$$\frac{d\mathcal{H}}{dt} = -\frac{\partial^T \mathcal{H}}{\partial x}\mathcal{R}\frac{\partial \mathcal{H}}{\partial x} + u^T y = u^T y \tag{1.8}$$

Eq. 1.8 verifies that energy is conserved. No loss occurs in the system. The rate of change of the Hamiltonian, $\mathcal{H}(x,p)$ is equal to the power injected into the system through the power port (u,y). If the input u is brought to and kept at 0, the system will continue to oscillate indefinitely.

The above development is still not sufficient to model systems since the mass-spring is a conservative system. We also need to be able to take care of dissipation which occurs in all systems. In the mass-spring-damper shown in Figure 1.7, energy is dissipated (lost) in the damper. The constitutive equation for the damper is taken to be linear i.e

$$F_d = b\dot{x} = bv \tag{1.9}$$

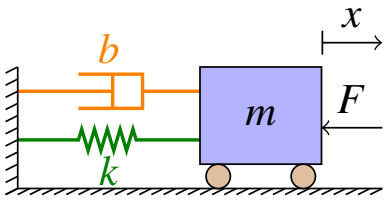

Figure 1.7: Mass Spring Damper System.

In the port-Hamiltonian formulation, dissipation is taken care by the $\mathcal{R}$ matrix. The Hamiltonian $\mathcal{H}$ stays the same while the formulation now includes $\mathcal{R}$ as follows

$$\begin{bmatrix}\dot{x}\\ \dot{p}\end{bmatrix} = \left(\underbrace{\begin{bmatrix}0 & 1\\ -1 & 0\end{bmatrix}}_{\mathcal{J}} - \underbrace{\begin{bmatrix}0 & 0\\ 0 & b\end{bmatrix}}_{\mathcal{R}}\right)\begin{pmatrix}\frac{\partial \mathcal{H}}{\partial x} = kx\\ \frac{\partial \mathcal{H}}{\partial p} = v\end{pmatrix} + \begin{bmatrix}0\\ 1\end{bmatrix}F$$

$$y = \begin{bmatrix}1 & 0\end{bmatrix}\begin{pmatrix}\frac{\partial \mathcal{H}}{\partial x}\\ \frac{\partial \mathcal{H}}{\partial p}\end{pmatrix} \tag{1.10}$$

In this case, power balance is given by:

$$\frac{d\mathcal{H}}{dt} = -\frac{\partial^T \mathcal{H}}{\partial x}\mathcal{R}\frac{\partial \mathcal{H}}{\partial x} + u^T y = u^T y - bv \tag{1.11}$$

And from 1.11, we infer that the system energy decreases. If input u is brought to and kept at 0 from some initial value, the system will stop after some time.

For simple systems, it is easy to find the interconnection matrix J, but for large systems consisting of many elements such as inductors, capacitors, masses, springs and/or resistances, systematic approaches exist to find the topology of the system. Two approaches are the bond-graph [56] and the

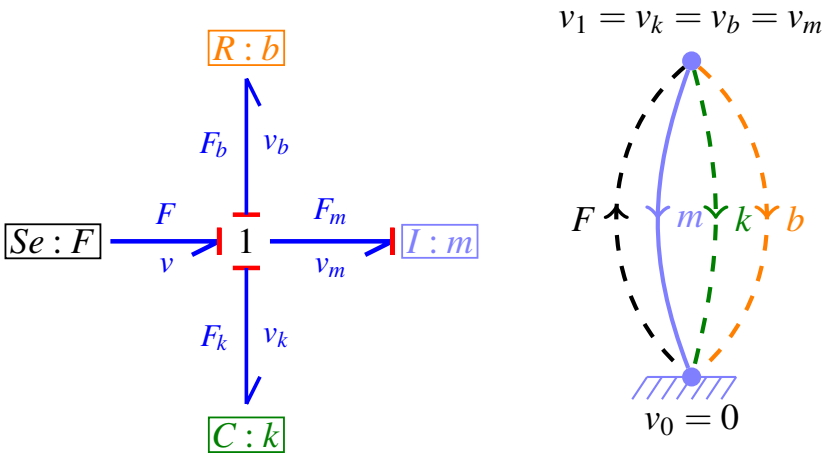

(a) Bond Graph of Mass-Spring Damper. The "1" junction indicates that all the bonds share the same velocity.

(b) Linear Graph of Mass-Spring Damper. The top node indicates equal velocities.

Figure 1.8: Bond Graph and Linear Graph of spring damper system.

linear graph [39]. More details about these 2 techniques will be given in subsequent chapters.

As a brief overview, both approaches are graphical in nature and they both make use of simple ideal elements such as *generalised inductances* or *generalised capacitances* to model elements. Bond graph makes use of junctions to connect elements whereas linear graph makes use of nodes as shown in Figure 1.8. The little vertical bars at the end of the bonds (half arrows) in Figure 1.8a indicate *causality* i.e which elements imposes the force and which elements impose the velocity. This information, although not missing from linear graph, is not so evident. It has to do with trees (solid lines representing a causal tree) and co-trees (dashed lines) in Figure 1.8b. On the other hand, linear graphs is more akin to give the topology directly without regards to what type of element is connected between the nodes whereas a little manipulation is required in bond graphs to get the $\mathcal{J} - \mathcal{R}$ interconnection matrix.

These 2 approaches can be used to find the interconnection matrix $\mathcal{J}$ for

any domain, electrical circuits for example or a mixture of domains. Since MSMAs are multi physics in nature, these 2 techniques are used to model the pathway of energy in the material.

The port Hamiltonian framework therefore seems well-adapted to model MSMA as there is a conversion of energy from electrical to mechanical. One further consideration regarding MSMAs and/or smart materials in general is their hysteretic behaviour [70].

1.4 Hysteresis

Hysteresis is a non-linear effect that arises in diverse disciplines ranging from physics to biology, from material science to mechanics, and from electronics to economics [73]. Ferromagnetism, illustrated in Figure 1.9, is a classical example of hysteresis in electrical engineering while in mechanical engineering, backslash and friction are the main source of hysteresis.

The physical causes of hysteresis are the existence of multiple metastable states of a free energy functional and energy dissipation [29]. In the micro magnetic theory of ferromagnetism, crystalline symmetry results in multiple minima for the thermodynamic free energy giving rise to multiple metastable states. These explanations are due to Landau and Lifshitz [43] who developed a qualitative theory of phase transitions which explains various kind of hysteretic behaviour.

This non-linear behaviour typically undermines our ability to control or perceive relations in physical, biological, and engineering systems. It is most of time seen as a detrimental and undesirable effect. Nonetheless it has been exploited successfully in some applications such as magnetic data storage and some emerging computer technology, such as ferroelectric nonvolatile thin-film memories. In power electronics, thermostats and digital circuits, hysteretic switching prevents chattering and its associated consequences.

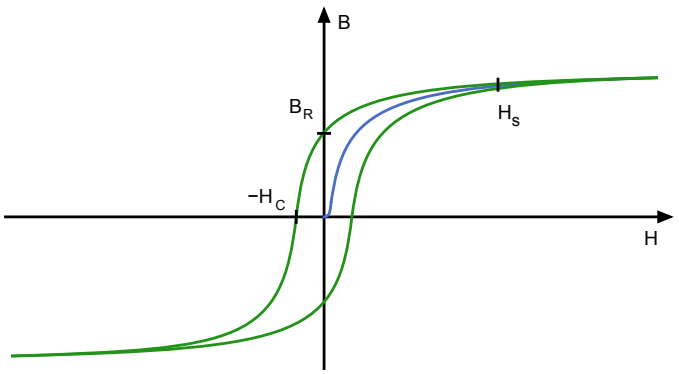

Figure 1.9: Typical hyster B-H curve which occurs in ferromagnetic materials.

Conversely for the purpose of precision positioning or micro assembly the effect of hysteresis has to be addressed. In smart materials, the constitutive coupling between mechanical and electrical/magnetic/thermal properties of these materials enables their inherent sensing and actuation capabilities. At the same time, their microstructure have multiple stable equilibria for one given external input. When hysteresis is present along with the electro-magneto-mechano-chemical dynamics of the material, the overall behaviour of smart sensors and actuators become very complex.

To mitigate and understand hysteresis, various models have been proposed. Hysteresis model can be roughly classified as physics-based or phenomenology based. An example of physics based model is the Jiles and Atherton [32] model for ferromagnetic hysteresis. Formulated in terms of switched differential equations, this theory characterises reversible and irreversible domain wall losses relative to the equilibrium anhysteretic magnetisation. This theory motivated the development of domain wall theory.

Phenomenological model on the other hand are independent of physical systems. One of the most common model is the Preisach model which was originally developed to physically explain ferromagnetic hysteresis[57, 46] but was later given a mathematical description and has since been mostly used as a phenomenological model. In brief, an elementary unit called a "relay" is used to construct the hysteresis operator. In its most basic form, the relay can switch between 2 states and a collection of such relays each switching at different values gives the hysteresis map. In the preisach model, a hysteron is totally defined by its values α and β. Or, it can be defined by its half width r and its centre s. Figure 1.10 shows the elementary Preisach hysteron (figure 1.10a) and a summation of these hysterics make up the hysteresis operators.

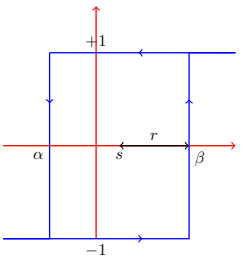

(a) Elementary Unit, a hysteron. α and β are the thresholds for switching.

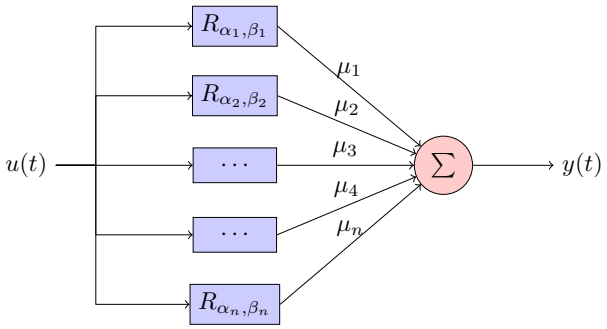

(b) A collection of hysterons whose outputs are summed to create the hysteresis operator. Each hysteron is multiplied by a weight μ. $R_{\alpha\beta}$ are the different relays (hysterons) who switches at different values of α and β.

Figure 1.10: Elementary hysteron and the hysteresis operator.

Other elementary units derived from the preisach are the *play* and *stop*

operator which make up the Prandtl Ishlinskii operator [77]. Their advantage over the Preisach is that they are more easily invertible. Such a property is very important as in many control design involving plant with hysteresis, an inverse model of the hysteresis is used with a linear model of the plant.

1.5 Objective of thesis and Outline of Manuscript

The main objective of the thesis is to build an actuator capable of controlled displacement. Magnetic Shape Memory will be employed as the transducer. It shall convert the electrical energy input to a mechanical energy output which can be used to do work. The port Hamiltonian framework which is energy based will be used to model and control the actuator. The outline of the thesis is as follows:

Chapter 2 presents a general actuator based on Magnetic Shape Memory Alloys. This actuator and its associated modeling was developed in a previous thesis by Gauthier [16] and from which this thesis is inspired. We present his dynamic model of the actuator and improve it using the port Hamiltonian formulation.

These improvements still being insufficient for a proper port-Hamiltonian control, we give in Chapter 3 the necessary theory for understanding MSMA. This chapter also shows how the constitutive equations for the MSMA is derived mainly the total strain and the thermodynamic driving force. Furthermore, we extend the distributed parameter modelling present to lumped parameter model more understandable and better suited for control.

Chapter 4 is then devoted to the Bond Graph Modeling of the actuator. The advantage of using Bond Graphs is first to have a systematic way of modeling the interconnection. Secondly being graphical in nature, it quickly gives an overview of the different elements and their relationship with each other. Thirdly, being power based, it naturally fits the port-Hamiltonian framework and finally we show that it is a powerful tool to incorporate hysteresis into an energetic framework.

Finally in chapter 5 we give some first ideas about possible control strategies for the actuator and some basic experimental results. And finally we conclude the thesis by giving some improvements and some future perspectives.

Chapter 2

A naive model

Contents

2.1 Introduction 17
2.2 Description of actuator 18
2.3 Modeling-Classical Hamiltonian Approach . . . 19
2.3.1 The electrical subsystem 20
2.3.2 The MSMA subsystem 21
2.3.3 The mechanical subsystem 22
2.3.4 Energy of the Actuator 22
2.3.5 Hamilton Equations 22
2.4 The Port-Hamiltonian Approach 25
2.4.1 The electrical subsystem 26
2.4.2 The MSMA+Load Subsystem 29
2.4.3 Interconnection of system I and system II 30
2.4.4 Model Reduction 31
2.5 Discussion 33

2.1 Introduction

In this chapter we extend the work performed by Gauthier [16] during his PhD. We start from his model of the MSMA, reported in [19], and cast it into a port-Hamiltonian model. We then discuss its merits and discrepancies from a Port-Hamiltonian point of view.

In Gauthier et al. [19], a classical Hamiltonian model [42] was built which contained 13 state equations and 3 Lagrange multipliers for a simple MSMA actuator shown in figure 2.1. Using the port-Hamiltonian framework, we were able to reduce the number of states from 13 to 8 with 3 equations of constraints. This reduction changes the set of differential-algebro equations (DAE) into a set of oridnary differential equations (ODE) best suited for

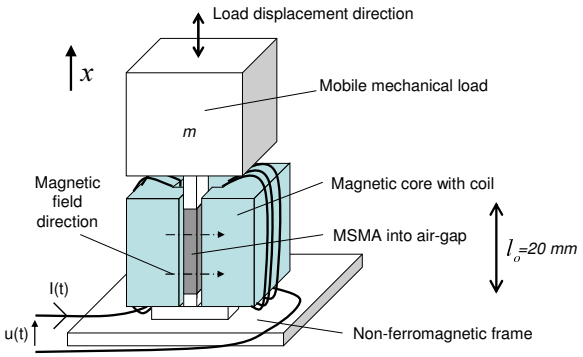

Figure 2.1: MSMA Actuator

.

simulation. These results, reported in Calchand et al. [8], will be presented in this chapter. We start by detailing the actuator and then proceed to derive the Port-Hamiltonian model.

2.2 Description of actuator

The actuator shown in Figure 2.1 consists of a piece of ferromagnetic core around which a piece of wire is wound to make a coil. Located in the core is an air gap in which the Magnetic Shape Memory Alloy (MSMA) is placed. Fixed on the top of the MSMA is a load, m, which applies a stress on the material. The purpose of the actuator is to convert electrical energy into mechanical energy. It can be divided into 3 subsystems namely the electrical subsystem, the MSMA, and the mechanical subsystem. The electrical subsystem is responsible for the generation of the magnetic field. When a voltage, $u(t)$, is applied at its terminals, a current flows in the wire which produces a magnetic field inside the core and in the air gap. The magnetic field in the air gap is converted by the second subsytem- the MSMA- into mechanical energy to lift the load which makes up the third system.

This transduction mechanism i.e the conversion of electrical energy to mechanical energy by the MSMA is possible due to the existence of two stable variants of the material, $M1$ and $M2$. As shown in figure 2.2a, these 2 variants co-exist together in the material. Application of a stress favours variant $M1$ while application of a magnetic field favours variant $M2$. Due to the different crystallographic arrangement of these variants, a macroscopic deformation is observed. Figure 2.2b shows a simplified structure of a unit cell of the MSMA. It has a long axis, a, and a short axis, c. An applied stress favours the $M1$ variant which has its *c-axis* parallel to it wheras a magnetic field favours the $M2$ variant which again has its *c-axis* parallel to it. A maximum macroscopic strain of the order of 6% has been observed in this material [45].

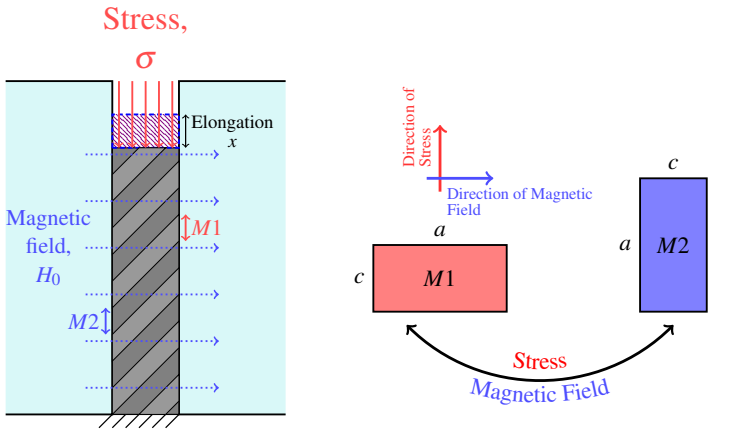

(a) MSMA in magnetic field and under stress.

(b) Transformation between M1 and M2.

Figure 2.2: Actuation Mechanism.

For the actuator to be useful in a range of applications, the displacement, x, of the material need to be controlled. For such purposes, appropriate models are needed to design the control systems. In Gauthier et al. [19], a classical Hamiltonian approach had been taken and in this work, we adopt the Port-Hamiltonian framework.

2.3 Modeling-Classical Hamiltonian Approach

In the classical Hamiltonian approach, a set of *generalised coordinates* denoted by q_i and a set of *generalised momentums* denoted p_i are used to describe a physical system [24, 44]. For a conservative system without external inputs, the time evolution of the system is then given by

$$\frac{dq_i}{dt} = +\frac{\partial \mathcal{H}}{\partial p_i}$$
$$\frac{dp_i}{dt} = -\frac{\partial \mathcal{H}}{\partial q_i}$$

where $\mathcal{H}$ is the Hamiltonian and corresponds to the total energy of the system. To take into account constraints, external inputs and dissipation, the extended formulation is used. In Gauthier et al. [19], it was described as

$$\begin{bmatrix} \dot{q} \\ \dot{p} \end{bmatrix} = \begin{bmatrix} 0 & I \\ -I & -R \end{bmatrix} \begin{bmatrix} \frac{\partial \mathcal{H}}{\partial q} \\ \frac{\partial \mathcal{H}}{\partial p} \end{bmatrix} + \begin{bmatrix} 0 \\ A^T(q) \cdot \mathbf{q} \end{bmatrix} \lambda + \begin{bmatrix} 0 \\ B \end{bmatrix} u(t) \tag{2.1}$$

where λ represents the lagrange multipliers, A the matrix of constraints where $A(q).\dot{\mathbf{q}} = 0$, $u(t)$ the external forces or inputs and R the dissipation

while $\mathcal{H}$ is the total stored energy of the system. For the actuator shown in Fig. 2.1, the different energies of the system is given in Fig. 2.3. There is transformation of energy which occurs along the energy path. The MSMA block shown in the figure is particularly interesting as it shows that the transformation of energy between magnetic and mechanical allowing for loss in the hysteresis. Now we will describe the model proposed by [19] in the next subsections.

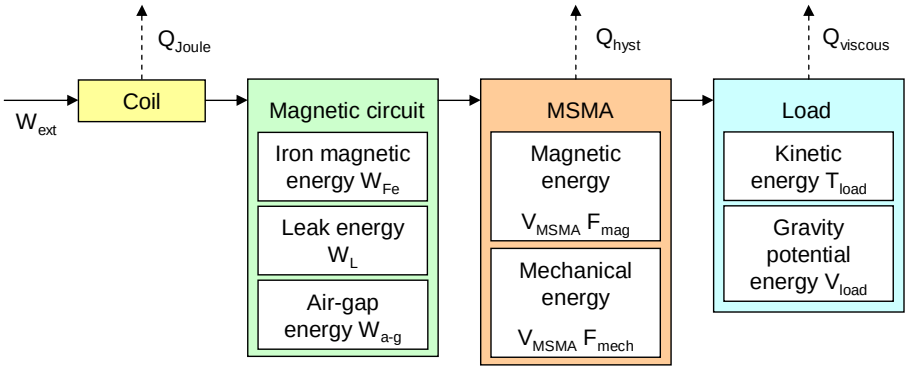

Figure 2.3: Energy repartition

2.3.1 The electrical subsystem

The electrical subsystem consist of an electrical part and a magnetic part. The electrical part generates a current in the coil which in turn produces a magnetic field in the core. As the magnetic part is non ideal, there are parasitic effects which occur along it. These are the *leakage flux* and the *fringing effect*. The leakage flux is due to some magnetic field lines not being confined to the core and the fringing effect is due to the distortion of the field lines near the air gap. After accounting for these effects, the magnetic field in the air gap depends on the inductance of the core and the inductance of the air gap. The core, air-gap, leakage flux and fringing effect have been modeled by inductances as shown in Figure 2.4 The inductances considered

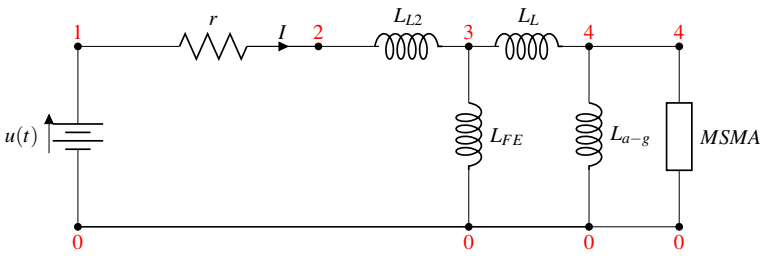

Figure 2.4: MSMA electrical subsystem

Table 2.1: Generalized Coordinates and Momentum for electrical part

	i	q_i	$\dot{q}_i$	p_i
Coil	1	charge,q_c	I	ϕ
Fe-Si core	2	D_{FE}	$H_{FE}.l_{FE}$	$B_{FE}.S_{FE}$
Fringing Effect	3	D_L	$H_L.l_L$	$B_L.S_L$
Air-Gap	4	D_{a-g}	$H_{a-g}.l_{a-g}$	$B_{a-g}.S_{a-g}$

Table 2.2: Generalized Coordinates and Momentum for MSMA

	i	q_i	$\dot{q}_i$	p_i
MSMA	5	field, D	$H.l$	$B.S$
MSMA	6	Fraction, z	$\dot{z}$	p_z
MSMA	7	Strain, ε	$\dot{\varepsilon}$	p_ε

are the leakage flux, L_{L2}, the inductance of the ferromagnetic core, L_{FE}, the fringe effect, L_L, and the inductance of the air gap, L_{a-g}. The generalised coordinates, q_i, and the generalised momentum for the electric part is given in Table 2.1.

For the coil, global[1] quantities are used where the generalised coordinate is the charge q_c, the generalized velocity is the current, I, and the generalized momentum is the flux linkage, ϕ. For the rest of the circuit, the local[2] form is used. The path integral of $H_i l_i$ over the path l_i is taken to be the generalized velocities and the fluxes $B_i.S_i$ through a surface S_i as the generalised momentum.

2.3.2 The MSMA subsystem

The MSMA itself only converts the electrical/magnetic energy into mechanical energy. The model used to quantify this conversion relies heavily on thermodynamics [9, 6]. Furthermore, the Coleman-Noll procedure [12] has been employed to introduce an internal variable, z, which models the material's dissipative nature and the memory effect of the material. Associated with this variable, there is a thermodynamic force which dictates the evolution of z. Physically, z, is the volume fraction of $M2$-the field preferred variant, in the material. Table 2.2 shows the generalised coordinates associated with the material. The magnetic field applied produces an elongation which, through the z variable, produces a strain, ε.

[1] Global quantities are variables integrated into subsystem to give lumped parameters.
[2] Local quantities are density variables which gives distributed parameters

Table 2.3: Generalized Coordinates and Momentum for Load

	i	q_i	$\dot{q}_i$	p_i
Load	8	displacement, x	$\dot{x}$	p_x

2.3.3 The mechanical subsystem

The mechanical subsystem consists of the load, m, being moved by the MSMA. Table 2.3 shows the generalised coordinate and momentum associated with the load. The mechanical subsystem consists of the kinetic and potential energy.

2.3.4 Energy of the Actuator

The total energy at play in the actuator is the sum of the energies of the different parts. For the electrical part, we have the energy associated with the air-gap, the energy stored in the ferromagnetic core, the energy associated with leakage flux and the enegy associated with the coil. These can be written as

$$\mathcal{H}_e = \frac{\phi^2}{2L_{L2}} + V_{FE}\int_0^{B_{FE}} H_{FE}(b)db + V_L\frac{1}{2\mu_0}B_L^2 + V_{a-g}\frac{1}{2\mu_0}B_{a-g}^2 \tag{2.2}$$

where V_i is the considered volume. For the material, it is the volume of the material . For the MSMA, the energy conversion process was quantified using irreversible thermodynamics [28] and is reported in [18] . It is given by

$$\mathcal{H}_{msma} = V_{msma}\left(\frac{E}{2}(\varepsilon-\gamma z)^2 + K_{12}.z.(1-z) + \int_0^B H(b)db\right) + \frac{p_z^2}{2m_z} + \frac{p_\varepsilon^2}{2m_\varepsilon} \tag{2.3}$$

where $\frac{E}{2}(\varepsilon-\gamma z)^2$ is the strain energy in the material, $K_{12}.z.(1-z)$ is an enegy interaction between the variants, $\int_0^B H(b)db$ is the part of magnetic energy stored in the material $\frac{p_z^2}{2m_z}$ is the kinetic energy associated with the movement of z and finally $\frac{p_\varepsilon^2}{2m_\varepsilon}$ which is the kinetic energy associated with the total strain of the material. Finally, the mechanical energy of the actuator is made up of the potential and kinetic energy which is given as

$$\mathcal{H}_{mec} = \frac{1}{2m}p_x^2 + mgx \tag{2.4}$$

2.3.5 Hamilton Equations

The total Hamiltonian is then given by

$$\mathcal{H}(q,p) = \mathcal{H}_e + \mathcal{H}_{msma} + \mathcal{H}_{mec} \tag{2.5}$$

The vector of generalized coordinates, $\mathbf{q}$, generalized momentum, $\mathbf{p}$ and λ which takes into account the Lagrange multipliers are given in (2.6), (2.7) and (2.8).

$$\mathbf{q}^T = [q_c, D_{Fe}, D_L, D_{a-g}, D, z, \varepsilon, x] \tag{2.6}$$
$$\mathbf{p}^T = [\phi, B_{Fe}S_{Fe}, B_L S_L, B_{a-g}S_{a-g}, BS, p_z, p_\varepsilon, p_x] \tag{2.7}$$
$$\lambda^T = (\lambda_1, \lambda_2, \lambda_3) \tag{2.8}$$

From equation (2.5), the equations of motions for the system can then be obtained. For each generalised coordinate and each generalised momentum, an equation can be written which gives 16 equations. The 8 equations relating to the coordinates are obtained as follows

- the first Hamilton equation is the definition of inductance L_{L2}:

$$L_{L2}\dot{q_c} = \phi \tag{2.9}$$

- the next four equation can be obtained from the definition of the magnetic field H_i for $i \in \{Fe, L, a-g, \emptyset\}$

$$\dot{D}_i = l_i H_i \tag{2.10}$$

  where $\emptyset$ (absence of index) represents the magnetic field in the MSMA.

- The next set of three equations relates the momentum p_i to the velocities q_i for $q_i \in \{z, \varepsilon, x\}$ and $i \in \{z, \varepsilon, x\}$.

$$p_i = m_i \dot{q_i} \tag{2.11}$$

The 8 equations relating the momentum are given by the one Kirchoff's voltage law, two magnetic conservation laws, one Newton' s law, one constitutive equation for the MSMA and finally by the 3 Lagrange multipliers.

- the dynamic electrical equation (Kirchoff's voltage law):

$$u = rI + N\dot{B_{Fe}}S_{Fe} \tag{2.12}$$

- the two equations for the conservation of magnetic fluxes in the magnetic circuit:

$$\dot{B}_L S_L = \dot{B}_{Fe}S_{Fe} - \dot{B}_{a-g}S_{a-g} \tag{2.13}$$
$$\dot{B}S = \dot{B}_{a-g}S_{a-g} \tag{2.14}$$

- the two dynamic equation for the load (Newton's Law):

$$m\ddot{x} = -mg - f\dot{x} - S_{msma}\sigma \tag{2.15}$$

- the quasi-static behaviour of the MSMA (constitutive equation)

$$\pi^f(z,\dot{z}) = -\sigma\gamma + K_{12}(1-2z) + \frac{\partial \int_0^B H(b)db}{\partial z} \tag{2.16}$$

- the values of the three Lagrange multipliers:

$$\begin{aligned}\lambda_1 =& \dot{B}_{Fe}S_{Fe}\\ \lambda_2 =& \dot{B}_{a-g}S_{a-g}\\ \lambda_3 =& S\sigma\end{aligned}$$

related to the following 3 constraints:

$$\begin{aligned}N.I =& H_{FE}.l_{FE} + H_L.i_L\\ H_L.l_L =& H_{a-g}.l_{a-g} + H.l\\ x =& l_0.\varepsilon\end{aligned}$$

The first two constraints pertain to the electrical circuit and the last to the mechanical side. Integrating the constraints yield the following 3 equations

$$\begin{aligned}c_1(\mathbf{q}) =& D_{FE} + D_l - N.q_c = 0\\ c_2(\mathbf{q}) =& D_L - D_{a-g} - D = 0\\ c_3(\mathbf{q}) =& x - l_0.\varepsilon = 0\end{aligned}$$

Furthermore we need to define the dissipation matrix, $\mathbf{R}$. The actuator dissipates energy in the resistance, r, of the wire making up the coil and through the hysteretic behaviour of the material. The variable, z, was introduced to model such a dissipation. The thermodynamic force, π^f, is related to the variable, z through the second law of thermodynamics and should obey the Clausius Duhem inequality which is

$$đ\mathcal{D} = \pi^f đz \geq 0 \tag{2.17}$$

In Gauthier et al. [18], to describe the hysteretic nature of the material, an expression of the form

$$\pi^f(z,\dot{z}) = \lambda_C\big[z + \frac{sign(\dot{z})}{2} - \frac{1}{2}\big] + \pi^{cr}.sign(\dot{z}) \tag{2.18}$$

is used and it is depicted in figure 2.5. Then from 2.18 the power dissipated due to hysteresis is given as

$$\mathcal{P}_{hyst} = V_{MSMA}.\dot{\mathcal{D}} \tag{2.19}$$

$$= V_{MSMA}.\big(\lambda_C\big[z + \frac{sign(\dot{z})}{2} - \frac{1}{2}\big] + \pi^{cr}.sign(\dot{z})\big).\dot{z} \tag{2.20}$$

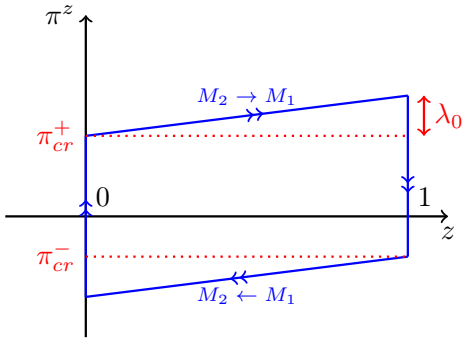

Figure 2.5: Expression for hysteresis. π^z is same as π^f

This power can be incorporated in the dissipation matrix by adding the following term

$$\left(\frac{\partial \mathcal{P}_{hyst}}{\partial \dot{z}}\right)/\dot{z} \tag{2.21}$$

.

Thus the dissipation matrix, $\mathbf{R}$, becomes

$$\mathbf{R} = \begin{pmatrix} r & 0 & 0 & 0 & 0 & 0 & 0 & 0 \\ 0 & 0 & 0 & 0 & 0 & 0 & 0 & 0 \\ 0 & 0 & 0 & 0 & 0 & 0 & 0 & 0 \\ 0 & 0 & 0 & 0 & 0 & 0 & 0 & 0 \\ 0 & 0 & 0 & 0 & 0 & 0 & 0 & 0 \\ 0 & 0 & 0 & 0 & 0 & \left(\frac{\partial \mathcal{P}_{hyst}}{\partial \dot{z}}\right)/\dot{z} & 0 & 0 \\ 0 & 0 & 0 & 0 & 0 & 0 & 0 & 0 \\ 0 & 0 & 0 & 0 & 0 & 0 & 0 & 0 \end{pmatrix} \tag{2.22}$$

The last 2 matrices that are needed to complete the model are the constraint matrix ,$\mathbf{A}$, and the input matrix, $\mathbf{B}$. From the equations above, they are given by

$$\mathbf{A}^T = \begin{pmatrix} -N & 1 & 1 & 0 & 0 & 0 & 0 & 0 \\ 0 & 0 & 1 & -1 & -1 & 0 & 0 & 0 \\ 0 & 0 & 0 & 0 & 0 & 0 & -l_0 & 1 \end{pmatrix} \tag{2.23}$$

and

$$\mathbf{B}^T = \begin{pmatrix} 1 & 0 & 0 & 0 & 0 & 0 & 0 & 0 \end{pmatrix} \tag{2.24}$$

2.4 The Port-Hamiltonian Approach

The previous section described the model as done by [19]. Though done with the Hamiltonian formalism, his model is not properly port-Hamiltonian. There are variables which are in excess. As described in [13], for lumped

electric circuits either (p) or (q) should be used. Using both results in redundancy. To cast that model in a proper port-Hamiltonian model, we will use linear graphs [39] to model the electric circuit in Figure 2.4. Then the MSMA element will be connected to the electrical circuit through its electrical port while the load will be connected at its mechanical port.

The advantage of using the port-Hamiltonian approach allows to separate the interconnection of the elements and the constitutive laws. The subsystem has been divided into two parts, the first part consists of the electrical subsystem and the second part consists of the MSMA element and the load. The electrical subsystem is modelled using linear graphs and then interconnected with the second subsystem.

2.4.1 The electrical subsystem

Figure 2.6 depicts the electrical subsystem of the actuator. It is made up of a network of inductances, the power supply and a resistor. The inductances considered are the leakage flux, L_{L2}, the inductance of the ferromagnetic core, L_{FE}, the fringe effect, L_L, and the inductance of the air gap, L_{a-g}. To

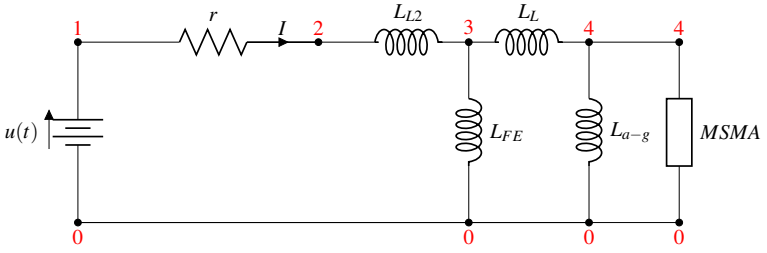

Figure 2.6: MSMA electrical subsystem

model this circuit, we make use of linear graph theory-a brief introduction is given in appendix A. This approach gives us the topology of our system i.e how the elements in the circuits are interconnected to each other.

Linear graph theory tend to translate the graphical representation of circuits into a mathematical form. It uses nodes and branches to represent voltages and current in elements. A node is similar to a potential whereas a branch is a connection between 2 nodes. Hence each branch represent an element (resistor, capacitor or inductor) in which a current flows whereas the nodes at the ends of the branch represent the voltage difference in that element. A tree is then defined as a subgraph which contains all tree nodes and the maximum number of branches without making a loop. A co-tree is then defined as the subgraph made up of the remaining branches. These branches are also called links and they are not present in the tree. To then derive the equations of the circuits, Kirchoff's Current Law (KCL) and Kirchoff's Voltage Law (KVL) are applied. Figure 2.7 shows the linear graph

of the electrical subsystem where u_i has been used to denote the potential difference across each branch.

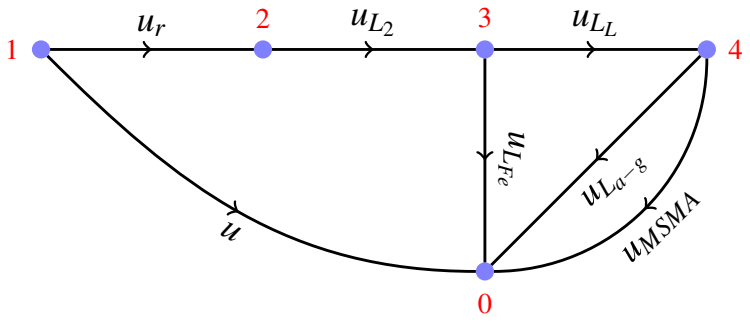

Figure 2.7: Linear graph of MSMA actuator

.

If all elements in a circuit were resistances and sources, the above concepts would have been enough to completely characterize circuits. But for circuits containing energy storage elements such as capacitors and inductors, a more systematic method is needed. Inductances should be put in the links while capacitors should be in tree [39]. Resistances can either be in the tree or co-tree. This makes deriving the equations easier and assures a minimal number of equations. Such a process is carried out because of the fundamental difference in the type of energy they store. Furthermore if the concept of linear graph were extended to the other domains such as mechanical, thermal or fluids, the concept of *across* and *through* variable should be used. Further details can be found in appendix A and [66].

Furthermore, loop-sets are loops which contains only one link. This link voltage can then be expressed in terms of the tree branch voltages. Cut sets are those subgraphs which when the graph is divided(cut) into 2 separate parts contain only 1 tree branch. Hence this tree branch current can be expressed in terms of link currents. KVL is then applied to the loop set and KCL to the cut set. To understand why inductance should be in the link, we need to look at the constitutive equation for an inductor which is

$$v_L = \frac{d\phi}{dt} = L\frac{di}{dt} \tag{2.25}$$

Hence $\dot{\phi}$ should be expressed in terms of all other voltages which is exactly what loop set does. As the inductor is the link, it expresses the voltage across it as a sum of all other voltages present in the loop set. Naturally since loop sets contain only 1 link, no other independent inductor is present. The same argument goes for why capacitors should be in the tree and therefore their equations are obtained using cut sets.

Keeping in mind that inductances are the links, the tree and links (co-tree) can be shown to be as in Figure 2.8.

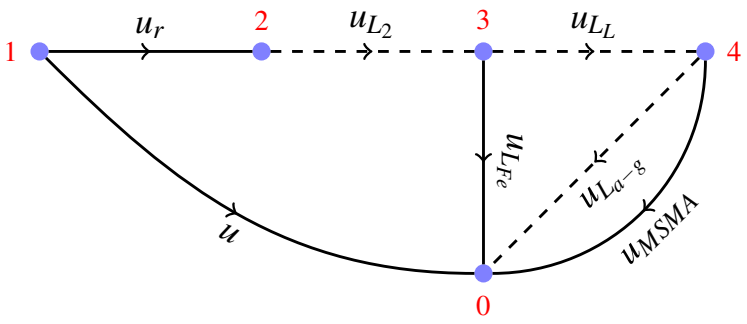

Figure 2.8: Tree and Co-Tree of Actuator. $u_{L_{FE}}$ is the dependent inductor as it is part of the tree.

A closer inspection reveals that one of the inductances is not independent. No tree can be found without adding at least an inductor . This problem can be resolved by either refining the model by incorporating eddy current losses in the core or if the actual model is to be kept, adding a constraint between the dependent and independent variable making the former independent. This is the Lagrange multiplier technique. The latter course is taken.

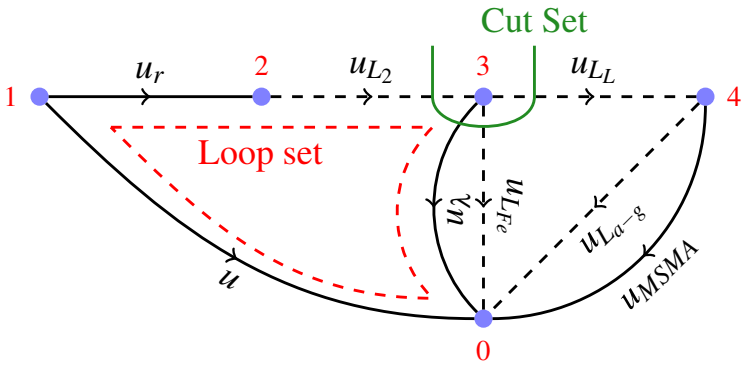

Figure 2.9: Addition of Lagrange Multiplier. Loop sets should contain only one link (dashed) and cut sets should have only one tree branch.

Figure 2.9 shows that the addition of the lagrange multiplier now makes the tree consistent. It also illustrates one loop set and one cut set. Following the discussion above, we pick our state variables to be the fluxes $\phi_{L2}, \phi_{L_{Fe}}, \phi_{L_L}, \phi_{L_{a-g}}$. We need the 4 loop set equations as they give the link voltages (state variable for inductor) and one cut set equation to express the resistor current in terms of a state variable.

The 4 loop set equations are

$$\begin{bmatrix} u_{L2} \\ u_{L_{Fe}} \\ u_{L_L} \\ u_{L_{a-g}} \end{bmatrix} = \begin{bmatrix} 1 & -1 & 0 & -1 \\ 0 & 0 & 0 & 1 \\ 0 & 0 & -1 & 1 \\ 0 & 0 & 1 & 0 \end{bmatrix} \begin{bmatrix} u \\ u_r \\ u_{msma} \\ u_\lambda \end{bmatrix} \tag{2.26}$$

and the 1 cutset equation is

$$i_{L_2} = i_r \tag{2.27}$$

Taking u and u_{msma} as inputs and u_λ as constraint, the Port-Hamiltonian formulation becomes:

$$\begin{bmatrix} \dot{\phi}_{L2} \\ \dot{\phi}_{L_{Fe}} \\ \dot{\phi}_{L_L} \\ \dot{\phi}_{L_{a-g}} \end{bmatrix} = \begin{bmatrix} -R & 0 & 0 & 0 \\ 0 & 0 & 0 & 0 \\ 0 & 0 & 0 & 0 \\ 0 & 0 & 0 & 0 \end{bmatrix} \begin{bmatrix} i_{L2} \\ i_{L_{Fe}} \\ i_{L_L} \\ i_{L_{a-g}} \end{bmatrix} + \begin{bmatrix} 1 & 0 \\ 0 & 0 \\ 0 & -1 \\ 0 & 1 \end{bmatrix} \begin{bmatrix} u \\ u_{msma} \end{bmatrix} + \begin{bmatrix} -1 \\ 1 \\ 1 \\ 0 \end{bmatrix} u_\lambda \tag{2.28}$$

2.4.2 The MSMA+Load Subsystem

The second subsystem consists of MSMA and the mechanical load. For this subsystem, as it was written in the thesis of [16], the input consisted of an input voltage (the voltage across the MSMA in 2.6), u_{ext3}, two thermodynamic variables z and p_z, the strain ε and finally the momentum of the mass p_{load}. p_ε shown in Table 2.2 is omitted. The energy, co-energy and input variables are given as

$$\begin{aligned} \mathbf{x}_{II} &= \begin{pmatrix} \phi_{msma} & z & p_z & \varepsilon & p_{load} \end{pmatrix}^T, \\ \mathbf{o}_{cII} &= \frac{\partial \mathcal{H}_{II}}{\partial \mathbf{x}_{II}} = \begin{pmatrix} i_{msma} & \frac{\partial \mathcal{H}_{II}}{\partial z} & \frac{\partial \mathcal{H}_{II}}{\partial p_z} & \frac{\partial \mathcal{H}_{II}}{\partial \varepsilon} & \frac{\partial \mathcal{H}_{II}}{\partial p_{load}} \end{pmatrix}^T, \\ \mathbf{o}_{extII} &= u_{ext3} = u_{MSMA} \quad \text{(voltage applied to msma).} \end{aligned}$$

where H_{II} is the total stored energy of second subsystem.The resulting Port-Hamiltonian equation is

$$\frac{d\mathbf{x}_{II}}{dt} = \underbrace{\begin{bmatrix} 0 & 0 & 0 & 0 & 0 \\ 0 & 0 & 1 & 0 & 0 \\ 0 & -1 & \star & 0 & 0 \\ 0 & 0 & 0 & 0 & 1 \\ 0 & 0 & 0 & -1 & 0 \end{bmatrix}}_{\mathcal{J}_{II} - \mathbf{R}_{II}} \cdot \frac{\partial \mathcal{H}_{II}}{\partial \mathbf{x}_{II}} + \underbrace{\begin{bmatrix} 1 \\ 0 \\ 0 \\ 0 \\ 0 \end{bmatrix}}_{\mathbf{G}_{II}} \cdot u_{ext3} \tag{2.29}$$

with $\star = \frac{(\partial \mathcal{P}_{hyst}/\partial \dot{z})}{\dot{z}}$ where $\mathcal{P}_{hyst}$ is the dissipated power due to the irreversibility of msma (see [16]). It can be shown, from the 2$^{\text{nd}}$ law of thermodynamics (Clausius-Duhem Inequality), that $\frac{\partial \mathcal{H}_{II}}{\partial \mathbf{x}_{II}}^T \cdot \mathbf{R}_{II} \cdot \frac{\partial \mathcal{H}_{II}}{\partial \mathbf{x}_{II}} \geq 0$ and hence subsystem II is passive.

2.4.3 Interconnection of system I and system II

The two subsystems are then interconnected where

$$u_{L_{a-g}} = u_{ext3} = u_{msma}$$

This interconnection causes a second causality problem as the MSMA and air-gap modelling both have an inductive behaviour and since they connected in parallel: one of them is necessarily dependent on the other. In a similar way to subsystem I, a Lagrange multiplier is added with a constraint defined by a second leakage current i_{λ_2} parallel to the air gap and the MSMA branch/edge:

$$i_{\lambda_2} = -i_{L_l} + i_{L_{a-g}} + i_{MSMA} = 0$$

Finally the Port-Hamiltonian equation for interconnection of subsystems I and II is:

$$\begin{aligned}\frac{d}{dt}\underbrace{\begin{pmatrix}\mathbf{x}_I\\ \mathbf{x}_{II}\end{pmatrix}}_{\mathbf{x}} &= \underbrace{\begin{pmatrix}\mathcal{J}_I - \mathbf{R}_I & 0\\ 0 & \mathcal{J}_{II} - \mathbf{R}_{II}\end{pmatrix}}_{\mathcal{J}-\mathbf{R}} \cdot \underbrace{\begin{pmatrix}\frac{\partial \mathcal{H}_I}{\partial \mathbf{x}_I}\\ \frac{\partial \mathcal{H}_{II}}{\partial \mathbf{x}_{II}}\end{pmatrix}}_{\frac{\partial \mathcal{H}}{\partial \mathbf{x}}}\\ &+ \underbrace{\begin{pmatrix}-1\\0\\0\\0\\0\\0\\0\\0\\0\end{pmatrix}}_{\mathbf{G}} \cdot \underbrace{u_{ext}}_{\mathbf{u}} + \underbrace{\begin{pmatrix}-1 & 0\\ 1 & 0\\ 1 & -1\\ 0 & 1\\ 0 & 1\\ 0 & 0\\ 0 & 0\\ 0 & 0\\ 0 & 0\end{pmatrix}}_{\mathbf{A}} \cdot \underbrace{\begin{pmatrix}u_{\lambda 1}\\ u_{\lambda 2}\end{pmatrix}}_{\mathbf{u}_\lambda}\end{aligned} \tag{2.30}$$

With two constraint equations:

$$\begin{cases} i_{\lambda 1} = i_{L_2} - i_{L_{Fe}} - i_{L_l} = 0\\ i_{\lambda 2} = -i_{L_l} + i_{L_{a-g}} + i_{msma} = 0 \end{cases}$$

These two constraint equations can be assigned in the Port-Hamiltonian formalism:

$$\underbrace{\begin{pmatrix}i_{\lambda 1}\\ i_{\lambda 2}\end{pmatrix}}_{\mathbf{y}_\lambda = \mathbf{i}_\lambda} = \underbrace{\begin{pmatrix}-1 & 1 & 1 & 0 & 0 & 0 & 0 & 0 & 0\\ 0 & 0 & -1 & 1 & 1 & 0 & 0 & 0 & 0\end{pmatrix}}_{\mathbf{A}^T} \cdot \underbrace{\begin{pmatrix}\frac{\partial \mathcal{H}_I}{\partial \mathbf{x}_I}\\ \frac{\partial \mathcal{H}_{II}}{\partial \mathbf{x}_{II}}\end{pmatrix}}_{\frac{\partial \mathcal{H}}{\partial \mathbf{x}}} = 0 \tag{2.31}$$

For quadratic dissipative systems, a Port-Hamiltonian output $\mathbf{y}$ power-conjugated with the external input $\mathbf{u}$ may be defined such as Schaft [64]

$$\frac{d\mathcal{H}}{dt} = -\frac{\partial \mathcal{H}}{\partial \mathbf{x}}^T \cdot \mathbf{R} \cdot \frac{\partial \mathcal{H}}{\partial \mathbf{x}} + \mathbf{y}^T \cdot \mathbf{u} \leq \mathbf{y}^T \cdot \mathbf{u} \tag{2.32}$$

For the device considered in this paper, the computation gives:

$$\begin{aligned}\frac{d\mathcal{H}}{dt} =& \frac{\partial \mathcal{H}}{\partial \mathbf{x}}^T \cdot \frac{d\mathbf{x}}{dt} \\ =& \frac{\partial \mathcal{H}}{\partial \mathbf{x}}^T \cdot \left[(\mathcal{J} - \mathbf{R}) \cdot \frac{\partial \mathcal{H}}{\partial \mathbf{x}} + \mathbf{G} \cdot \mathbf{u} + \mathbf{A} \cdot \mathbf{u}_\lambda \right] \\ =& \frac{\partial \mathcal{H}}{\partial \mathbf{x}}^T \cdot \mathcal{J} \cdot \frac{\partial \mathcal{H}}{\partial \mathbf{x}} - \frac{\partial \mathcal{H}}{\partial \mathbf{x}}^T \cdot \mathbf{R} \cdot \frac{\partial \mathcal{H}}{\partial \mathbf{x}} \\ &+ \left(\mathbf{G}^T \cdot \frac{\partial \mathcal{H}}{\partial \mathbf{x}} \right)^T \cdot \mathbf{u} + \left(\mathbf{A}^T \cdot \frac{\partial \mathcal{H}}{\partial \mathbf{x}} \right)^T \cdot \mathbf{u}_\lambda\end{aligned}$$

Because $\mathcal{J} = -\mathcal{J}^T$ (antisymmetric in accordance with Tellegen principle [74]) and $\mathbf{A}^T \cdot \frac{\partial \mathcal{H}}{\partial \mathbf{x}} = 0$ (constraints), the first and the last parts of the second hands are nul and we obtain:

$$\frac{d\mathcal{H}}{dt} = -\frac{\partial \mathcal{H}}{\partial \mathbf{x}}^T \cdot \mathbf{R} \cdot \frac{\partial \mathcal{H}}{\partial \mathbf{x}} + \left(\mathbf{G}^T \cdot \frac{\partial \mathcal{H}}{\partial \mathbf{x}} \right)^T \cdot \mathbf{u} \tag{2.33}$$

The output $\mathbf{y}$ of this Port-Hamiltonian system is then defined as:

$$\mathbf{y} = \mathbf{G}^T \cdot \frac{\partial \mathcal{H}}{\partial \mathbf{x}} = i_{L_2} \tag{2.34}$$

The number of state variables is 9 in this Port-Hamiltonian modeling whereas it was 16 in the "canonical" Hamiltonian modeling. This system-oriented modeling procedure already allows to reduce the size of the dynamical problem by keeping only state variables instead of generalized coordinates and momenta. We also obtain a minimal realization of the system.

2.4.4 Model Reduction

The "canonical" Hamiltonian modeling procedure gives $2n + n_c$ DAE in the case of n generalized coordinates constraint by n_c interconnections. The Port-Hamiltonian modeling procedure gives $n_x + n_{cx}$ DAE in the case of n_x conservative components constraint by n_{cx} equations. As previously noticed, it is still necessary to reduce them to gain insight into the design and control issues and especially to transform the DAE system into an ODE system

This section presents the reduction of DAE Port-Hamiltonian equations into a set of ODE Port-Hamiltonian equations by using changes of variables and state space projection according to Schaft [65]. The first step consists in decoupling the n_{cx} Lagrange multipliers to $n_x - n_{cx}$ states of the system. It is done by the following change of coordinates: $\tilde{\mathbf{x}} = \mathbf{T_A} \cdot \mathbf{x}$ with $\mathbf{T_A} = \begin{pmatrix} \mathbf{S} & \mathbf{A} \end{pmatrix}^T$ s.t. $\mathbf{A}^T \cdot \mathbf{S} = 0$. $\mathbf{S}$ being a real matrix of size $(n_x, n_x - n_{cx})$. In our case the

following matrix presents the required characteristics:

$$\mathbf{S}^T = \begin{pmatrix} 1 & 1 & 0 & 0 & 0 & 0 & 0 & 0 & 0 \\ 0 & -1 & 1 & 1 & 0 & 0 & 0 & 0 & 0 \\ 0 & 0 & 0 & 1 & -1 & 0 & 0 & 0 & 0 \\ 0 & 0 & 0 & 0 & 0 & 1 & 0 & 0 & 0 \\ 0 & 0 & 0 & 0 & 0 & 0 & 1 & 0 & 0 \\ 0 & 0 & 0 & 0 & 0 & 0 & 0 & 1 & 0 \\ 0 & 0 & 0 & 0 & 0 & 0 & 0 & 0 & 1 \end{pmatrix} \tag{2.35}$$

Because of the dissipative term $\mathbf{R}$ this first coordinate transformation is not sufficient. Indeed after this change of variables the Lagrange multipliers only act on the two last states of the system but these states remain connected to the other ones through $\mathbf{T_A}\left(\mathcal{J}-\mathbf{R}\right)\mathbf{T_A}^T$ due to the dissipative term $\mathbf{R}$. Furthermore the input is still coupled to the constraints as: $\mathbf{T_A}\cdot\mathbf{G} = \begin{pmatrix} -1 & 0 & 0 & 0 & 0 & 0 & 0 & \mathbf{1} & 0 \end{pmatrix}^T$. Hence, after the first coordinate transformation $\mathbf{T_A}$ a second transformation $\mathbf{T_G}$ is applied to remove this residual coupling coming from the dissipation term:

$$\tilde{\tilde{\mathbf{x}}} = \mathbf{T_G}\cdot\tilde{\mathbf{x}} = \underbrace{\mathbf{T_G}\cdot\mathbf{T_A}}_{\mathbf{T}}\cdot\mathbf{x} \tag{2.36}$$

with the following matrix transformations:

$$\mathbf{T_G} = \begin{pmatrix} 1 & 0 & 0 & 0 & 0 & 0 & 0 & 0 & 0 \\ 0 & 1 & 0 & 0 & 0 & 0 & 0 & 0 & 0 \\ 0 & 0 & 1 & 0 & 0 & 0 & 0 & 0 & 0 \\ 0 & 0 & 0 & 1 & 0 & 0 & 0 & 0 & 0 \\ 0 & 0 & 0 & 0 & 1 & 0 & 0 & 0 & 0 \\ 0 & 0 & 0 & 0 & 0 & 1 & 0 & 0 & 0 \\ 0 & 0 & 0 & 0 & 0 & 0 & 1 & 0 & 0 \\ 1 & 0 & 0 & 0 & 0 & 0 & 0 & 1 & 0 \\ 0 & 0 & 0 & 0 & 0 & 0 & 0 & 0 & 1 \end{pmatrix}, \mathbf{T} = \begin{pmatrix} 1 & 1 & 0 & 0 & 0 & 0 & 0 & 0 & 0 \\ 0 & -1 & 1 & 1 & 0 & 0 & 0 & 0 & 0 \\ 0 & 0 & 0 & 1 & -1 & 0 & 0 & 0 & 0 \\ 0 & 0 & 0 & 0 & 0 & 1 & 0 & 0 & 0 \\ 0 & 0 & 0 & 0 & 0 & 0 & 1 & 0 & 0 \\ 0 & 0 & 0 & 0 & 0 & 0 & 0 & 1 & 0 \\ 0 & 0 & 0 & 0 & 0 & 0 & 0 & 0 & 1 \\ 0 & 2 & 1 & 0 & 0 & 0 & 0 & 0 & 0 \\ 0 & 0 & -1 & 1 & 1 & 0 & 0 & 0 & 0 \end{pmatrix}$$

The change of states $\mathbf{x} \mapsto \tilde{\tilde{\mathbf{x}}}$ gives the following Port-Hamiltonian equations:

$$\begin{cases} \dfrac{d\tilde{\tilde{\mathbf{x}}}}{dt} = \mathbf{T}\cdot\left(\mathcal{J}-\mathbf{R}\right)\cdot\mathbf{T}^T\cdot\dfrac{\partial\tilde{\tilde{\mathcal{H}}}}{\partial\tilde{\tilde{\mathbf{x}}}} + \mathbf{T}\cdot\mathbf{G}\cdot\mathbf{u} + \mathbf{T}\cdot\mathbf{A}\cdot\mathbf{u}_\lambda \\ \mathbf{y} = \left(\mathbf{T}\cdot\mathbf{G}\right)^T\cdot\dfrac{\partial\tilde{\tilde{\mathcal{H}}}}{\partial\tilde{\tilde{\mathbf{x}}}} \\ \mathbf{y}_\lambda = \left(\mathbf{T}\cdot\mathbf{A}\right)^T\cdot\dfrac{\partial\tilde{\tilde{\mathcal{H}}}}{\partial\tilde{\tilde{\mathbf{x}}}} = 0 \end{cases} \tag{2.37}$$

With the following state vectors and matrix:

$$\tilde{\tilde{\mathbf{x}}} = \begin{pmatrix} \phi_{L_2} + \phi_{L_{Fe}} \\ -\phi_{L_{Fe}} + \phi_{L_l} + \phi_{L_{a-g}} \\ \phi_{L_{a-g}} - \phi_{msma} \\ z \\ p_z \\ \varepsilon \\ p_{load} \\ 2\phi_{L_{Fe}} + \phi_{L_l} \\ -\phi_{L_l} + \phi_{L_{a-g}} + \phi_{msma} \end{pmatrix}, \ \mathbf{T}\cdot\mathbf{A} = \begin{pmatrix} 0 & 0 \\ 0 & 0 \\ 0 & 0 \\ 0 & 0 \\ 0 & 0 \\ 0 & 0 \\ 0 & 0 \\ 3 & -1 \\ -1 & 3 \end{pmatrix}$$

$$\mathbf{T}\cdot(\mathcal{J}-\mathbf{R})\cdot\mathbf{T}^T = \begin{pmatrix} -R & 0 & 0 & 0 & 0 & 0 & 0 & 0 & 0 \\ 0 & 0 & 0 & 0 & 0 & 0 & 0 & 0 & 0 \\ 0 & 0 & 0 & 0 & 0 & 0 & 0 & 0 & 0 \\ 0 & 0 & 0 & 0 & 1 & 0 & 0 & 0 & 0 \\ 0 & 0 & 0 & -1 & * & 0 & 0 & 0 & 0 \\ 0 & 0 & 0 & 0 & 0 & 0 & 1 & 0 & 0 \\ 0 & 0 & 0 & 0 & 0 & -1 & 0 & 0 & 0 \\ 0 & 0 & 0 & 0 & 0 & 0 & 0 & 0 & 0 \\ 0 & 0 & 0 & 0 & 0 & 0 & 0 & 0 & 0 \end{pmatrix}, \ \mathbf{T}\cdot\mathbf{G} = \begin{pmatrix} -1 \\ 0 \\ 0 \\ 0 \\ 0 \\ 0 \\ 0 \\ 0 \\ 0 \end{pmatrix}$$

This model reduction procedure allows finally to isolate the two constraint equations (algebraic) from the rest of the other equations (ordinary differential) as it can be seen in the last two rows of $\mathbf{T}\cdot(\mathcal{J}-\mathbf{R})\cdot\mathbf{T}^T$, $\mathbf{T}\cdot\mathbf{G}$ and $\mathbf{T}\cdot\mathbf{A}$: the corresponding 7 ODE can be solved independently of the 2 AE. The final 7 order model usable for control can be derived by using projection.

This reduced model has been a very important milestone in this thesis.

2.5 Discussion

The model as described in Section 2.3 was developed in [18, 19]. This model as regards to port-Hamiltonian control is unsuitable. Firstly, in his approach, there is a mixture of local and global form. Either everything should be in local or everything should be global else the model becomes intractable. Secondly, for the description of electric circuits, we have two choices. Either the circuit can be described in terms of *charges* and *current* or the system can be described in terms of *voltages* and *flux linkages* as explained in [13]. Then instead of having 2 equations for one conservative circuit element, only one is required. Considering the the first line in Table 2.1, $\frac{\partial \mathcal{H}}{\partial \phi} = \dot{q}_c$ exists but $\frac{\partial H}{\partial q_c}$ does not. Also, it is not seen how the MSMA converts the electrical energy to the mechanical energy. Though present, it has been drowned within equations.

Also, 3 Lagrange multipliers had to be used in both models. The first one is used as the inductances modelled are not independent. The second

because the MSMA also presents an inductive nature and the third was used because the MSMA was considered an *effort* source when in fact it is a *flow* source acting by means of variable z. The term *effort* and *flow* will be dealt with in later chapters.

And finally in treating hysteresis, no explicit expression for $\dot{z}$ is given. In the static case, the dynamics of $\dot{z}$ is not essential whereas for control purposes this dynamics becomes very important. An ad-hoc solution has been used to include hysteresis. The term $\frac{\partial \mathcal{P}_{hyst}}{\partial \dot{z}}$ is inconsistent with either the energy framework or state-space formulation in general.

The port-Hamiltonian model in this section, only solves the problem partially. It has reduced the number of states but the Lagrange multipliers and the hysteresis problem are still here. In the remaining of this thesis, we propose solutions to resolve these problems and give explicit dynamics on z. We will also propose a model and a graphical view of the energy conversion process throughout the material.

The next chapter is the first step towards resolving the problems. It details the physics of the MSMA as well as the derivation of the lumped parameters for the actuator.

Chapter 3

MSMA: An energy conversion device

Contents

3.1 Introduction 36
3.2 Magnetism 36
3.2.1 Magnetization 37
3.3 Physics of the MSMA 39
3.3.1 Motion of Magnetic Wall 40
3.3.2 Rotation of Magnetization vector 41
3.3.3 Strain Mechanism 41
3.4 Distributed Parameter Modelling of MSMA . . 42
3.4.1 Representative Volume 43
3.4.2 Thermodynamics of MSMA 44
3.4.3 Magnetization of MSMA 46
3.4.4 Magnetic Energy 47
3.4.5 Mechanical Energy 50
3.4.6 Gibbs Free Energy 51
3.5 Lumped Parameters Modelling of MSMA . . . 52
3.5.1 Terminal Variables 52
3.5.2 Reluctances 55
3.5.3 MSMA Actuator lumped Parameters 56
3.5.4 Energy Considerations 59
3.6 Discussion 66

3.1 Introduction

The purpose of this chapter is to explain the detailed working of the MSMA. We start from the thermodynamics model done by Gauthier [16] and extend it for our purposes. The first aim is to understand how energies functionals proper to thermodynamics such as Gibbs free energy and/or Helmholtz free energies relates to energy functional as defined in the port Hamiltonian framework. Then, using constitutive equations for magnetization and strain, we derive the thermodynamic force which govern the evolution of the z variable. This model only takes into consideration the material but for the actuator, we need to also take into account the associated part such as the electromagnet and the load. In a second step therefore, we convert our model of the material to a lumped parameter model then extends it taking into account the associated parts. We will differentiate between energy densities which will be written using the symbol $\mathscr{W}$ and lumped energy which will be written using W. We start by giving a brief overview of magnetism which will be used throughout this chapter.

3.2 Magnetism

In MSMA, magnetism plays a dominant role as it is this kind of energy that is converted to mechanical work. More specifically, the material magnetization changes when there is an elongation and vice-versa. Hence, we define some basics of magnetism to understand the terminology used in this chapter (see Appendix B for a brief treatment of magnetism).

The Magnetic Flux Density in free space

The magnetic flux density, B, produced by a current carrying conductor is given by the **Biot-Savart** law which states that

$$B(p) = \frac{\mu_0}{4\pi} \int \frac{\bar{I} \times \hat{r}}{r^2} = \frac{\mu_0 I}{4\pi} \int \frac{d\bar{l} \times \hat{r}}{r^2} \tag{3.1}$$

where I is the current flowing through the conductor, $\hat{r}$ is the vector between an element $d\bar{l}$ of the conductor and the point at which B is measured. I can be taken out of the integral since $d\bar{l}$ is in the same direction as the current I. μ_0 is called the *permeability* of free space and has a value of $4\pi \times 10^{-7} N/A^2$ [25, 82].

Two results which will be stated without proof are the curl and divergence of B. The proof of these resu lts can be found in any standard textbook such as Griffiths [25] and Zahn [82]. The divergence of B is

$$\nabla \cdot B = 0 \tag{3.2}$$

which states that no magnetic monopoles exist. And the curl in free space is given by

$$\nabla \times B = \mu_0 J \tag{3.3}$$

where J is the current density. Apart from current, another source of the magnetic flux density are permanent magnets. They can produce a magnetic field due to their magnetisation.

3.2.1 Magnetization

MSMA are ferromagnetic materials which gets **magnetized** in a magnetic field. All magnetic phenomena are due to electric charges moving. In a material, there are electrons moving around orbits which produce a magnetic field. These orbiting electrons can be considered to be magnetic dipoles. Usually this magnetic field cancel each other so that no net field is observed. The effect of applying an external magnetic field to a material gives rise to three main types of magnetism. They are diamagnetism, paramagnetism and ferromagnetism.

In media where the induced dipole moment produces a field which opposes B, is called "diamagnetic" medium. Some media contain permanent dipoles which are oriented at random even when there is no magnetic field. But under the action of a magnetic field, the dipoles becomes oriented resulting in a dipole moment which is proportional to the external field. These are called "paramagnetic" medium [68, 25].

The last type of magnetism which is ferromagnetism is an extreme case of paramagnetism. If the permanent dipoles are very close to each other in the medium, there proves to be an effect only, explainable only by quantum theory [25], and called "exchange", which results in the strong tendency for the spins (direction of orbit of rotation of electron) of adjacent atoms or molecules to line up parallel to each other even in the absence of any field. Such a parallel orientation can extend, in an unmagnetized body over volumes of a considerable scale on an atomic order, though a very small volume by ordinary standards. Such a volume is called a "domain", and an ordinary ferromagnetic body contains many such domains, each with a strong permanent moment, but oriented in different directions. In the presence of a magnetic field, such domains change their orientation and align with the external field until finally at very large field all moments are aligned and the further increasing the field has no effect. This is called saturation of the material. Reversing the field reverses the moments, but there is an effect similar to friction, hindering this reorientation, so that, by the time the external field is zero, there can still be a considerable moment. The effect of the moment lagging behind the field is what gives rises to the phenomenon of hysteresis in ferromagnetic materials [68].

It has been shown that a magnetized [25] body produces a magnetic field outside it. Also, the magnetization can be attributed to surface and

volume currents flowing in the material. And these bounded currents can be calculated knowing the magnetization, M of the material. The bounded currents, J_b, is given by

$$J_b = \nabla \times M \tag{3.4}$$

The Magnetic field intensity

Now since the magnetic field, B, derives from currents, we can rewrite it as a sum of free currents (those produced by a battery or a circuit), J_f and bounded currents, J_b.

$$\nabla \times B = \mu_0(J_f + J_b) \tag{3.5}$$

which is equal to

$$\nabla \times B = \mu_0(J_f + \nabla \times M) \tag{3.6}$$

from which we can deduce

$$\nabla \times \left(\frac{B}{\mu_0} - M\right) = J_f \tag{3.7}$$

The quantity $\frac{B}{\mu_0} - M$ is so important in engineering that it has been given a special name and symbol. Usually it is called the "magnetic field intensity" and is denoted by H. Its importance lies in the fact that it gives the free current directly or can be calculated directly from free currents. The field produced by a coil of wire is usually calculated using H instead of B. And in laboratory setting, it is the magnetic field intensity H that we can control by varying the current passing in a circuit. The constitutive equation relating B, H and M is

$$B = \mu_0(H + M) \tag{3.8}$$

It has already been stated that in diamagnetic and paramagnetic materials, M is proportional to B and hence proportional to H we can therefore write

$$B = \mu_r \mu_0 H \tag{3.9}$$

where μ_r is called the relative permeability of the material. Then the ratio of magnetization to magnetic field intensity becomes

$$M = \chi_m H, \qquad \mu_r = 1 + \chi_m \tag{3.10}$$

where χ_m is the susceptibility of the material.

It will be seen later that MSMA exhibit nonlinear magnetization when subjected to a field H_0. Its relative permeability μ_r and susceptibility χ varies with elongation of the material.

3.3 Physics of the MSMA

MSMA exhibit a deformation under the action of a magnetic field. This magnetic induced deformation depends on the stress applied. The property which changes and can be exploited for sensor and actuator application is the permeability of the material. Figure 3.1 shows the deformation curve under different loading conditions [36]. The stress dependent deformation is clearly visible as well as the highly hysteretic nature of the material.

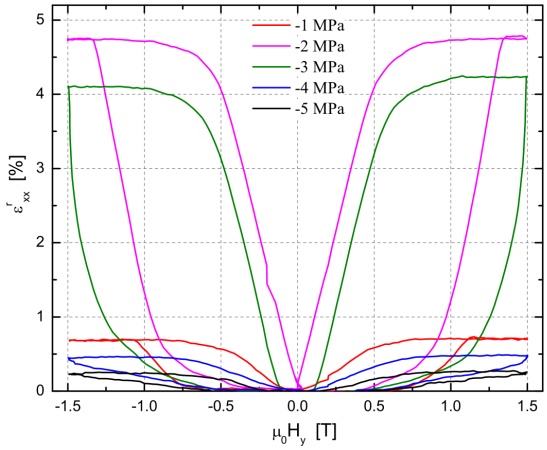

Figure 3.1: Deformation with different applies stress [38].

In MSMA, the macroscopic response is driven by 3 mechanisms

1. The motion of magnetic wall domains,
2. The local rotation of magnetization vectors,
3. The field induced variant orientation

The first two are common to ferromagnetic material whereas the last one is proper to Magnetic Shape Memory alloys. Nevertheless all of them contribute to the magnetization of the material. On cooling down from the austenite phase, all three martensite variants exists. Applying a stress in one direction say x[100], favours one particular variant, in figure 1.5 it would be variant $M2$, which has its short axis, c, parallel to the stress.

This stress can be further increased until only one variant is present. Then if this stress is lower than the *blocking stress*, martensitic variant orientation can still take place on applying a magnetic field in the z[001] direction. Such a magnetic field, would promote the appearance of variant *M1*. At the blocking stress, σ^b, this third mechanism will not take place hence no deformation will be observed.

Magnetic domains form in order to reduce the magnetization of the material and is termed the magnetostatic energy. They are separated by magnetic

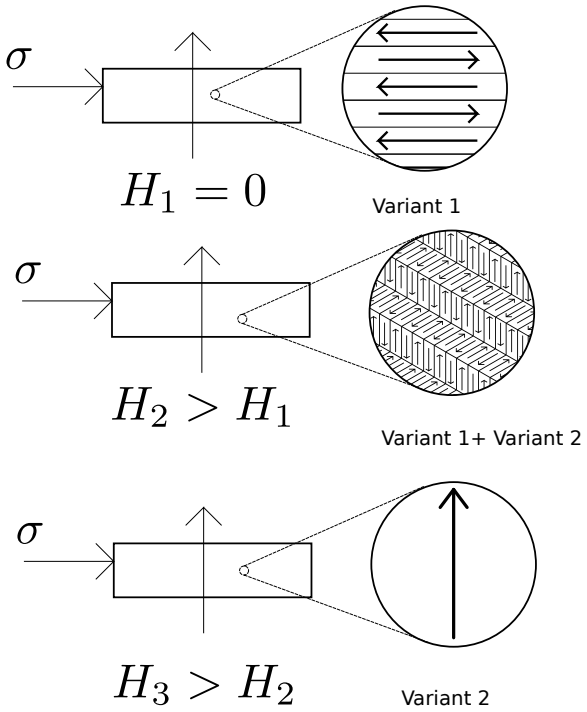

Figure 3.2: Crystallographic Change

domain walls. In these walls, the magnetization vectors (magnetic dipole moments) are rotated over short distances to accommodate the magnetization direction of their neighboring domain. (Hence near positively directed domains, negatively directed domains will be formed as such a configuration is energetically more favorable.)

MSMA also behave in an anisotropic way. Such a behavior is characteristic of materials which have different magnetization along different crystallographic direction. Hence more energy is required to magnetize one direction than the other. The easy magnetization direction is called the easy axis whereas the hard axis is where more energy is required to magnetize.

3.3.1 Motion of Magnetic Wall

Before the application of a magnetic field, the magnetization vectors are distributed in a positive and negative direction evenly in the material such that they cancel each other and there is no net magnetization. On application of a magnetic field which coincides with the easy axis of magnetization, one of domain will grow at the expense of the other until all the magnetization vectors are in the same direction as the applied field.

3.3.2 Rotation of Magnetization vector

When the applied field is not in the direction of easy axis ,c, the magnetization has to rotate in order to align itself with the magnetic field. Since in both domains, it is equally unfavorable, no domain wall motion is available to accommodate the magnetization. Energy has to be expended against the magnetocrystalline anisotropy energy. The amount of energy required is higher than that for domain wall motion. This therefore becomes the hard axis of magnetization. Figure 3.3 shows the normalized response to an applied magnetic field for the hard and easy axis. It is clear that the magnetization energy which is defined as

$$\mathcal{U}_m = \mu_0 \int_0^{M^{sat}} H(M)dM \tag{3.11}$$

is greater for the hard axis.

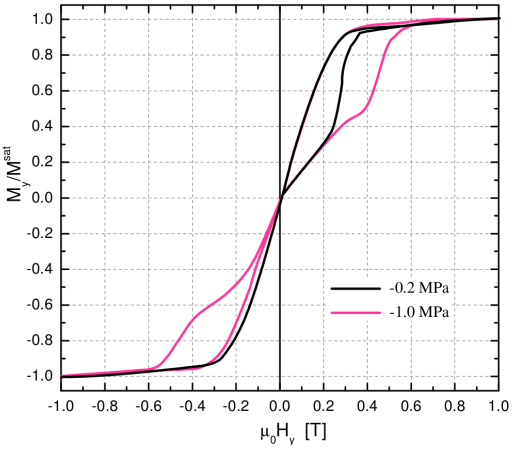

Figure 3.3: Relative Magnetization Response as reported by Heczko et al. [27].

3.3.3 Strain Mechanism

When under no magnetic field, there exists equal proportions of 3 variants. Since we are interested only in motion in the xy plane we will consider only 2 of them. The 2 variants called M1 and M2 are separated by a twin boundary. Also, within each variants, magnetic domains exist which are seperated by 180° walls. If no stress is applied to the material, the twin boundary will start to move, the field preferred variant will grow at the expense of the stress-preferred variant. If a stress, greater than the blocking stress is applied, no deformation can take place. Hence the strain is governed by an interplay between the magnetic field applied and the stress on the material.

3.4 Distributed Parameter Modelling of MSMA

In this section, we show how thermodynamics is applied to give the constitutive equation on the evolution of the volume fraction z. We use a continuum media description of the material. All the variables used in this section are densities.

In literature, numerous models have been developed for the characterization of the twinning rearrangement. Most of the models are based on the construction of a free energy function to find equilibrium configuration for mechanical, magnetic and thermal load conditions. A model by James and Wutting [30] relies on the theory of constrained micromagnetics. The terms contributing to the free energy are the Zeeman energy, the magnetostatic energy and the elastic energy. The magnetization is assumed to be fixed to the magnetic easy axis of each martensitic variant because of high magnetic anisotropy. The microstructural deformations and the resulting macroscopic strain and magnetization response are predicted by detecting low-energy paths between initial and final configurations. They conclude that the typical strains observed in martensite, together with the typical easy axes observed in ferromagnetic materials lead to layered domain structures that are simultaneously mechanically and magnetically compatible.

O'Handley [48] proposed a 2-D model in which two variants are separated by a single twin boundary and each variant itself consists of a single magnetic domain. The local magnetization is not necessarily constrained to the crystallographic easy axis. Depending on the magnitude of the magnetic anisotropy, either the magnetic anisotropy difference (low magnetic anisotropy case) or the Zeeman energy (high magnetic anisotropy case) are identified as the driving force for twin boundary motion. For the intermediate case a parametric study is conducted showing the influence of varying elastic and magnetic anisotropy energies. All cases assume an initial variant distribution that implies a remnant magnetization.

Likhachev and Ullakko [45] presented a model which identifies the magnetic anisotropy energy difference in the two variant twinned-martensite microstructure as the main driving force for the reorientation process. The effect of magnetic domains is taken into account in an average sense through the incorporation of curve fitted magnetization data, corresponding to the magnetization along different crystallographic directions, into their model. They argue that, regardless of the physical nature of the driving force, twin boundary motion should be initiated at equivalent load levels. With this assumption experimentally obtained detwinning-under-stress data in addition to the magnetization data of magnetic shape memory alloy martensite can be used to predict the constitutive behavior associated with the variant reorientation process under the application of external magnetic fields.

Hirsinger and Lexcellent [28] introduced the outline of a non-equilibrium thermodynamics based model. The free energy contains chemical, mechan-

ical, magnetic and thermal contributions. The magnetic term is given by the Zeeman energy. Two internal state variables, the martensitic variant volume fraction and the magnetic domain volume fraction, are introduced to represent the influence of the microstructure. The rate independent nature of their approach motivates the definition of driving forces for the twin boundary motion and the domain wall motion.

Mogylnyy et al. [47] proposed a constitutive model for the martensitic twin rearrangement based on a statistical approach, in which the magnetic-field-induced strains are related to the relaxation of the internal stresses in martensite due to magnetoelastic interactions. It should be mentioned that several other groups have contributed to the literature on modeling of MSMAs, which can not all be mentioned in this brief overview.

3.4.1 Representative Volume

To model our material, we will consider a small representative volume of the material which is transforming from M2 to M1 as shown in figure 3.4. Internal variables as proposed in [28] are used to describe the micro-macro behaviour of the material. These variables are α, θ and z. When the material cools down from the austenite phase, equal amounts of variants $M1$ and $M2$ exist. Parameter α represents the fraction of domain wall which is aligned in the same direction as the field whereas θ represents the angle between the applied magnetic field and the natural orientation of the magnetization vector in M1. As discussed previously, on increasing the magnetic field, domains walls in the same direction as the field tends to grow whereas those not aligned disappear. Similarly for sufficiently high stress, when rearrangement is not possible, rotation of the magnetization vector occurs to align itself with the plane of the magnetic field.

Figure 3.5 shows the evolution of other wall domain and the magnetization vector under different loading conditions.

Domain wall motion represented by α saturates at quite low applied field value. If then, the external magnetic field is increased, two situations may occur. If no stress is applied, the field preferred variant grows at the expense of the stress preferred variant until there is only 1 variant in the sample. If there is an applied stress, the magnetization vector starts to rotate and there in an increase in the field preferred variant. These processes are thought to occur simultaneously such that for some low stresses, complete reorientation does occcur while for stresses above a certain value, the magnetization vector saturates before complete reorientation and hence a mixture of both variants is present.

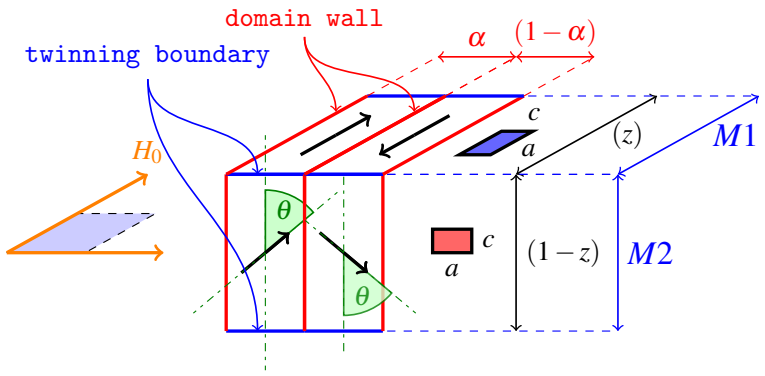

Figure 3.4: Representative volume. The direction of the magnetization vector in α is in the same direction as H_0.

3.4.2 Thermodynamics of MSMA

Thermodynamics has proven a very useful tool to model this material as shown in Likhachev and Ullakko [45], Kiefer and Lagoudas [38] and Sarawate [63]. There are two types of variables used in thermodynamics namley *extensive* and *intensive*. Extensive variables are those variables which depend on size of the system such as volume, mass, strain etc. whereas intensive variables are those variables which are energetically dual of extensive variables. They are temperature, pressure, stress etc.

For the MSMA, the extensive variables are the magnetization, M, the strain of the material, ε and entropy S. The associated conjugate variable which is intensive in nature associated with each of the previous extensive variables are the magnetic field, H_0, the stress, σ and the temperature, T. The extensive variables are the *generalised coordinates* whereas the intensive variables are the *generalised forces*. The internal energy $U(M, \varepsilon, S)$ which depends on the extensive variables then completely characterises the state of the system at thermodynamic equilibrium. Futhermore, in our case we need 3 more variables, the internal variables, α, θ and z to complete the state during irreversible behaviour. The internal energy is then given by

$$U = U(M, \varepsilon, S, \alpha, \theta, z) \tag{3.12}$$

In (3.12), the extensive variables are the independent variables i.e variables which can be varied independently by some external means. Unfortunately in our case, we cannot vary the magnetization or the strain. It is the applied magnetic field, H_0, which can be varied by changing the current. And instead of the strain, we can control the stress by changing the load applied. Also, it is easier to work with the temperature, T, instead of entropy,

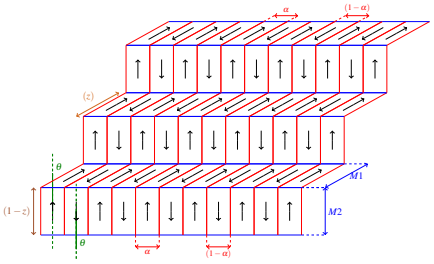

(a) On cooling both variants exist in same quantity.

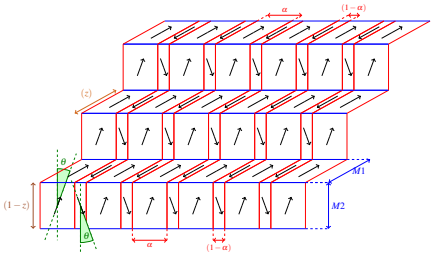

(b) Application of a magnetic field makes α appears rapidly while θ rotates slowly.

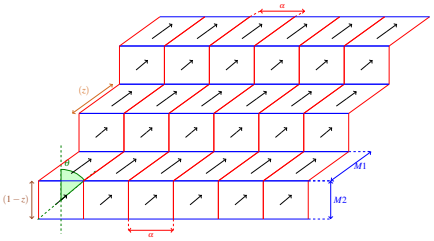

(c) After critical value of magnetic field has reached. Twinning start M1 grows at expense of M2. Domain walls $1-\alpha$ have disappeared.

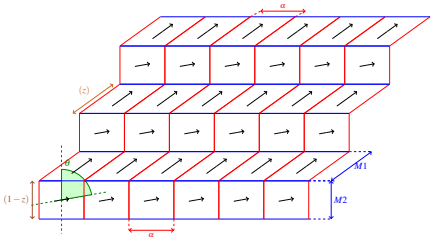

(d) If specimen is blocked, no twinning motion occurs. θ rotates on increasing magnetic field.

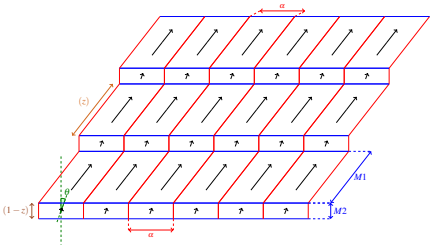

(e) If speciment not blocked, M2 dissappears.

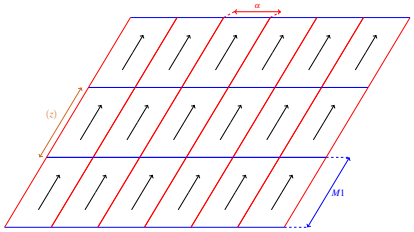

(f) At saturation, if not blocked, only one variant exist-M1-the field preferred variant.

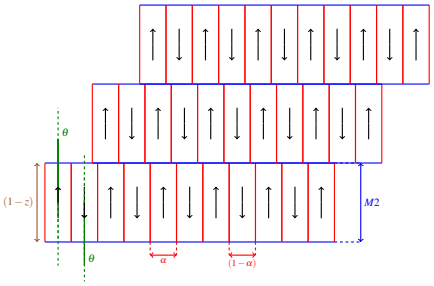

(g) On applying a very high stress with no magnetic field, only M2 is present. All M1 dissappears.

Figure 3.5: Twinning mechanism. Formation of domain walls and rotation of magnetization vector.

S for isothermal processes. For such purposes, instead of internal energy, U, we must make use of the Gibbs free energy, $\mathcal{G}$, which is given by a Legendre transform as follows

$$\mathcal{G} = U - \sum_{i}^{n} X_i q_i \tag{3.13}$$

where X_i is the generalised force and q_i the generalised coordinate.

Taking the independent variables as the stress, σ, the magnetic field H_0, the temperature, T, and the internal state variables α, θ and z, the constitutive dependencies are

$$\begin{aligned}\mathcal{G} =& \mathcal{G}(\sigma, H_0, T, \alpha, \theta, z)\\ \varepsilon =& \varepsilon(\sigma, H_0, T, \alpha, \theta, z)\\ M =& M(\sigma, H_0, T, \theta, z)\end{aligned}$$

And finally the main purpose of using thermodynamics is to derive a thermodynamic driving force, $\pi^z(H_0, \sigma, T, \alpha, \theta, z)$ which gives the evolution of internal variable z. The driving force for α and θ are taken to be 0 as they are assumed to be reversible i.e purely magnetic hysteresis is negligible. On removal of the magnetic field, α and θ return to their original position. To arrive at π^z, a total Gibbs free energy, $\mathcal{G}$, is derived and then differentiated to obtain the driving force:

$$\pi^z = -\frac{\partial \mathcal{G}}{\partial z} \tag{3.14}$$

These constitutive dependencies, will follow in the following subsections.

3.4.3 Magnetization of MSMA

To quantify the magnetization, M, of the material in a field of intensity, H_0, all 3 internal variables α, θ, z are needed. In other words, $M = f(\alpha(H_0), \theta(H_0), z)$. Variables α and θ take care of the saturation whereas z gives the proportion of magnetization that each variant contribute. As proposed in Gauthier et al. [18] and Hirsinger and Lexcellent [28], α, a function of H_0, is taken to be

$$\alpha = \frac{M}{2M_s} + \frac{1}{2} = \frac{\chi_a H_0}{2M_s} + \frac{1}{2} \quad , \quad \alpha \in [0, 1] \tag{3.15}$$

which gives

$$M = M_s(2\alpha - 1) \tag{3.16}$$

for the field preferred variant $M2$ and θ, also a function of H_0, is taken to be

$$\sin\theta = \frac{M}{M_s} = \frac{\chi_t H_0}{M_s} \quad , \quad \theta \in [-\frac{\pi}{2}, \frac{\pi}{2}] \tag{3.17}$$

which gives for variant $M1$

$$M = M_s \sin(\theta) \tag{3.18}$$

M_s is the saturation magnetization, χ_t and χ_a are the domain susceptibilities. Then again from Gauthier et al. [18], Hirsinger and Lexcellent [28], it is proposed that the total magnetization is the sum of the magnetization for each variant (refer to figure 4.19 for a pictorial representation of α and θ).

$$M = M_s\big((2\alpha - 1)z + (\sin\theta)(1 - z)\big) \tag{3.19}$$

Figure 3.6 shows the variation of α and θ where it can be seen that α saturates at a much lower value than θ.

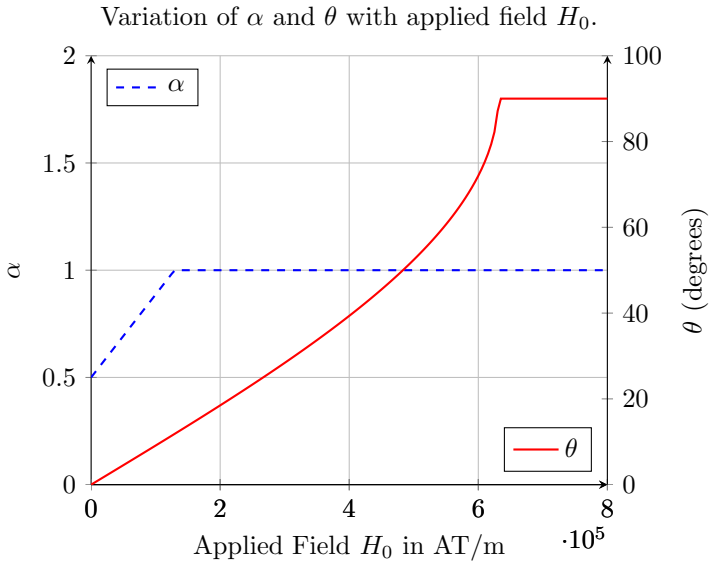

Figure 3.6: Variation of α, θ with applied H_0

Similarly, figure 3.7 shows the magnetization for different values of z. Both curves were simulated using values from the Adaptamat's datasheet which specifies an $M_s = \frac{0.65T}{\mu_0}$, $\chi_a = 40$ and $\chi_t = 1$.

3.4.4 Magnetic Energy

The magnetic energy stored or converted by the material can be found out from the constitutive (H_0, M) relationship. The work done by a battery is to establish the magnetic field in the air gap as well as to increase the magnetization of the material (see Appendix B). Considering only the differential work $d\mathscr{W}_{mag}$ we require to magnetize the material, we have

$$d\mathscr{W}_{mag}(M) = \mu_0 H_0 . dM \tag{3.20}$$

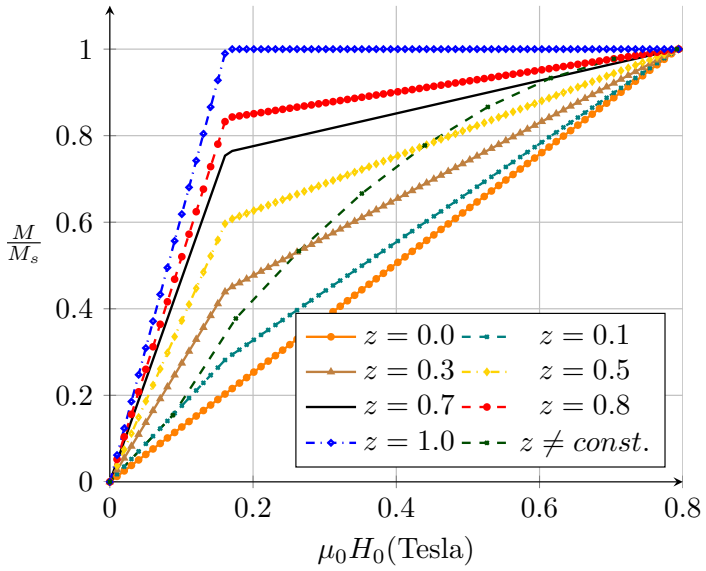

Figure 3.7: Magnetization for different values of z. Dotted line shows a possible magnetization curve of the material as z changes. Solid lines show magnetization at constant z.

The energy density $\mathscr{W}_{mag}$ is then obtained as follows

$$\mathscr{W}_{mag}(M) = \int_0^M \mu_0 H_0 dM \tag{3.21}$$

Due to the complicated nature of (3.19), no attempt has been made to invert it. In such cases, it is easier to work with the co-energy density. Figure 3.8 shows the co-energy (density) and energy (density) for the magnetization of the material. The energy is the area under the *y-axis* whereas co-energy is the area under the *x-axis*. It also depicts where α and θ get saturated.

From figure 3.8, we have

$$\mathscr{W}_{mag} + \mathscr{W}^*_{mag} = \mu_0 H_0 . M \tag{3.22}$$

Differentiating, we obtain

$$d\mathscr{W}_{mag} + d\mathscr{W}^*_{mag} = \mu_0 H_0 dM + \mu_0 M dH_0 \tag{3.23}$$

And finally replacing $d\mathscr{W}_{mag} = \mu_0 H_0 dM$, results in

$$d\mathscr{W}^*_{mag} = \mu_0 M dH_0 \tag{3.24}$$

The above steps is called a Legendre transformation, i.e we pass from an energy representation to a co-energy representation.

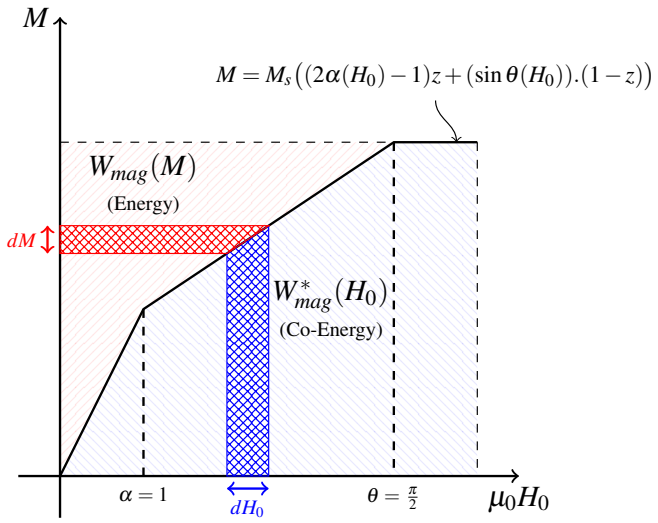

Figure 3.8: Energy and Co-energy for Magnetic part of MSMA.

Applying thermodynamics principles, we can now derive the magnetic Gibbs free energy, $\mathcal{G}_{mag}$. Starting from the internal energy (assuming it depends on M and T only) we have

$$dU(M,S) = \mu_0 H_0 dM + TdS$$

We can then apply a Legendre transformation to make H_0 and T independent variables.

$$\mathcal{G}_{mag}(H_0,T) = U - TS - \mu_0 HM$$

Then

$$\begin{aligned} d\mathcal{G}_{mag} =& dU - TdS - SdT - \mu_0 H_0 dM - \mu_0 M dH_0 \\ =& \mu_0 H_0 dM + TdS - TdS - SdT - \mu_0 H_0 dM - \mu_0 M dH_0 \\ =& -\mu_0 M dH_0 - SdT \end{aligned}$$

Since we are working at isothermal conditions, $dT = 0$. Then

$$d\mathcal{G}_{mag} = -\mu_0 M dH_0 = -d\mathscr{W}^*_{mag} \tag{3.25}$$

The magnetic Gibbs free energy can then be calculated from the following equation

$$\begin{aligned} \mathcal{G}_{mag} = -\mathscr{W}^*_{mag}(H_0) &= -\int_0^{H_0} \mu_0 M dH \\ &= -\int_0^{H_0} \mu_0 M_s\big((2\alpha-1)z + (\sin\theta)(1-z)\big) dH_0 \end{aligned} \tag{3.26}$$

To be able to integrate (3.26), it has to be expressed in terms of H_0. For this purpose, the saturation of α and θ has to be taken into consideration.

Note that we have 3 cases

1. $\alpha < 1$ and $\theta < \frac{\pi}{2}$. $H_0 < \frac{M_s}{\chi_a}$.
2. $\alpha = 1$ and $\theta < \frac{\pi}{2}$. $\frac{M_s}{\chi_a} \leq H_0 < \frac{M_s}{\chi_t}$.
3. $\alpha = 1$ and $\theta = \frac{\pi}{2}$. $H_0 \geq \frac{M_s}{\chi_t}$.

For the first case, the integral becomes

$$\begin{aligned} \mathcal{G}_{mag} &= -\mu_0 M_s \int_0^{H_0} \frac{\chi_a H_0}{M_s} z + \frac{\chi_t H_0}{M_s}(1-z)\, dH_0 \\ &= -\mu_0 \left(\frac{\chi_a H_0^2}{2} z + \frac{\chi_t H_0^2}{2}(1-z) \right) \end{aligned} \tag{3.27}$$

For the second case we have

$$\begin{aligned} \mathcal{G}_{mag} &= -\mu_0 M_s \left(\int_0^{\frac{M_s}{\chi_a}} \frac{\chi_a H_0}{M_s} z\, dH_0 + \int_{\frac{M_s}{\chi_a}}^{H_0} 1.z\, dH_0 + \int_0^{H_0} \frac{\chi_t H_0}{M_s}(1-z)\, dH_0 \right) \\ &= -\left(\mu_0 H_0 M_s - \frac{\mu_0 M_s^2}{2\chi_a} \right) z - \mu_0 \frac{\chi_t H_0^2}{2}(1-z) \end{aligned} \tag{3.28}$$

and finally for the last case

$$\begin{aligned} \mathcal{G}_{mag} &= -\mu_0 M_s \big(\int_0^{\frac{M_s}{\chi_a}} \frac{\chi_a H_0}{M_s} z\, dH_0 + \int_{\frac{M_s}{\chi_a}}^{H_0} 1.z\, dH_0 \\ &\quad + \int_0^{\frac{M_s}{\chi_t}} \frac{\chi_t H_0}{M_s}(1-z)\, dH_0 + \int_{\frac{M_s}{\chi_t}}^{H_0} (1-z) \big) \\ &= -\mu_0 M_s \left(H_0 - \frac{M_s z}{2\chi_a} - \frac{M_s(1-z)}{2\chi_t} \right) \end{aligned} \tag{3.29}$$

Equations (3.27), (3.28) and (3.29) will take part in the final Gibbs free energy.

3.4.5 Mechanical Energy

The mechanical work done by or on the material consists of 2 parts. The first part is the work done on the material to compress it elastically and the second part is the work done by the twinning strain in moving against the stress. If ε_e is the elastic strain, γz the twinning strain, σ the applied and E the young modulus of the material, we have for infinitesimal work

$$d\mathscr{W}_{mech} = -\sigma\, d\varepsilon_e + \gamma\, dz \tag{3.30}$$

If the constitutive equation between stress and elastic strain is linear i.e $\sigma = E\varepsilon_e$, we have as the mechanical energy density

$$\begin{aligned} \mathscr{W}_{mech}(\varepsilon_e, z) &= -\int_0^{\varepsilon_e} \sigma d\varepsilon_e + \int_0^z \sigma\gamma dz \\ &= -\frac{1}{2}E\varepsilon_e^2 + \sigma\gamma z \end{aligned} \tag{3.31}$$

The first term on the right of (3.31) represents the elastic deformation of the material while the second term is the work done by the rearrangement of the martensite (twinning). σ is the stress applied to the material. γ is the maximum deformation which can occur due to rearrangement of the martensite. It is typically taken as 0.06. Note that the elastic deformation is in opposition to the twinning rearrangement.

Since the elastic constant of the material is taken to be constant, the energy $\mathscr{W}_{mech}$ is equal to the co energy $\mathscr{W}^*_{mech}$.

$$\mathscr{W}^*_{mech}(\sigma, z) = -\frac{\sigma^2}{2E} + \sigma\gamma z \tag{3.32}$$

This is the expression that will take part in constructing the Gibbs energy where $\mathcal{G}_{mech} = -\mathscr{W}^*_{mech}$.

3.4.6 Gibbs Free Energy

The total Gibbs free energy can now be written

$$\mathcal{G}(H_0, \sigma, z) = \mathcal{G}_{mag} + \mathcal{G}_{mech} + K_{12}z(1-z) \tag{3.33}$$

The last term in the left hand side of (3.33) is a term, called interaction energy, which has been added to account for the interaction between the variants. This term was taken from previous work [16]. In later chapters, we will see how this term arises and give a proper explanation for its inclusion. Explicitly, the Gibbs free energy can now be written as

$$\begin{aligned} \mathcal{G}(H_0, z, \sigma) &= \sigma\gamma z - \frac{\sigma^2}{2E} + K_{12}z(1-z) \\ -\mu_0 M_s\Bigg[z&\left((2\alpha-1)H_0 - \frac{M_s}{2\chi_a}(2\alpha-1)^2\right) \\ &+(1-z)\left((\sin(\theta)H_0 - \frac{M_s}{2\chi_t}\sin^2(\theta)\right)\Bigg] \end{aligned} \tag{3.34}$$

From (3.34), the thermodynamic potential appropritate to z can then be found

$$\pi^z = -\frac{\partial \mathcal{G}}{\partial z} =$$
$$\sigma\gamma - K_{12}(1-2z) + \mu_0 Ms\left[(2\alpha-1)H_0 - \frac{M_s}{2\chi_a}(2\alpha-1)^2 - H_0\sin\theta + \frac{M_s}{2\chi_t}\sin^2\theta\right] \tag{3.35}$$

which can be reduced to

$$\pi^z = \sigma\gamma - K_{12}(1-2z) - \mu_0 M_s^2\left[\frac{(1-2\alpha)\sin\theta}{\chi_t} + \frac{(2\alpha-1)^2}{2\chi_a} + \frac{\sin^2\theta}{2\chi_t}\right] \tag{3.36}$$

π^z is the thermodynamic potential that dictates the evolution of z and carries the dissipation of the material.

3.5 Lumped Parameters Modelling of MSMA

The purpose of this section is to write the model in terms of lumped-parameter variables. Lumped-parameters are defined as follows: the electromagnetic fields are quasi-static and electrical terminal properties can be described as functions of a finite number of electrical variables [81].

In the last section, we derived the model of the MSMA element only in terms of field parameters such as M and H_0. For our purposes, we need to relate those parameters to lumped parameters such as current, i, and voltage, v as in a laboratory settings, these are the variables that can be measured. More specifically we need to study the effect of induced emf due to the element's change in length on the circuit parameters of the actuator.

From the MSMA constitutive relations derived above, we will find their lumped equivalent. Furthermore, instead of Gibbs free energy ($\mathcal{G}$), we will use energy (W) and co-energy(W^*) since we are assuming that our actuator will be working at constant temperature.

3.5.1 Terminal Variables

The lumped parameters of interest when magnetism is involved is the *flux linkage*, λ , the current, i and the induced emf, v_{ind} when the magnetic field changes. Consider the arrangement shown in figure 3.9. On application of a voltage to the terminals a and b, a magnetic flux Φ appears in the ferromagnetic core and the air-gap. From *Faraday's Law* it can be shown that the closed integral around the contour $a' - b'$ gives the induced emf [25, 82], v_{ind} as follows

$$v_{ind} = \oint_L E.dl = -N\frac{d\Phi}{dt} = -N\frac{d}{dt}\int_{S_t} B.dS_t \tag{3.37}$$

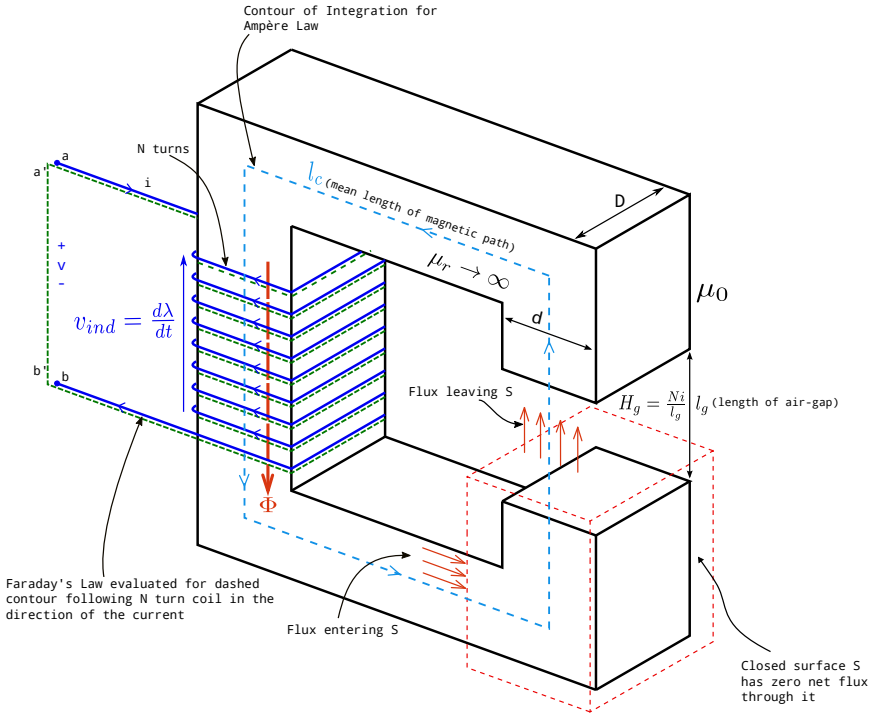

Figure 3.9

where E is the electric field and L is the contour $a' - b'$, S_t is the area spanned by 1 turn of the coil and B is the magnetic flux density produced by the current in the wire. Furthermore the total flux through any closed, S_c, is zero

$$\oint_{S_c} B.dS_c = 0 \tag{3.38}$$

Therefore, all the flux leaving the core, enters the air gap if we neglect leakage flux and fringing effect. Note in this case we have $S_t = S$ and thus we have $\Phi = SB$.

To calculate B, we need to find the magnetic field intensities H_c and H_l and then use the relationship $B = \mu_0 H_g$ for the air gap and $B = \mu_0 \mu_r H_c$ for the core. This can be achieved by using Ampere circuital law [25, 82] which is no more than $\nabla \times H = J_f$ in integral form

$$\oint_{l_c} H.dl = H_c.(l_c - l_g) + H_g.l_g = I_{total \quad enclosed} = Ni$$

The permeability μ_r of the core is usually very high for a ferromagnetic material and can be approximated by an infinite permeability. Then to keep the flux and the coil voltage constant, B has to be finite and H_c should be

zero.

$$\lim_{\mu_r \to \infty} = \mu_0 \mu_r H_c \implies \begin{cases} H_c & = 0 \\ B & finite \end{cases} \tag{3.39}$$

Then we have all the magnetic field intensity which appears across the air-gap and is given by

$$H_g = \frac{Ni}{l_g} \tag{3.40}$$

The magnetic flux density B is then given by

$$B = \mu_0 H_g = \mu_0 \frac{Ni}{l_g} \tag{3.41}$$

from which we can deduce Φ

$$\Phi = S.B = \frac{\mu_0 SNi}{l_g} \tag{3.42}$$

As Φ which is the flux for one loop cuts the coil N times, λ the magnetic flux linkage becomes

$$\lambda = N\Phi = \frac{\mu_0 SN^2 i}{l_g} \tag{3.43}$$

from which the inductance, L, of the circuit is found to be

$$L = \frac{\lambda}{i} = \frac{\mu_0 SN^2}{l_g} \tag{3.44}$$

As seen from equation (3.44), the inductance depends only on the geometry of the circuit and in this case is a constant. In the case that μ_r is not infinity, we have

$$\lambda = \frac{\mu_0 SN^2 i}{l_g(1 - \frac{1}{\mu_r}) + \frac{l_c}{\mu_r}} = Li \tag{3.45}$$

where $L = \frac{\mu_0 SN^2}{l_g(1-\frac{1}{\mu_r})+\frac{l_c}{\mu_r}}$. The dynamics of the system can then be written as

$$L\frac{di}{dt} = v - iR \tag{3.46}$$

where R is the resistance of the coil. The above development has shown how the field variables can be related to the lumped parameters. Furthermore, it has been seen that inductance is a property of the whole circuit and we cannot subdivide a magnetic circuit into separate inductances as was done in Chapter 2. Although in theory, the latter is a very valid way of modeling, physically calculating individual inductances is not possible. To palliate this shortcoming, instead of inductances, ***reluctances*** should be used.

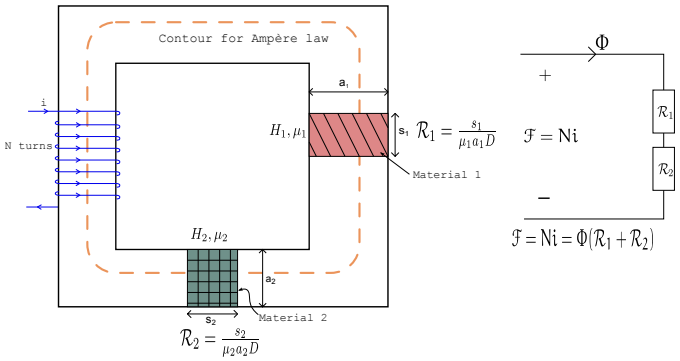

(a) Equivalent Series Circuit.

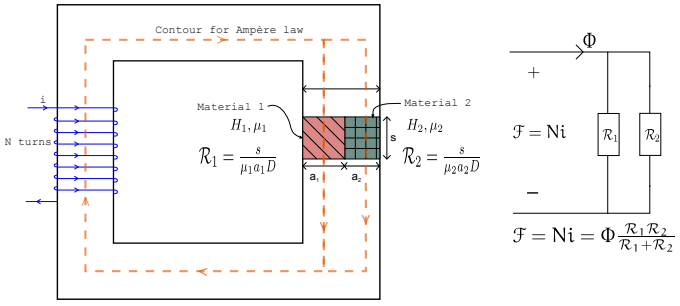

(b) Equivalent Parallel Circuit.

Figure 3.10: Magnetic Circuit with 2 different magnetic materials embedded in the core. The cross-sectional length is D.

3.5.2 Reluctances

Magnetic circuits can be taken as analogous to resistive electronic circuit if we define the magnetomotive force (MMF) $\mathscr{F}$ analogous to the voltage (EMF) as

$$\mathscr{F} = Ni \tag{3.47}$$

The flux then becomes analogous to the current of electronic circuits so that the magnetic analog of resistance is reluctance, $\mathscr{R}$ defined as

$$\mathscr{R} = \frac{\mathscr{F}}{\Phi} = \frac{N^2}{L} \tag{3.48}$$

The advantage of reluctances is that the rules of adding reluctances in series and parallel are the same as for a resistances in electric circuits. Figure 3.10 illustrates the concepts. For the iron core with infinite permeability with 2 finitely permeable material, the reluctance of each gap is given by

$$\mathscr{R}_1 = \frac{s_1}{\mu_1 a_1 D}, \qquad \mathscr{R}_2 = \frac{s_2}{\mu_2 a_2 D} \tag{3.49}$$

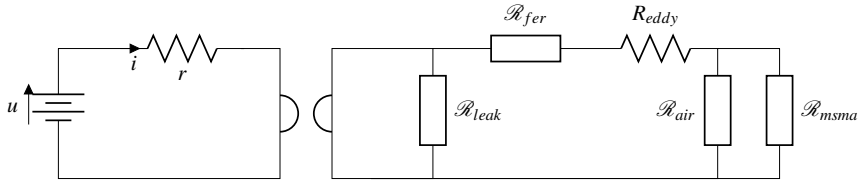

Figure 3.11: Reluctance model of the MSMA Actuator

so that the flux is

$$\Phi = \frac{\mathscr{F}}{\mathscr{R}_1 + \mathscr{R}_2} = \frac{Ni}{\mathscr{R}_1 + \mathscr{R}_2} \implies L = \frac{N\Phi}{i} = \frac{N^2}{\mathscr{R}_1 + \mathscr{R}_2} \tag{3.50}$$

Again we see that the inductance, L, depends on the whole circuit whereas the reluctances characterize the individual element.

We will later see that reluctances are more equivalent to capacitors when bond graph modeling is introduced. In the static case, reluctances can be treated as equivalent resistances without any major problems but this cannot be so in the dynamic case. The main reason is that reluctances are energy storing element (an air gap stores magnetic energy) whereas resistances dissipate energy. The more appropriate electronic circuit element analogous to reluctance is the *capacitor* or more precisely $\frac{1}{(Capacitor)}$.

Figure 3.11 shows the reluctance circuit of the MSMA. The electric circuit consist of the battery and the resistance of the coil, then between the electric circuit and the magnetic circuit there is a gyrator which transforms the current into an equivalent magnetomotive force and the voltage into an equivalent flux ϕ.

The reluctance of the air-gap, $\mathscr{R}_{fer}$, $\mathscr{R}_{gap}$, $\mathscr{R}_{msma}$ can be calculated knowing their geometries whereas $\mathscr{R}_{leak}$ should be measured.

Now having the necessary tool to model electric and magnetic circuit, we proceed to find the MSMA lumped parameters.

3.5.3 MSMA Actuator lumped Parameters

In this section, we will use the theory developed previously to write the lumped parameters of the MSMA actuator. Consider a MSMA sample in a magnetic field H_0 as in Fig 3.12. The sample length is l, its width is a and its depth is d. It is located in air gap of same width and depth but of different length w. In deriving the constitutive equations, as a first approximation we will consider that the change in length of the MSMA is negligible i.e the air gap remains constant. We will use the magnetization M and the equation $B = \mu_0(H_0 + M)$ to find the flux ,Φ. Then we will write the energy and co-energy of the magnetic part of the actuator. This will be useful for the port-Hamiltonian model.

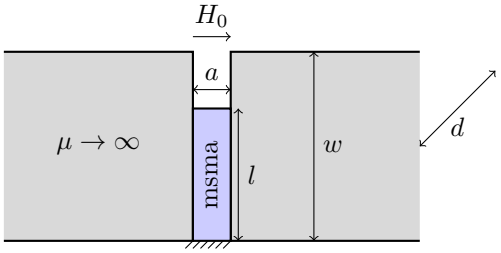

Figure 3.12: MSMA in Air Gap

Magnetization to Flux

From (3.19), the magnetisation of the material is given as :

$$\frac{\partial \mathcal{G}}{\partial H_0} = \mu_0 M = \mu_0 M_s\big((2\alpha - 1)z + sin(\theta)(1 - z)\big) \tag{3.51}$$

where $\alpha = \frac{\chi_a H_0}{2Ms} + \frac{1}{2}$ and $sin(\theta) = \frac{\chi_t H_0}{Ms}$ are the internal variables representing weiss domain and z is the volume fraction of variant $M2$.

The three cases to be considered are $(\alpha < 1, \theta < \frac{\pi}{2})$, $(\alpha = 1, \theta < \frac{\pi}{2})$ and $(\alpha = 1, \theta = \frac{\pi}{2})$. The magnetisation equation (3.51) then becomes:

$$M = \begin{cases} M_s\big((2\alpha - 1)z + sin(\theta)(1 - z)\big), & \text{if } (\alpha < 1, \theta < \frac{\pi}{2}) \\ M_s\big(z + sin(\theta)(1 - z)\big), & \text{if } (\alpha = 1, \theta < \frac{\pi}{2}) \\ M_s, & \text{if } (\alpha = 1, \theta = \frac{\pi}{2}) \end{cases} \tag{3.52}$$

Also from electromagnetic theory,

$$B = \mu_0(M + H_0) \tag{3.53}$$

Hence in terms of B, (3.52) becomes :

$$B = \begin{cases} \mu_0\big(\chi_a H_0 z + \chi_t H_0(1 - z)\big) + \mu_0 H_0, & \text{if } (\alpha < 1, \theta < \frac{\pi}{2}) \\ \mu_0 M_s z + \mu_0 H_0(\chi_t(1 - z) + 1), & \text{if } (\alpha = 1, \theta < \frac{\pi}{2}) \\ \mu_0 M_s + \mu_0 H_0, & \text{if } (\alpha = 1, \theta = \frac{\pi}{2}) \end{cases} \tag{3.54}$$

Since we are assuming that the permeability of the core generating the field in the air gap is infinite, all the magnetic field appears in the air gap. And if it is generated from a solenoid containing N turns and in which a current of i amperes is flowing, then it is given as:

$$H_0 = \frac{Ni}{a} \tag{3.55}$$

where a is the width of the air gap (see Fig 3.12).

Substituting (3.55) into (3.54), we obtain:

$$B = \begin{cases} \mu_0\big(\chi_a z + \chi_t(1 - z) + 1\big)\frac{Ni}{a}, & \text{if } (\alpha < 1, \theta < \frac{\pi}{2}) \\ \mu_0 M_s z + \mu_0 \frac{Ni}{a}(\chi_t(1 - z) + 1), & \text{if } (\alpha = 1, \theta < \frac{\pi}{2}) \\ \mu_0 M_s + \mu_0 \frac{Ni}{a}, & \text{if } (\alpha = 1, \theta = \frac{\pi}{2}) \end{cases} \tag{3.56}$$

Having B we can relate it to the flux, ϕ_{msma}, which passes through the MSMA.

$$\phi_{msma} = AB = ldB \tag{3.57}$$

where , $A = l \times d$ is the cross sectional area of the MSMA. Hence (3.57) can be writted as:

$$\phi_{msma} = \begin{cases} \frac{Ni\mu_0 ld}{a}\big(\chi_a z + \chi_t(1-z)+1\big), & \text{if } (\alpha < 1, \theta < \frac{\pi}{2}) \\ \mu_0 M_s zld + \frac{Nild\mu_0}{a}(\chi_t(1-z)+1), & \text{if } (\alpha = 1, \theta < \frac{\pi}{2}) \\ \mu_0 M_s ld + \frac{Nild\mu_0}{a}, & \text{if } (\alpha = 1, \theta = \frac{\pi}{2}) \end{cases} \tag{3.58}$$

Constitutive Relations

Relations in the electrical domain can be derived as follows. The electrical part and magnetic part should be treated as a whole. Since the current i across the MSMA does not quite have a meaning, to derive the equations, we need to consider the whole circuit generating the H field. Then only we can relate the current i flowing in the solenoid to λ, the total flux linkage.

The net flux flowing in the circuit is given by

$$\begin{aligned} \phi =& \phi_{air} + \phi_{msma} \\ =& \frac{Ni(w-l)d\mu_0}{a} + \frac{Ni\mu_0 ld}{a}\big(\chi_a z + \chi_t(1-z)+1\big) \end{aligned} \tag{3.59}$$

We know from electric circuits that

$$\lambda = N\phi \tag{3.60}$$

Therefore our 3 piecewise continous equations (3.61) becomes:

$$\lambda = \begin{cases} \frac{N^2 i(w-l)d\mu_0}{a} + \frac{N^2 i\mu_0 ld}{a}\big(\chi_a z + \chi_t(1-z)+1\big), & \text{if } (\alpha < 1, \theta < \frac{\pi}{2}) \\ \frac{N^2 i(w-l)d\mu_0}{a} + N\mu_0 M_s zld + \frac{N^2 ild\mu_0}{a}(\chi_t(1-z)+1), & \text{if } (\alpha = 1, \theta < \frac{\pi}{2}) \\ \frac{N^2 i(w-l)d\mu_0}{a} + N\mu_0 M_s ld + \frac{N^2 ild\mu_0}{a}, & \text{if } (\alpha = 1, \theta = \frac{\pi}{2}) \end{cases} \tag{3.61}$$

which can be reduced to

$$\lambda = \begin{cases} \frac{N^2 i(w)d\mu_0}{a} + \frac{N^2 i\mu_0 ld}{a}\big(\chi_a z + \chi_t(1-z)\big), & \text{if } (\alpha < 1, \theta < \frac{\pi}{2}) \\ \frac{N^2 i(w)d\mu_0}{a} + N\mu_0 M_s zld + \frac{N^2 ild\mu_0}{a}(\chi_t(1-z)), & \text{if } (\alpha = 1, \theta < \frac{\pi}{2}) \\ \frac{N^2 i(w)d\mu_0}{a} + N\mu_0 M_s ld, & \text{if } (\alpha = 1, \theta = \frac{\pi}{2}) \end{cases} \tag{3.62}$$

Taking $K_0 = \frac{N^2(w)d\mu_0}{a}$, $K_1 = \frac{N^2(l)d\mu_0}{a}$ and $K_2 = N\mu_0 M_s ld$ further simplification is possible.

$$\lambda = \begin{cases} K_0 i + K_1 i\big(\chi_a z + \chi_t(1-z)\big), & \text{if } (\alpha < 1, \theta < \frac{\pi}{2}) \\ K_0 i + K_2 z + K_1 i(\chi_t(1-z)), & \text{if } (\alpha = 1, \theta < \frac{\pi}{2}) \\ K_0 i + K_2, & \text{if } (\alpha = 1, \theta = \frac{\pi}{2}) \end{cases} \tag{3.63}$$

Table 3.1: Values used for simulation

N	w	l	a	d	χ_a	χ_t
1200	25 mm	20mm	3mm	5mm	4	0.82

Equation (3.63) being invertible, we can now write the current, i, in terms of the λ. This will prove useful in writing the energy equation.

$$i = \begin{cases} \frac{\lambda}{K_0+K_1(\chi_a z+\chi_t z(1-z))}, & \text{if } (\alpha < 1, \theta < \frac{\pi}{2}) \\ \frac{\lambda-K_2 z}{K_0+K_1(\chi_t(1-z))}, & \text{if } (\alpha = 1, \theta < \frac{\pi}{2}) \\ \frac{\lambda-K_2}{K_0}, & \text{if } (\alpha = 1, \theta = \frac{\pi}{2}) \end{cases} \tag{3.64}$$

Figure 3.13 shows the graph of the constitutive equations for different values of z. The figure was obtained using values shown in Table 3.1. These values are very close to the circuit values. The two saturation values $\alpha = 1$ and $\theta = \frac{pi}{2}$ are clearly seen. One difference to be noted with the magnetization curve of figure 3.7 is that no plateau of saturation exists. This is because of the air-gap present which never saturates. Finally, in deriving the equation, it was assumed that the air-gap is not affected by the change in length of the MSMA. This proved to be a valid assumption as seen from Figure 3.14. It is seen that very little change occurs due to this change in length. The deformation of the MSMA is related to z. At $z = 1$, the deformation is around 6%. This has been taken into consideration to produce these results.

3.5.4 Energy Considerations

As has been done for the case of the local parameters, we derived a thermodynamics force, π^z, which gives the evolution of z, we will in this section derive the same driving force in terms of the lumped parameters. For such a purpose we will apply energy relations which is common for systems where there is a coupling between different domains.

It has been shown that the electrical terminal relations are in the form expressed by

$$\lambda = \lambda(i, z) \tag{3.65}$$

Applying a force on the MSMA results in a change in "inductance" and hence in the magnetic energy stored. We can now make an assumption that the lumped driving force, f^{mag} of magnetic origin which does work also depends on

$$f^{mag} = f^{mag}(i, z) \tag{3.66}$$

Then if the total magnetic energy stored by the *system* is denoted by W_{mag}, we can write

$$id\lambda = dW_{mag} + f^{mag}dz \tag{3.67}$$

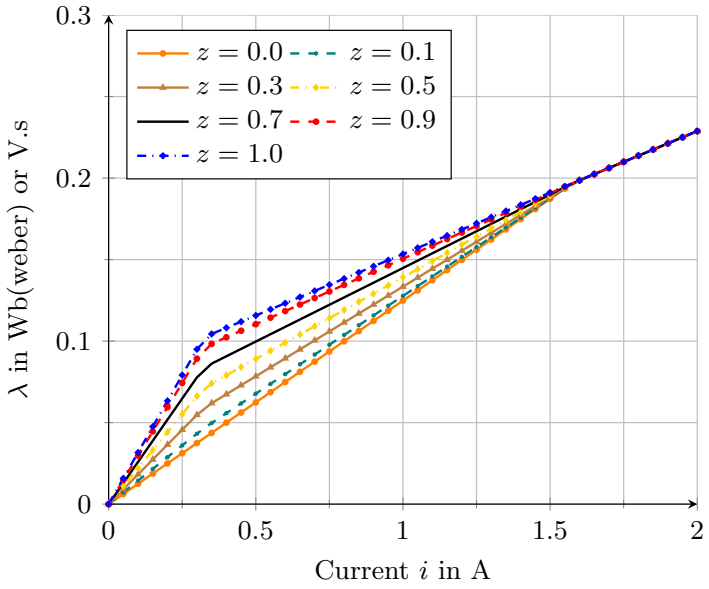

Figure 3.13: Constitutive Equations between total magnetic flux λ and i for the actuator. The curves are shown for the different values of z.

Equation (3.67) states that the work done by the electric circuit is either stored as magnetic energy (in case the MSMA is blocked) or can be used to do work. The evaluation of the change in W_{mag} when λ or z is varied is given by the integration of (3.67). This is a line integration through the variable space (λ, z). These two variables are the independent variables i.e they can be varied independently of each other. Suppose we want to find the change in stored energy when the independent variables change from (λ_a, z_a) to (λ_b, z_b). Figure 3.15 shows the possible paths in the variable space. Thus using path C, we have

$$W_{mag}(\lambda_b, z_b) - W_{mag}(\lambda_a, z_a) = -\int_{z_a}^{z_b} f^{mag}(\lambda_a, z)dz + \int_{\lambda_a}^{\lambda_b} i(\lambda, z_b) \quad (3.68)$$

One property of conservative systems is that the energy does not depend on the path taken. It is a state function. Our system though being dissipative in nature, we can divide it in a conservative part and a dissipative part. The dissipative part will be added later. Hence if we take the conservative part, we can choose any path which makes the integration easier. One commonly used method [81] is to assemble the system mechanically keeping $d\lambda = 0$, then no force is required to overcome forces of magnetic origin hence $f^{mag} = 0$. Then, we put the energy through the electrical ports by keeping the geometry fixed ($dz = 0$). We then have all the energy accounted for only by

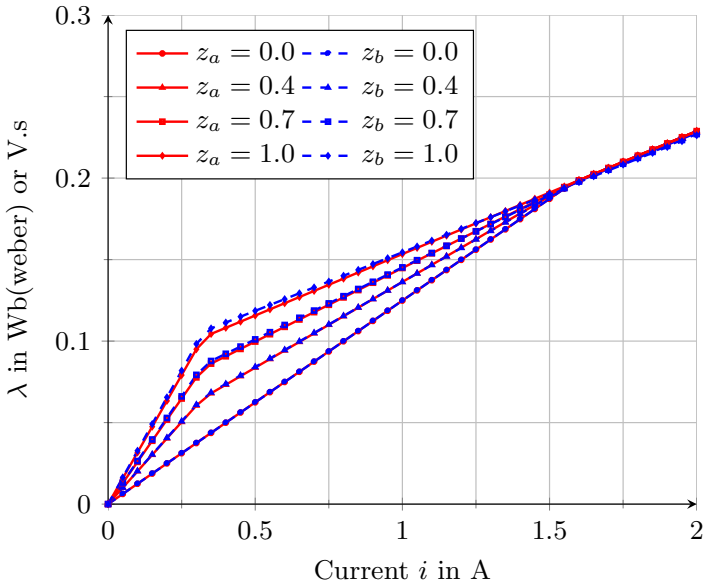

Figure 3.14: Comparaison of constitutive equations taking into account change in length of air-gap, w, as well as change in length of MSMA, l. Dashed lines show the constitutive equations when the changes in length are taken into consideration while Solid lines show the equations when the changes are assumed negligible.

the electrical part. So W_{mag} is then given by

$$W_{mag} = \int_0^{\lambda} i(\lambda, z) d\lambda \tag{3.69}$$

As W_{mag} is a function of the two independent variables λ and z

$$W_{mag} = W_{mag}(\lambda, z) \tag{3.70}$$

its total differential is

$$dW_{mag} = \frac{\partial W_{mag}}{\partial \lambda} d\lambda + \frac{\partial W_{mag}}{\partial z} dz \tag{3.71}$$

From (3.67) and (3.71) we have

$$0 = \left(i - \frac{\partial W_{mag}}{\partial \lambda}\right) d\lambda - \left(f^{mag} + \frac{\partial W_{mag}}{\partial z}\right) dz \tag{3.72}$$

This from (3.72), we have

$$i = \frac{\partial W_{mag}}{\partial \lambda}$$
$$f^{mag} = -\frac{\partial W_{mag}}{\partial z}$$

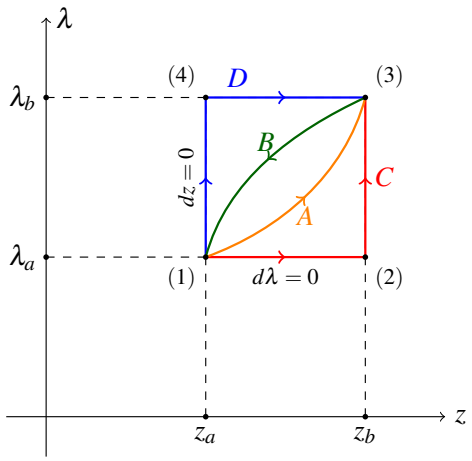

Figure 3.15: Variable Space.

Sometimes instead of the energy, it is easier to work with the co-energy, $W^*_{mag}(i,z)$. One of the reason is because the constitutive relationships are easier in one sense than the other. For our case, the $\lambda(i)$ relationship is easier to work with rather than the $i(\lambda)$. Another reason is that the co-energy variables in a particular system are the independent variables rather than the energy variables. Such transformations are very common in thermodynamics where the co-energies are given different names such as Gibbs, Helmholtz etc.. The co-energy is obtained from a Legendre transformation such as

$$W^*_{mag}(i,z) = i\lambda - W_{mag}(\lambda,z) \tag{3.73}$$

Using the co-energy, then the force of magnetic origin is given by

$$f^{mag} = \frac{\partial W^*_{mag}}{\partial z} \tag{3.74}$$

To construct the energy and co-energy using a path where the system is assembled mechanically first i.e all the energy input to the system is accounted by the electrical part only, we have to integrate the constitutive equations (3.64) and (3.63) taking into account the piecewise continuous nature of these equations. We will now derive in detail the co-energy functional and then for the energy functional and the associated driving force for z, the reader is referred to Table 3.2.

Taking into account the saturation, the corresponding current, i_α for $\alpha = 1$, using equations (3.15) and (3.54), becomes

$$i_\alpha = \frac{M_s a}{N\chi_a} \tag{3.75}$$

and for $\theta = \frac{\pi}{2}$, the corresponding saturation current, i_θ is

$$i_\theta = \frac{M_s a}{N\chi_t} \tag{3.76}$$

The co-energy $W^*_{mag}(i,z)$ is given by

$$W^*_{mag}(i,z) = \int_0^i \lambda di \tag{3.77}$$

Then for $i < \frac{M_s a}{N\chi_a}$

$$W^*_{mag} = \int_0^i (K_0 i + K_1 i\big(\chi_a z + \chi_t(1-z)\big))di \tag{3.78}$$

$$= \frac{1}{2}\left(K_1\chi_a z + K_1\chi_t\left(1-z\right) + K_0\right) i^2 \tag{3.79}$$

for $\frac{M_s a}{N\chi_a} < i < \frac{M_s a}{N\chi_t}$

$$\begin{aligned} W^*_{mag} &= \int_0^{\frac{M_s a}{\chi_a}} (K_1\chi_a z i)di + \int_{\frac{M_s a}{N\chi_a}}^i (K_2 z) + \int_0^i (K_0 i + K_1 i\chi_t(1-z))di \\ &= \frac{1}{2}\frac{K_1 z {M_s}^2 a^2}{\chi_a N^2} + K_2 z\left(i - \frac{M_s a}{N\chi_a}\right) + \frac{1}{2}\left(K_1\chi_t\left(1-z\right) + k_0\right) i^2 \end{aligned} \tag{3.80}$$

and finally for $i > \frac{M_s a}{N\chi_t}$

$$\begin{aligned} W^*_{mag} &= \int_0^{\frac{M_s a}{\chi_a}} \left(K_1\chi_a z i\right) di + \int_{\frac{M_s a}{N\chi_a}}^i \left(K_2 z\right) di \\ &+ \int_0^{\frac{M_s a}{N\chi_t}} \left(K_1 i\chi_t(1-z)\right) di + \int_{\frac{M_s a}{N\chi_t}}^i \left(K_2(1-z)\right) di + \int_0^i K_0 i\, di \\ &= \frac{1}{2}\frac{K_1 z {M_s}^2 a^2}{\chi_a N^2} + K_2 z\left(i - \frac{M_s a}{N\chi_a}\right) \\ &+ \frac{1}{2}\frac{K_1\left(1-z\right){M_s}^2 a^2}{\chi_t N^2} + K_2\left(1-z\right)\left(i - \frac{M_s a}{\chi_t N}\right) + \frac{1}{2}K_0 i^2 \end{aligned} \tag{3.81}$$

The above development is also carried out for the energy function $W_{mag}(\lambda, z)$ and then the driving force,f^{mag} is given by

$$f^{mag} = -\frac{\partial W_{mag}}{\partial z} = \frac{\partial W^*_{mag}}{\partial z} \tag{3.82}$$

The resulting equations are presented in Table 3.2 which shows that f^{mag} depends only on the current but is a function of both λ and z. Using the values from Table 3.1 and the driving force equations from Table 3.2, Fig. 3.16 shows how f^{mag} varies with current and Fig. 3.17 shows the same dependance on λ and z. In both cases, the same driving force is observed for whatever values of z as expected.

Table 3.2: Energy Relation

	Energy	*Co-Energy*
Conservation of Energy	$dW = id\lambda - fdz$	$dW^* = \lambda di + fdz$
Constitutive Equations	$i = \begin{cases} \frac{\lambda}{K_0+K_1(\chi_a z+\chi_t z(1-z))}, & (\alpha<1,\theta<\frac{\pi}{2}) \\ \frac{\lambda-K_2 z}{K_0+K_1(\chi_t(1-z))}, & (\alpha=1,\theta<\frac{\pi}{2}) \\ \frac{\lambda-K_2}{K_0}, & (\alpha=1,\theta=\frac{\pi}{2}) \end{cases}$	$\lambda = \begin{cases} K_0 i + K_1 i\big(\chi_a z + \chi_t(1-z)\big), & (\alpha<1,\theta<\frac{\pi}{2}) \\ K_0 i + K_2 z + K_1 i(\chi_t(1-z)), & (\alpha=1,\theta<\frac{\pi}{2}) \\ K_0 i + K_2, & (\alpha=1,\theta=\frac{\pi}{2}) \end{cases}$
Energy Relation	$W_{mag}(\lambda,z) = \begin{cases} \frac{1}{2}\frac{\lambda^2}{K_0+K_1(\chi_a z+\chi_t(1-z)}, & (\alpha<1,\theta<\frac{\pi}{2}) \\ \frac{1}{2}i_\alpha C_1 + \frac{\lambda^2-2K_2 z\lambda}{2C_2} - \frac{C_1^2-2K_2 zC_1}{2C2}, & (\alpha=1,\theta<\frac{\pi}{2}) \\ \frac{1}{2}i_\alpha C_1 + \frac{C_3^2-2K_2 zC_3}{2C_2} - \frac{C_1^2-2K_2 zC_1}{2C2} + \frac{\lambda-K2}{K_0} - \frac{C_3-K_2}{K_0}, & (\alpha=1,\theta=\frac{\pi}{2}) \end{cases}$	
Co-Energy Relation		$W^*_{mag}(i,z) = \begin{cases} \frac{1}{2}(K_1\chi_a z + K_1\chi_t(1-z)+K_0)i^2, & (\alpha<1,\theta<\frac{\pi}{2}) \\ \frac{K_1 z M_s^2 a^2}{2\chi_a N^2} + K_2 z\big(i - \frac{M_s a}{N\chi_a}\big) + \frac{1}{2}(K_1\chi_t(1-z)+K_0)i^2, & (\alpha<1,\theta<\frac{\pi}{2}) \\ \big(\frac{1}{2}\frac{K_1 M_s^2 a^2}{N^2} - \frac{K_2 M_s a}{N}\big)\big(\frac{z}{\chi_a} + \frac{(1-z)}{\chi_t}\big) + K_2 i + \frac{1}{2}K_0 i^2, & (\alpha=1,\theta=\frac{\pi}{2}) \end{cases}$
Force Relation	$-\frac{\partial W_{mag}}{\partial z} = \begin{cases} \frac{1}{2}\frac{\lambda^2(K_1(\chi_a-\chi_t))}{(K_0+K_1(\chi_a z+\chi_t(1-z)))^2}, & (\alpha<1,\theta<\frac{\pi}{2}) \\ \frac{i_\alpha C_1'}{2} - \frac{K_2\lambda}{C_2} - \frac{K_2\lambda z C_2'}{C_2^2} - \frac{2C_1C_1'}{C_2} - \frac{C_1^2C_2'}{C_2^2} + \frac{2K_2C_1}{C_2} + \frac{K_2 zC_1'}{C2} + \frac{K_2 zC_1C_2'}{C_2^2}, & (\alpha=1,\theta<\frac{\pi}{2}) \\ , & (\alpha=1,\theta=\frac{\pi}{2}) \end{cases}$	
		$\frac{\partial W^*_{mag}}{\partial z} = \begin{cases} \frac{1}{2}K_1(\chi_a-\chi_t)i^2, & (\alpha<1,\theta<\frac{\pi}{2}) \\ \frac{K_1 M_s^2 a^2}{2\chi_a N^2} + K_2\big(i - \frac{M_s a}{N\chi_a}\big) - \frac{1}{2}K_1\chi_t i^2, & (\alpha<1,\theta<\frac{\pi}{2}) \\ \big(\frac{1}{2}\frac{K_1 M_s^2 a^2}{N^2} - \frac{K_2 M_s a}{N}\big)\big(\frac{1}{\chi_a} - \frac{1}{\chi_t}\big), & (\alpha=1,\theta=\frac{\pi}{2}) \end{cases}$
Constants	$C_1 = i_\alpha K_1(\chi_a z + \chi_t(1-z))$, $C_2 = K_0 + K_1\chi_t(1-z)$, $C_3 = K_0 i_\theta + K_2 z + K_1 i_\theta \chi_t(1-z)$ $i_\alpha = \frac{M_s a}{N\chi_a}$, $i_\theta = \frac{M_s a}{N\chi_t}$	

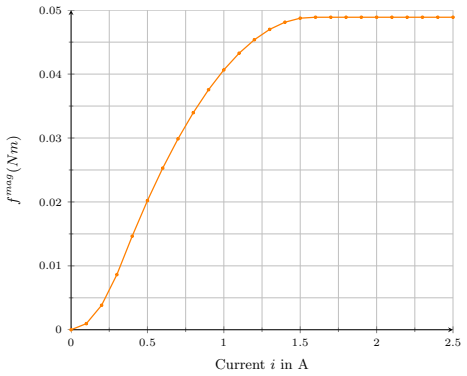

Figure 3.16: Driving force f^{mag} derived from co-energy, W^*_{mag}.

The other mechanism which drives the reorientation of martensite in MSMA is the stress applied to the material. And when subjected to both a magnetic field and a stress, the thermodynamic driving force, f^{tot}, is given by

$$f^{tot} = f^{mag} + f^{mech} \tag{3.83}$$

where f^{mech} is the driving force due to the mechanical stress.

The infinitesimal lumped parameter mechanical work consists of the work done by the twinning displacement $\gamma z l$ and the elastic displacement $x_e = \varepsilon_e l$. If the force acting on the material is F_{ext} (in the case of our actuator its mg) and the material spring constant (lumped Young modulus) is k, then the infinitesimal work is

$$dW_{mec} = \int_0^{x_e} F_{ext}\, dx_e + \int_0^{z} F_{ext}\gamma l\, dz \tag{3.84}$$

Integrating yields

$$W_{mec} = \frac{1}{2}kx_e^2 + F_{ext}\gamma l z \tag{3.85}$$

and the mechanical co-energy is given by

$$W^*_{mec} = \frac{1}{2}\frac{F_{ext}^2}{k} + F\gamma l z \tag{3.86}$$

The total strain x_t is then given by

$$x_t = \frac{\partial W^*_{mec}}{\partial F_{ext}} = \frac{F_{ext}}{k} + \gamma l z = x_e + \gamma z l \tag{3.87}$$

while f^{mech}, the thermodynamics driving force due to the mechanical energy is

$$f^{mech} = \frac{\partial W^*_{mec}}{\partial z} = F_{ext}\gamma l \tag{3.88}$$

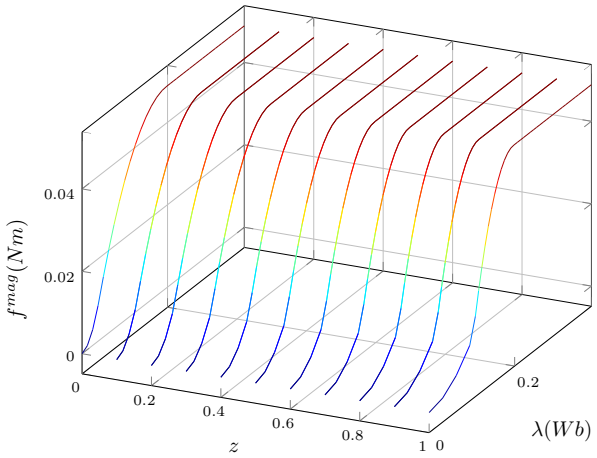

Figure 3.17: Driving force f^{mag} derived from energy, W_{mag}.

Finally as in the thermodynamics case, the total energy is given by

$$W(x_e, z, \lambda) = W_{mag} + W_{mec} \tag{3.89}$$

and the driving force, f^z is given by

$$f^{tot} z = \frac{\partial W_{mag}}{\partial z} + \frac{\partial W_{mech}}{\partial z} \tag{3.90}$$

And finally if to be coherent with the thesis of Gauthier [16], we add the term called interaction energy which gives

$$f^{tot} z = \frac{\partial W_{mag}}{\partial z} + \frac{\partial W_{mech}}{\partial z} + K_{12}(1 - 2z) \tag{3.91}$$

3.6 Discussion

In this chapter, we used thermodynamics to model the material. Thermodynamics being quite universal, from its premises we were able to derive two very important constitutive relations. The first is the driving force which dictates the evolution of the internal variable z and the second was to obtain the relation between the total strain x_t from the elastic and twinning strain.

In the distributed parameter section, we used thermodynamics free energies (Gibbs) to get to the driving force while in the lumped parameter section, we employed a more classical view. What we have called energy and denoted W in the lumped parameter part is actually the Helmholtz free energy, F. The Helmholtz free energy is actually $F = U - TS$ and it gives the available energy at constant temperature.

Hence in the port Hamiltonian modelling for electric circuits, mechanical circuits where temperature and entropy are neglected, we are actually using the Helmholtz free energy.

Truly speaking if a strict view of energy is to be adopted as the ability to produce heat and/or work, we should always include entropy as it is a natural variable for internal energy.

Secondly we have shown that employing co-energies sometimes result in easier derivation of relationship between generalised forces and generalised coordinates. In any energetic framework, both energy and co-energy should be employed consistently as one representation may give better insight or simpler results than the other.

Furthermore, this chapter has given an explicit form of the magnetic and mechanical energy and their derivation in terms of the lumped parameters, something that was missing in [16] and in general literature. Thus we can now embark to derive the port Hamiltonian equation of the actuator where these energies will play a central part. We will also give an explanation in the next chapter as to where the term $K_{12}(1-2z)$ associated with interaction energy comes from.

Chapter 4

Bond Graph Modeling

Contents

4.1 Introduction 69
4.2 Network Modelling 70
4.3 Energy flow in Bond Graph 71
4.3.1 The inductive element 72
4.3.2 The capacitive element 73
4.3.3 The resistive element 73
4.4 Bond Graphs 74
4.4.1 Junctions 74
4.4.2 Transformers and Gyrators 76
4.4.3 Causality 77
4.4.4 Bond Graph Examples 80
4.5 MSMA Actuator Bond Graph 83
4.5.1 Electric/Magnetic Subsystem Bond Graph 83
4.5.2 Mechanical subsystem Bond Graph 85
4.5.3 MSMA subsystem Bond Graph 87
4.5.4 Hysteresis in MSMA 90
4.6 Discussion 95

4.1 Introduction

In the last chapter, we have used thermodynamics to derive the constitutive equation regarding the internal variable z. Unfortunately though powerful, thermodynamics has its limitations. It deals only with initial and final states of a system. It provides no information about the dynamical behaviour between these 2 states. As stated by Oster et al. [54]: Thermodynamics tells us where we have been and where we are, but not how we got there.

To be able to control the MSMA actuator, it is important to know the entire dynamical trajectory. The bond graph approach provides a very systematic way to derive the mathematical model. Not only does it provide to derive the equations but it also helps visualise the flow of power in the system. The energy conversions and different couplings that exist between domains is easily discernible much unlike the 2 models in chapter 2 where it was impossible to see how the electrical energy of the actuator was converted to mechanical energy. Finally, it reveals one other very important feature of the actuator-its topology. Topology of a circuit refers to the way different elements are connected. The interconnection of these elements impose a set of constraints on the system which further determines the system behaviour.

Oster and Desoer [55] states that there are 2 underlying structures to most physical models-one topological and one dynamic. The port Hamiltonian framework just employs such a representation. It separates the constitutive equations ('dynamic') from the interconnection ('topological') and it is very closely related to the bond graph methodology as both uses energy as a central theme.

4.2 Network Modelling

To model simple systems consisting entirely of mechanical or electrical domain, it is sufficient to use the traditional methods such as Newton laws for mechanical systems or Kirchhoff current/voltage laws for electrical systems. For more complicated systems, Lagrangian or Hamiltonian formalism can be used and they usually yield very good results.

But unfortunately for systems consisting of a large number of such elements the amount of equations can rapidly grow very large.

Linear graph theory or network graphs has been widely used [39] in electrical circuit analysis to analyze and establish their properties. This approach first models the topology of the circuit without regards to any particular element and then afterward only the circuit elements are taken into consideration to derive the dynamical equations using *through* and *across* variables.

Bond Graphs, invented by Paynter [56], is another systematic approach widely used to derive system equations. Using *effort* and *flow* variables, it models in a graphical way the power exchange between elements in a systems. While linear graphs has a sound mathematical basis, bond graph does not possess such a rich mathematical background even though attempts have been made in [3, 2, 4].

Other methods such as behavioral modeling proposed by Willems [80] is a very powerful method but it is mathematically very demanding.

These methods have the advantage that unlike an input/output (i/o) representation, the system description is viewed as a constraint on a set of

variables and systems are connected without any i/o assignment beforehand. State space description is derived from basic system representation only after having decided on the inputs and the outputs.

The different types of modelling described above relies in one way or the other on Kirchoff's current law (KCL) and Kirchoff's voltage law. They apply very well to lumped systems. Using both Kirchoff's laws, implies Tellegen theorem which is a purely topological results but applied to a physical system, it means that energy is conserved. Furthermore KCL and KVL which are proper to electric circuits also have their corresponding counterparts in other domains. Any conservation law (conservation of charge, conservation of momentum, conservation of matter or conservation of energy) is a KCL statement more generally known as an equation of continuity whereas a KVL statement more generally known as an equation of compatibility is a kind of uniqueness condition or constraint such as geometrical constraint in mechanical systems (equal position and by extension velocities at same points) or same electrical potential at same point etc [66].

A rapid review of bond graphs will follow in the following sections before deriving the MSMA actuator dynamic model.

4.3 Energy flow in Bond Graph

A set of primitive elements which form the building blocks for the construction of dynamic models for physical systems may be defined from energy flows within the system, and between the system and its environment. The principle of conservation of energy provides a fundamental basis for characterizing such elements.

Basically there are 4 types of elements, two energy storage elements, one dissipative element and source elements.

Example of source elements in the electrical domain would be a current source or a voltage source whereas in the mechanical domain it would be a velocity source such as a cam or a force source.

The dissipative element in electrical domain would be a resistor whereas in mechanical domain it would be a damper.

The 2 different energy storage are related to the type of energy they store. In mechanical domain, there exists the kinetic energy and the potential energy whereas in the electrical domain we can distinguish between electric energy (energy stored in a capacitor due to charges) and magnetic energy (energy stored in an inductor).

From the law of conservation of energy, the change in energy, ΔE, is equal to the work done ,ΔW, by or on the system and the heat exchanged, ΔQ. Namely the power flow in any branch is given by

$$\mathcal{P}(t) = \underbrace{effort}_{e} \times \underbrace{flow}_{f} = \underbrace{v \times i}_{electrical} = \underbrace{F \times v}_{mechanical} \tag{4.1}$$

Furthermore two additional useful variables can be defined called *generalized momenta*, p, which is the integral of the effort variable and, q, the *generalized displacement* which is the integral of the flow variable as shown by equation (4.2).

$$\begin{aligned} p(t) =& p(t_0) + \int_0^t e(\tau)\, d\tau \qquad \text{or} \qquad dp = e\, dt \\ q(t) =& q(t_0) + \int_0^t f(\tau)\, d\tau \qquad \text{or} \qquad dq = f\, dt \end{aligned} \tag{4.2}$$

These 2 variables are called the energy variables. The relationship between the energy variables and their power counterpart (e, f) is what gives and dictates the dynamics of any system. Also, the change in internal energy of a system in a time, dt can be written as

$$\boxed{\begin{array}{llll} \Delta U = & e(fdt) & = edq & \Delta(\text{Potential or Electrical Energy}) = \Delta W \\ \Delta U = & f(edt) & = fdp & \Delta(\text{Kinetic or Magnetic Energy}) = \Delta W \\ \Delta U = & (ef)dt & = (fe)dt & (\text{Dissipation}) = \Delta Q \end{array}} \tag{4.3}$$

The first 2 equations of (4.3) are energy which can be stored and retrieved later whereas the third one is energy loss as heat. Nonetheless, they suggest that 3 types of elements are responsible for energy exchange or conversion.

4.3.1 The inductive element

The inductive element or "I"-element is an energy storing device which is characterized by a static relationship between flow f and generalized momentum p. The constitutive equation is given by

$$p = p(f) \tag{4.4}$$

For an inductor, the flux linkage (generalized momentum), λ, in the linear case is given by

$$\lambda = Li \tag{4.5}$$

The relationship between the flow (current, i) and the effort (voltage, v) variable is given by

$$\begin{aligned} \frac{d\lambda}{dt} &= L\frac{di}{dt} \\ v &= L\frac{di}{dt} \end{aligned}$$

and the energy stored in the inductor is

$$\mathcal{E} = \int_0^\lambda i d\lambda = \frac{1}{2L}\lambda^2 \tag{4.6}$$

while the co-energy is given by

$$\mathcal{E}^* = \int_0^i \lambda di = \frac{1}{2} L i^2 \tag{4.7}$$

A clear distinction will always be made between energy and co-energy as they are equal in the linear case but for the non-linear case, they are not.

4.3.2 The capacitive element

The capacitive element is one in which there is a static relationship between the generalized displacement and the effort variable.

$$q = q(e) \tag{4.8}$$

In a capacitor, the charge, q, is a generalized displacement variable and the effort variable is the voltage v across the plates. In a linear capacitor,

$$q = Cv \tag{4.9}$$

C is termed the capacitance.

In a similar fashion to the inductor, the energy and co-energy are given by:

$$\mathcal{E} = \int_0^q v dq = \frac{1}{2C} q^2$$
$$\mathcal{E}^* = \int_0^v q dv = \frac{1}{2} C v^2$$

4.3.3 The resistive element

The resistive is an element in which power is dissipated. It relates the effort variable to the flow variable.

$$e(t) = e(f) \tag{4.10}$$

In this case, the integration of

$$\mathcal{D} = \int_0^e f de \tag{4.11}$$

where $\mathcal{D}$ is called the content and the co-content is given by

$$\mathcal{D}^* = \int_0^f e df \tag{4.12}$$

The sum $D + \bar{D}$ is the total power supplied or extracted from the system.

Figure 4.1 gives the relationship between the four types of variables. The diagonal gives the relationship between the effort or flow variable and the generalized displacement or generalized momentum variable. The edges gives the relationship between the different elements.

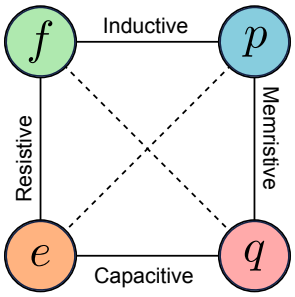

Figure 4.1: The four-element quadrangle

4.4 Bond Graphs

The bond graph method [56, 34] is a graphical approach to modeling in which component energy ports are connected by bonds that specify the transfer of energy between system components. Power, the rate of energy transport between components, is the universal currency of physical systems. The graphical nature of bond graphs separates the system structure from the equations, making bond graphs ideal for visualizing the essential characteristics of a system [20].

In a bond graph a half arrow head is used to indicate the power flow between elements and junctions and they are called a bonds. The direction of the arrow is the direction of power flow and each arrow is labeled with an effort, e, and a flow variable, f. And these arrows connected to the elements above, junctions, transformers and gyrators makes up a bond graph.

Finally, *causality*, which relates cause to effect, helps to gain insight into the system. Due to the simplicity of the representation, causality appears naturally and is much more evident in bond graphs. In linear graph, causality is determined by the tree and co-tree whereas in bond graph it is a casual stroke (vertical line) added to the arrows. In this thesis, causality has been fundamental in determining relationships and equations which will be discussed shortly.

4.4.1 Junctions

Central to the idea of bong graph are junctions. There are two kinds of junctions the *0*-junction and the *1*-junction. These junctions are ideal in the sense that they neither store or dissipate power and mathematically they are just a simple graphical notation for a set of linear constraint equations such as KVL and KCL. Figure 4.2 shows the 2 junctions and how they are constructed.

Each junction contains a KVL(continuity), KCL(conservation) and conservation of energy statement, any two implying the third. A 0-junction is effectively a point where flows are distributed where a 1-junction is where

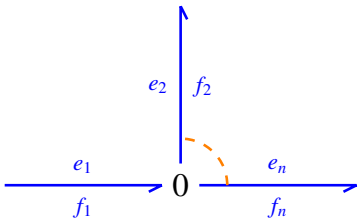

(a) 0-junction where $\sum_i^n f_i = 0$ and $e_1 = e_2 = .. = e_n$.

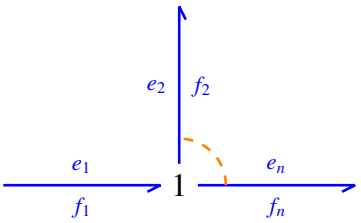

(b) 1-junction where $\sum_i^n e_i = 0$ and $f_1 = f_2 = .. = f_n$.

Figure 4.2: 0-junction and 1-junction. In both cases, $\sum_i^n e_i f_i = 0$.

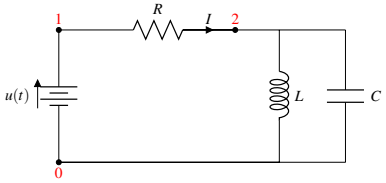

(a) RLC circuit.

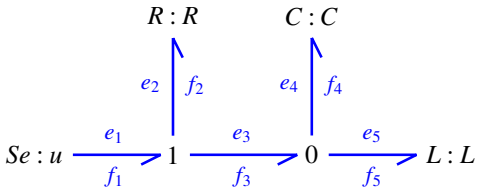

(b) Associated Bond Graph.

Figure 4.3: Bond Graph of RLC circuit.

efforts are distributed. Figure 4.3 shows the example RLC circuit and its associated bond graph.

The bond graph depicts the power flow from the source, $Se : u$, called an effort source, towards the elements. Parts having the same current are linked by a 1-junction and those having same voltage are linked by a 0-junction.

Taking current to be flows and voltages to be efforts and assuming that all causalities are respected, the equation for the system are dervived as follows. Taking the inductor flux $p = \lambda$ and the capacitor charge q as state variables, we have $\dot{p} = e_5$ and $\dot{q} = f_4$.

The junctions give the following relationship

$$\begin{array}{llll} f_3 = \mathbf{f_4} + f_5 & , & e_3 = e_4 = \mathbf{e_5} & \text{(0-junction).} \\ f_1 = f_2 = f_5 & , & e_1 = e_2 + e_3 & \text{(1-junction).} \end{array} \tag{4.13}$$

while the constitutive relationships are

$$\begin{array}{llll} \dot{q} = f_4 & , & e_4 = \frac{1}{C} q & \text{(Capacitor).} \\ \dot{p} = e_5 & , & f_5 = \frac{1}{L} p & \text{(Inductor).} \\ f_2 = \frac{e_2}{R} & , & & \text{(Resistor).} \end{array} \tag{4.14}$$

From the above relationships, we see that $e_5 = e_4$ and hence

$$\dot{p} = \frac{q}{C} \tag{4.15}$$

and

$$\begin{aligned} f_4 =& f_3 - f_5 \\ f_4 =& f_3 - \frac{p}{L} \\ =& \frac{e_2}{R} - \frac{p}{L} \\ =& \frac{e_1}{R} - \frac{e_3}{R} - \frac{p}{L} \\ f_4 =& \dot{q} = \frac{u}{R} - \frac{q}{RC} - \frac{p}{L} \end{aligned}$$

which be can be written in port-Hamiltonian form. Since $\mathcal{H}(q,p)$ is

$$\mathcal{H} = \frac{q^2}{2C} + \frac{p^2}{2L}$$

the port Hamiltonian representation becomes:

$$\begin{bmatrix} \dot{q} \\ \dot{p} \end{bmatrix} = \begin{bmatrix} -\frac{1}{R} & -1 \\ 1 & 0 \end{bmatrix} \begin{bmatrix} \frac{q}{C} = v_C \\ \frac{p}{L} = i_L \end{bmatrix} + \begin{bmatrix} \frac{1}{R} \\ 0 \end{bmatrix} u \tag{4.16}$$

$$y = \begin{bmatrix} \frac{1}{R} & 0 \end{bmatrix} \begin{bmatrix} \frac{q}{C} \\ \frac{p}{L} \end{bmatrix} \tag{4.17}$$

4.4.2 Transformers and Gyrators

In addition to elements such as Effort Source (Se), Flow Source (Sf), I-element, R-element, C-element, 0-junction and 1-junction, two other important elements are the gyrator(GY) and the transformer(TF). The former elements are called one-ports elements while gyrator and transformers are called two-port elements.

These elements are power converting elements i.e they either convert power within a single domain or from one domain to another. As in an electrical transformer, in a bond graph transformer also, the ratio of efforts is equal to the inverse ratio of flows whereas in a gyrator, the effort at one end of the port depends on flow at the other port and vice-versa. Examples of transformers are gear trains and electrical transformer among others whereas an example of gyrator would be the conversion of electrical energy to mechanical energy in DC motors or the voice coil transducer.

Figure 4.4 shows the graphical representation of a transformer and a gyrator. The governing equations for these two-ports elements are, for a transformer,

$$\begin{bmatrix} e_2 \\ f_2 \end{bmatrix} = \begin{bmatrix} \frac{1}{n} & 0 \\ 0 & n \end{bmatrix} \begin{bmatrix} e_1 \\ f_1 \end{bmatrix}$$

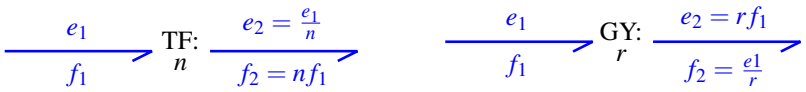

(a) Transformer. (b) Gyrator.

Figure 4.4: Two-port devices.

and for a gyrator:

$$\begin{bmatrix} e_2 \\ f_2 \end{bmatrix} = \begin{bmatrix} 0 & r \\ \frac{1}{r} & 0 \end{bmatrix} \begin{bmatrix} e_1 \\ f_1 \end{bmatrix}$$

4.4.3 Causality

Causality is an important feature of modeling. It dictates which bond sets the effort and which bond set the flow. It represents a constraint between the flow and effort variable. One immediate consequence is that the flow and effort cannot be specified independently. For example if a mass is being pulled with a certain velocity, then the force, F, experienced by the mass, m, at velocity, v is given by:

$$F = m\frac{dv}{dt} \tag{4.18}$$

On the other hand if the mass is subjected to a force then the velocit is given by:

$$v(t) = v_0 + \int_0^t \frac{F}{m} dt \tag{4.19}$$

Equation (4.18) is called *derivative* causality whereas equation (4.19) is called *integral* causality. It can be shown that all *independent* energy elements can be represented in integral causality. This also dictates the input and output of such an element.

Once the bond graph has been obtained, it is acausal in nature. Once the input has been decided, a state space model can be found. Furthermore, for a state space model, integral causality is preferred as it does take into consideration initial conditions. Causality is also important in simulations as it reveals if algebraic loops are present in the systems. Systems in which causality cannot be assigned are usually ill-posed.

In bond graph, causality is indicated by means of the casual stroke added at the end or at the start of a bond. The element adjacent to the casual stroke sets f whereas the other element sets e as shown in figure 4.5.

In bond graph, efforts and flows sources always have fixed causality which is natural. Effort sources will set e whereas flow sources will set f as shown in figure 4.6.

Storage elements i.e "I" and "C" elements are assigned their preferred causality which is the integral causality as shown in figure 4.7. If on propa-

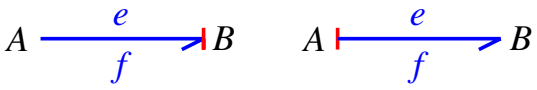

(a) A sets e and B sets f.

(b) A sets f and B sets e.

Figure 4.5: Causal Stroke.

(a) Effort sources always sets e.

(b) Flow Sources always sets f.

Figure 4.6: Effort and flow Sources.

gating causalities, the integral form cannot be assigned, then there is either a problem in the model or there are storage elements which are dependent. This will give rise to algebraic loops in the simulation.

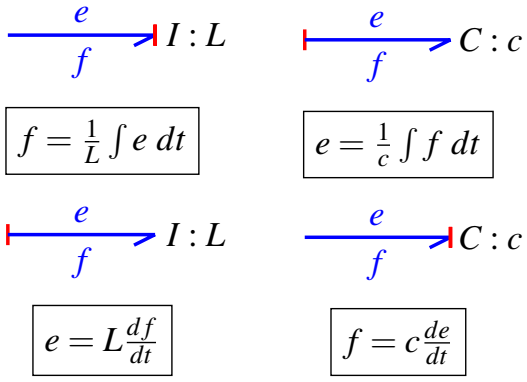

(a) I-element

(b) C-element.

Figure 4.7: Integral (top) and Derivative Causality of "I" and "C" elements.

Transformers and gyrators can take one of their 2 fixed causalities as shown in 4.8. This is also a consequence of how the elements were defined. If any other causalities are assigned to those elements, then they no longer work as intended.

And finally, figure 4.9 shows the resistive element. It can take both causalities. Usually one causality is preferred over the other if the inverse of constitutive law does not exist or it is difficult to obtain such as in Coulomb friction.

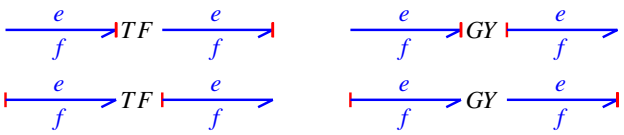

(a) Tranformers. (b) Gyrators.

Figure 4.8: Both can only take one of these allowed causalities.

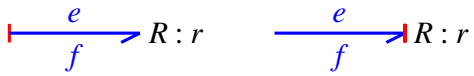

$e = rf$ $f = \frac{1}{r}e$

Figure 4.9: Resistive element can take both causalities.

Causalities are assigned only after having drawn the bond graph and the inputs are known. Sources are assigned their causalities first, then storage elements are put in their preferred causalities and then causality is propagated throughout the bond graph for the other elements until every bond has a casual stroke.

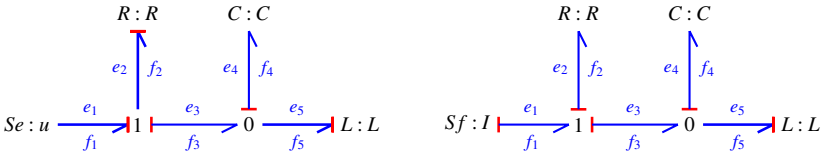

(a) RLC with voltage input. (b) RLC with current input.

Figure 4.10: Causality assignment for voltage input and current input.

Figure 4.10 shows the causality assignment for our RLC circuit example. It is to be noted that on a 0-junction there is only 1 causal stroke whereas on a 1-junction, all but 1 bond has a casual stroke. This is due to the fact that on a 0-junction only 1 bond sets the effort and on a 1-junction, only 1 bond sets the flow.

In addition, for comparison, the voltage input was changed to a current input and the bond graph is shown in 4.10a. This completely changes the dynamics of the circuits. Firstly, the resistor is no longer the element which sets the current as is shown by the causality change. This can also be seen in the state space equation (4.20).

$$\begin{bmatrix} \dot{q} \\ \dot{p} \end{bmatrix} = \begin{bmatrix} 0 & -1 \\ 1 & 0 \end{bmatrix} \begin{bmatrix} v_c \\ i_l \end{bmatrix} + \begin{bmatrix} 1 \\ 0 \end{bmatrix} i \tag{4.20}$$

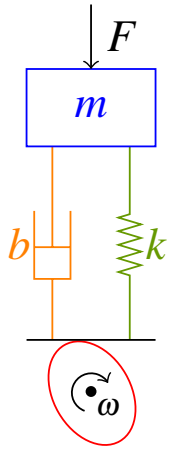

(a) Spring dashpot with velocity input (cam).

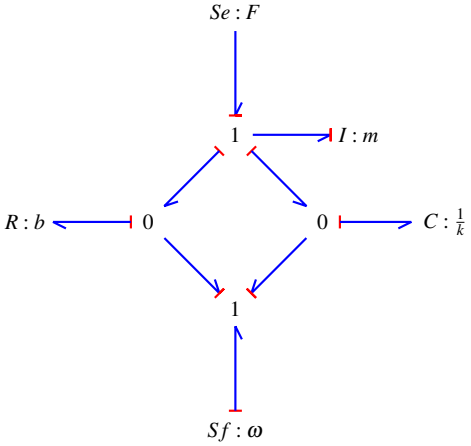

(b) Causal Bond Graph.

Figure 4.11: Mechanical System Bond Graph.

4.4.4 Bond Graph Examples

Till now, we have only seen an electrical example, all the power of bond graphs shows up in modelling coupled domains. We will illustrate examples which will help us understand the MSMA.

Mechanical Example

Figure 4.11 shows an example of a mechanical system and its corresponding bond graph. The systems is a class mass-spring system but with an additional velocity input. For mechanical systems, *force* is taken as the *effort* variable whereas *velocity* is taken as the *flow*. The bond graph is then written as follows, a "1" is written for each distinct velocities and then "0" added where there is common force. Once the bond graph is obtained, the power flow as well as the causality are found and then the equations can be written as described above. For this particular system, the state space equations are:

$$\begin{bmatrix} \dot{q} \\ \dot{p} \end{bmatrix} = \begin{bmatrix} 0 & \frac{1}{m} \\ -k & -\frac{b}{m} \end{bmatrix} \begin{bmatrix} q \\ p \end{bmatrix} + \begin{bmatrix} 0 & -1 \\ 1 & -b \end{bmatrix} \begin{bmatrix} F \\ \omega \end{bmatrix} \tag{4.21}$$

Taking the Hamiltonian $\mathcal{H}$ to be

$$\mathcal{H} = \frac{kq^2}{2} + \frac{p^2}{2m}$$

the port Hamiltonian representation becomes:

$$\begin{bmatrix}\dot{q}\\ \dot{p}\end{bmatrix} = \begin{bmatrix}0 & 1\\ -1 & -b\end{bmatrix}\begin{bmatrix}kq\\ \frac{p}{m}\end{bmatrix} + \begin{bmatrix}0 & -1\\ 1 & -b\end{bmatrix}\begin{bmatrix}F\\ \omega\end{bmatrix} \tag{4.22}$$

$$y = \begin{bmatrix}1 & 0\\ 0 & 1\end{bmatrix}\begin{bmatrix}kq\\ \frac{p}{m}\end{bmatrix} \tag{4.23}$$

Electromechanical Example

The DC motor is a very popular electromechanical device. It converts electrical energy to mechanical energy. As seen in the bond graph of figure 4.12, it is the gyrator which couples the electrical side and the mechanical side. The back emf induced is proportional to the speed at which the motor is turning wheras the torque is proportional to the current. This constant of proportionality is K, found on the gyrator.

$$\begin{aligned} E &= K\omega \\ \tau &= Ki \end{aligned}$$

The state space equation for this dc motor is given by:

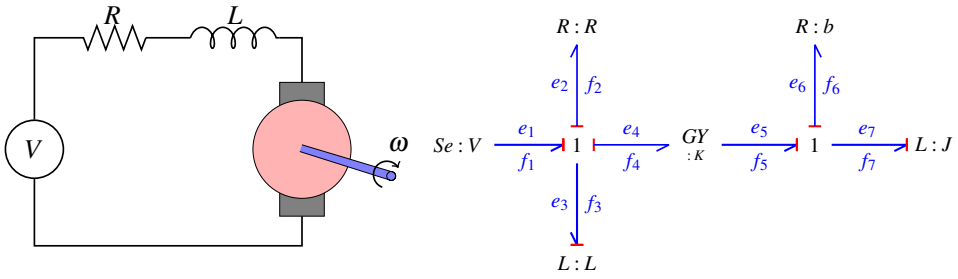

Figure 4.12: DC Motor and its Bond Graph.

$$\begin{bmatrix}\dot{p}_e\\ \dot{p}_m\end{bmatrix} = \begin{bmatrix}-\frac{R}{L} & -\frac{K}{J}\\ \frac{K}{L} & -\frac{b}{J}\end{bmatrix}\begin{bmatrix}p_e\\ p_m\end{bmatrix} + \begin{bmatrix}1\\ 0\end{bmatrix}V \tag{4.24}$$

A non-linear example: Magnetic Levitation

The magnetic levitation system is a good example of a non-linear system. The system consists of a sphere of ferromagnetic material which is levitated using a magnetic field. In this typical example, the inductance varies with the position, q, of the ball. An approximate constitutive law can be given by

$$L(q) = \frac{k}{a+q} \tag{4.25}$$

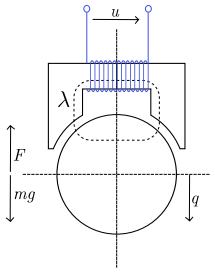

(a) Magnetic Levitation.

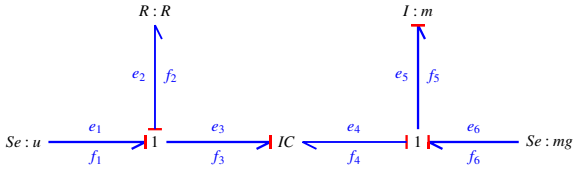

(b) Causal Bond Graph.

Figure 4.13: Non-Linear Example.

where a and k are constants. The energy stored in the magnetic field is given by

$$W = \frac{\lambda^2.(a+q)}{2k} \tag{4.26}$$

This energy has been represented by an "IC" field. It is commonly used to represent energy elements who depend on multiple set of coordinates. This does not add any more complexity to our model except that our constitutive equation now depends on more than one variable. In the maglev case, the constitutive equations are

$$i(\lambda, q) = \frac{\partial W}{\partial \lambda} = \frac{\lambda(a+q)}{k}$$
$$F(\lambda, q) = \frac{\partial W}{\partial q} = \frac{\lambda^2}{2k}$$

The state equations are then found to be as follows:

$$e_3 = \dot{\lambda}$$
$$f_3 = \frac{\partial W}{\partial \lambda} = \frac{\lambda(a+q)}{k} \qquad e_4 = \frac{\partial W}{\partial q} = \frac{\lambda^2}{2k} \qquad e_5 = \dot{p}$$
$$\dot{\lambda} = e_1 - e_2 \qquad f_4 = \dot{q} = f5 \qquad f_5 = \frac{p}{m}$$
$$\dot{\lambda} = u - Rf_2 = u - Rf_3 \qquad \dot{q} = \frac{p}{m} \qquad e_5 = e_6 - e_4$$
$$\dot{\lambda} = u - R\frac{\lambda(a+q)}{k} \qquad \dot{p} = mg - \frac{\lambda^2}{2k}$$

By taking $x_1 = \lambda$, $x_2 = q$ and $x_3 = p$, the Port Hamiltonian model can be written as:

$$\dot{x} = \left[\underbrace{\begin{pmatrix} 0 & 0 & 0 \\ 0 & 0 & 1 \\ 0 & -1 & 0 \end{pmatrix}}_{\mathbf{J}} - \underbrace{\begin{pmatrix} R & 0 & 0 \\ 0 & 0 & 0 \\ 0 & 0 & 0 \end{pmatrix}}_{\mathbf{R}} \right] \frac{\partial \mathcal{H}}{\partial x} + \begin{bmatrix} 1 \\ 0 \\ 0 \end{bmatrix} u \tag{4.27}$$

with $\mathcal{H}$ being the Hamiltonian of the system.

$$\mathcal{H} = \frac{x_1^2.(a + x_2)}{2k} - mgx_2 + \frac{x_3^2}{2m} \tag{4.28}$$

4.5 MSMA Actuator Bond Graph

The purpose of this section is to derive the dynamic equations of the actuator. In chapter 3, we only considered the actuator in a static case. We derived all the necessary constitutive equations. Thermodynamics methods were applied to derive the constitutive relation between z and the thermodynamic driving force π (distributed parameter). As explained in the last chapter, this parameter is integrated to give the lumped parameter, f. It is an intensive parameter with its dual z the extensive parameter. It is an effort variable just like voltage/force in electrical/mechanical domain.

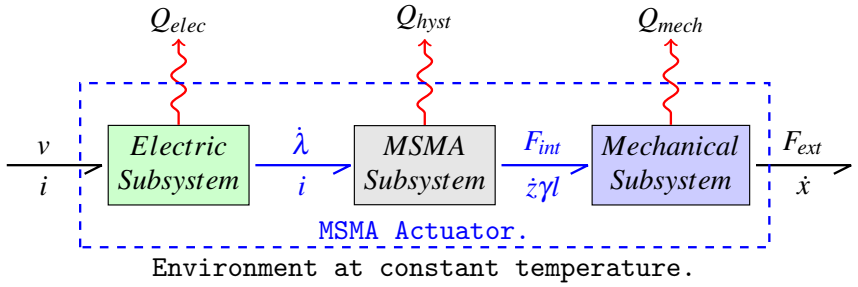

Figure 4.14: Schematic diagram showing the subsystems of the actuator with the arrows showing the power exchanging ports.

As stated before, the actuator consists of 3 parts. The electric/magnetic part, the MSMA part and the mechanical part. Figure 4.14 depicts a schematic diagram of the actuator. It exchanges energy with its environment through an electrical port and a mechanical port. Losses in the form of heat is dissipated to its surroundings. Q_{elec} is the joule heating which occurs in the resistor of the electrical circuit, Q_{hyst} is the losses due to hysteresis and Q_{mech} is the heat generated by viscous friction on the mechanical side.

Each part will be considered separately and they will be connected together. Also, hysteresis which has been treated sparsely will be detailed and it will be shown how an energy consistent formulation can be made.

4.5.1 Electric/Magnetic Subsystem Bond Graph

For the electric/magnetic part, there are 2 possible representations depending on the level of detail that is required. We can adopt an inductance representation or a reluctance representation.

For an inductance representation, lets consider the electric circuit of the actuator shown in Figure 4.15a. This circuit shows the resistance of the coil as r as well as a non-linear inductor. This non-linear inductor represent the relationship between λ, i and z. The relationship between these 3 variables is given in (3.63). From an energetic point of view, it means that the energy stored in the inductor is affected by both the electrical side and the MSMA side. For a fixed current, this energy can be changed by applying a force on the MSMA or for a fixed applied force, this energy can be modified by changing the current. As in the magnetic levitation model, when the energy depends on more than one coordinate, an "IC" field as seen in figure 4.15b , is used to model such phenomena.

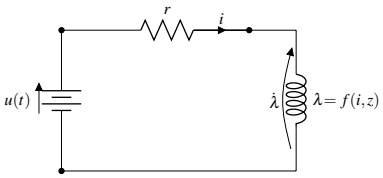

(a) Electric circuit of MSMA Actuator. $f(i,z)$ denotes that the flux linkage λ is a function of i and z.

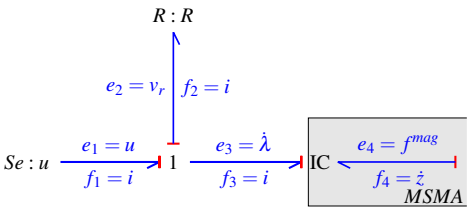

(b) Bond Graph of Electric subsystem.

Figure 4.15: Electric susbsystem Bond Graph.

Using W_{mag} (from Table 3.2), as the energy stored in the "IC" field, the equation for the electrical subsystem is derived as follows:

$$\begin{aligned} e_3 &= \dot{\lambda} \\ f_3 &= \frac{\partial W_{mag}}{\partial \lambda} \\ e_3 &= e_1 - e_2 \\ \dot{\lambda} &= u - R f_3 \\ &= u - R\frac{\partial W_{mag}}{\partial \lambda} \end{aligned} \tag{4.29}$$

The port-Hamiltonian representation of this circuit, taking u as input and i as output, given the Hamiltonian $\mathcal{H}_e = W_{mag}$ is

$$\dot{\lambda} = \underbrace{(0-R)}_{\mathcal{J}-\mathcal{R}} \frac{\partial \mathcal{H}_e}{\partial \lambda} + u$$
$$y_{elec} = \frac{\partial \mathcal{H}_e}{\partial \lambda} = i$$

so that the product of input and output is *power*.

Reluctance Model Bond Graph

Just for the sake of completeness, we show in Figure 4.16 the bond graph of the reluctance circuit shown in Figure 3.11. The reluctances have been modelled by capacitors as they are energy storing elements. Throughout this thesis, we have assumed that all the magnetic field H_0 produced by the coil appears in the air gap. This assumption relies on the fact that we have neglected parasitic effects, eddy current losses and we have taken the permeability of the ferromagnetic core to be infinite. Usually this is not the case. The reluctance circuit is useful if we need a finer model and it helps to model each individual magnetic element separately. Also, it gives access to one more measurement, the magnetic field in the air gap. Furthermore, if any saturation is present in the ferromagnetic core, this can easily be incorporated with this model.

The model shows that the MSMA and the air gap have been lumped together. This has been done for 2 reasons. Firstly since they are in parallel they are not independent (causality problem) and secondly it is easier to incorporate it in the "IC" field in this manner. Our constitutive equations for the "IC" thus remain the same else we would have to separate the air gap part from the msma part.

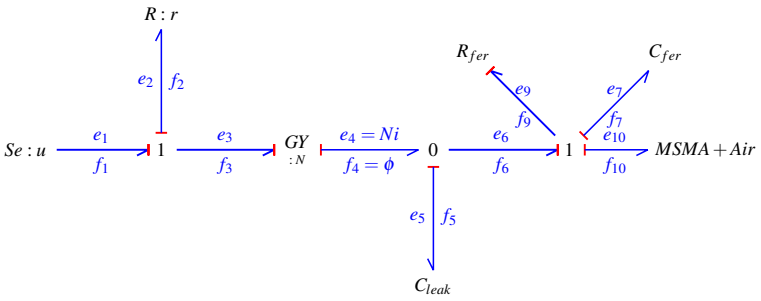

Figure 4.16: Bond graph model of reluctance circuit

This model will not be further discussed, we will adopt its ideal circuit equivalent to keep things manageable else the number of equations will quickly get unwieldy.

4.5.2 Mechanical subsystem Bond Graph

The MSMA mechanical model is shown in Figure 4.17a. The MSMA has a Young's modulus E, a cross-sectional area, A and its longitudinal length is l. The elastic part of the MSMA is modelled by a spring of stiffness, $k = \frac{AE}{l}$. The damper models the dissipation due to viscous friction experienced by the load. The coefficient of damping is taken to be b. And finally when the MSMA converts electrical energy to mechanical energy, it acts as a flow source by means of the variable z. The figure also shows the forces acting

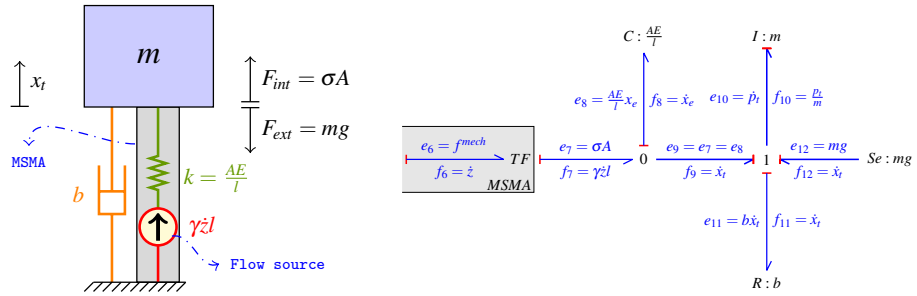

(a) MSMA mechanical model with load.

(b) Bond Graph of Mechanical Subsystem.

Figure 4.17: Mechanical subsystem and its Bond Graph.

on the system and the total displacement x_t. The latter is made up of the elastic displacement x_e which in a uniformly deformed rod

$$x_e = \int_0^l \varepsilon_e \, dl = \varepsilon_e l \tag{4.30}$$

and the displacement due to twinning strain $\gamma z l$ which is

$$x_z = \int_0^l \gamma z \, dl = \gamma z l \tag{4.31}$$

The variable γ is the maximum twinning strain achievable. Finally, the momentum of the mass is denoted by p_t.

The bond graph of the mechanical model in Figure 4.17b shows that there exists a constraint between $\dot{x}_e$, $\gamma \dot{z} l$ and $\dot{x}_t$. Notably only 2 of them are independent.

$$\dot{x}_t = \gamma \dot{z} l - \dot{x}_e \tag{4.32}$$

It should be emphasized that the direction of x_e and $\gamma z l$ are opposite when operating in actuation mode whereas in sensing mode, they would be in the same direction. The bond (e_8, e_9) can take both directions. Hence it depends really how power is flowing-i.e is the magnetic field increasing or decreasing when the applied load is constant. The kinetic energy of the mechanical system is given by

$$W_k(p_t) = \frac{1}{2} \frac{p_t^2}{m} \tag{4.33}$$

and the potential energy is

$$W_p(x_t, z) = \frac{1}{2} k x_e^2 = \frac{1}{2} k (x_t - \gamma z l)^2 \tag{4.34}$$

Using (4.33) and (4.34) and the bond graph in Figure 4.17b and choosing state variables as x_t, p_t, and z the following equation can be written

$$\dot{x}_t = \frac{p_t}{m} = \frac{\partial W_k}{\partial p_t} \tag{4.35}$$

and for p_t

$$\begin{aligned} e_{10} &= \dot{p}_t \\ e_{10} &= e_8 - e_{11} + e_{12} \\ \dot{p}_t &= -\frac{AE}{l}x_e - b\dot{x}_t + mg \\ &= -\frac{\partial W_p}{\partial x_t} - b\frac{\partial W_k}{\partial p_t} + mg \end{aligned} \tag{4.36}$$

In the mechanical part, the state variables are x_t and p_t. The state variable z is in the MSMA part. The port Hamiltonian representation for the mechanical subsystem, taking the Hamiltonian $\mathcal{H}_m$ as

$$\mathcal{H}_m = \frac{1}{2}k(x_t - \gamma z l)^2 + \frac{1}{2}\frac{p_t^2}{m} \tag{4.37}$$

is

$$\begin{bmatrix} \dot{x}_t \\ \dot{p}_t \end{bmatrix} \underbrace{\begin{bmatrix} 0 & 1 \\ -1 & -b \end{bmatrix}}_{\mathcal{J}-\mathcal{R}} \begin{pmatrix} \frac{\partial \mathcal{H}_m}{\partial x_t} \\ \frac{\partial \mathcal{H}_m}{\partial p_t} \end{pmatrix} + \underbrace{\begin{bmatrix} 0 \\ 1 \end{bmatrix}}_{B} \underbrace{F_{ext}}_{mg} \tag{4.38}$$

with output

$$y = \begin{bmatrix} 1 & 0 \end{bmatrix} \begin{pmatrix} \frac{\partial \mathcal{H}_m}{\partial x_t} \\ \frac{\partial \mathcal{H}_m}{\partial p_t} \end{pmatrix} = \dot{x}_t \tag{4.39}$$

and again $(F_{ext}.\dot{x}_t)$ is a power.

4.5.3 MSMA subsystem Bond Graph

The bond graph of the MSMA is made up of two ports. The electric port represented by the "IC" field and the mechanical port represented by the transformer "TF" as shown in Figure 4.18. The 2 ports represents the energy conversion process between the electrical subsystem to the MSMA subsystem and then from the MSMA subsystem to the mechanical subsystem.

The "IC" field is used because of the non-linear energy function. In fact it is just a non-linear capacitor coupled to a non-linear inductor through a non-linear transformer. These kinds of energy storage element are very common where the energy stored depends on one or more generalised coordinate and one or more generalised momentum. A common example is the solenoid [81, chap. 3] or the previously explained magnetic levitation system where the energy stored depends both on the flux and the position.

In the MSMA, thus, both types of conservative elements exists (I and C), since z is the volume fraction, a change in its value directly related to the change in the elongation of the material. Hence from a bond graph point of view, on the mechanical side, it is a transformer.

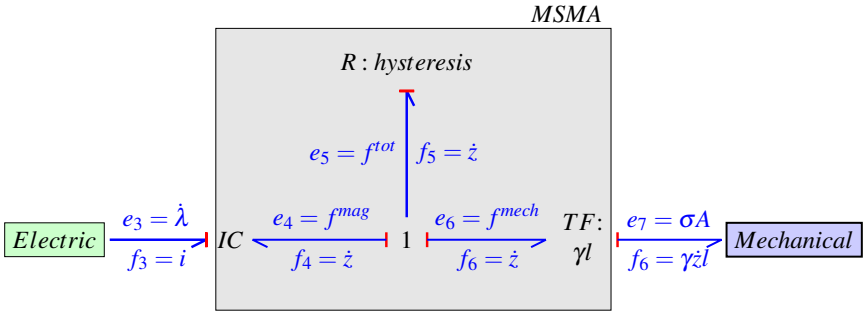

Figure 4.18: The Bond Graph of the MSMA. The "IC" field and the transformer "TF" act as energy converting ports.

On the electrical side on the other hand, the two internal variables α and θ were taken to be reversible variables. Figure 4.19 shows the elementary representative volume. The effect of the magnetic field H_0 is to make domains parallel to it align in the same direction i.e α grows and θ aligns with the plane of the magnetic field as shown in figure 4.19. Once the magnetic field is removed they return to their original position if the pre-stress is sufficient i.e the energy which can be recovered depends greatly on the value of z. This is due to the hysteretic nature of z.

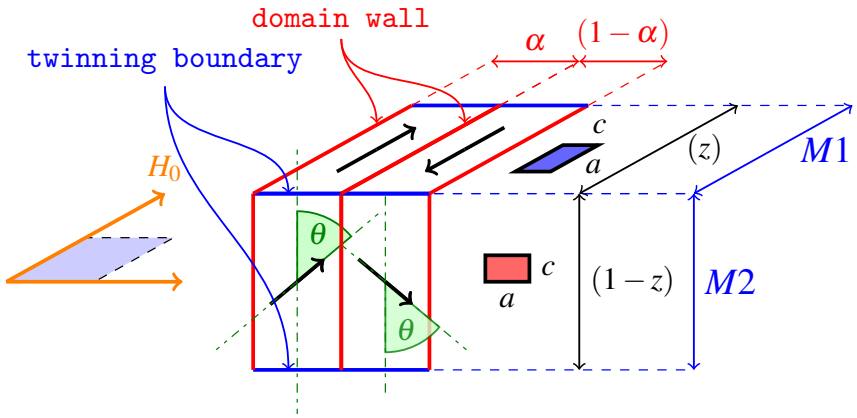

Figure 4.19: Energy is stored in the MSMA by the rotation of magnetisation vector θ and the change in size of α.

The hysteretic part (e_5, f_5) in figure 4.18 has as input the effort e_5 (deduced from location of causal stroke) which is the total thermodynamics driving force related to the mechanical part and the electrical part. As the dynamics of z is related to these 2 competing forces, it is this force that

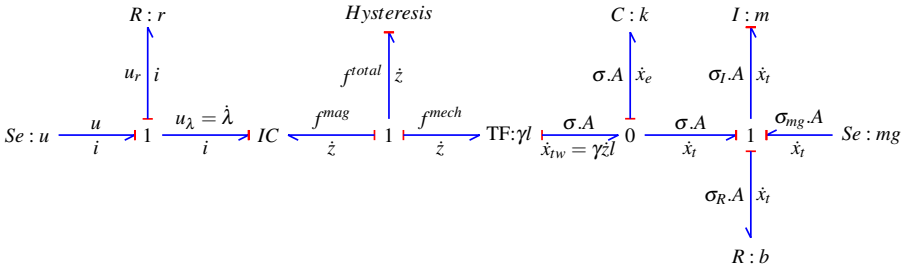

Figure 4.20: Complete Bond Graph without hysteresis details.

moves the z. The mechanical thermodynamics driving force is given by

$$f^{mech} = \frac{\partial \mathcal{H}_m}{\partial z}$$

whereas the electrical thermodynamics driving force is given by

$$f^{mag} = \frac{\partial \mathcal{H}_e}{\partial z}$$

where $\mathcal{H}_m$ and $\mathcal{H}_e$ are the Hamiltonians of the electric and mechanical subsystem. From the bond graph, it is seen that this total thermodynamics driving force, f^{tot} is

$$f^{tot} = -f^{mag} - f^{mech} \tag{4.40}$$

and that $\dot{z}$ is common to all the bonds in the MSMA subsytem. Hence the $R : hysteresis$ part takes in the effort $e_5 = f^{total}$ and gives $\dot{z}$ to the system hence

$$\dot{z} = g(.) \tag{4.41}$$

where $g(.)$ is a possibly non-linear operator which characterises hysteresis. The latter will be made explicit in the next section.

As of now, our bond graph for the actuator is as shown in figure 4.20. Taking the Hamiltonian to be

$$\begin{aligned} \mathcal{H}(\lambda, x_t, p_t, z) &= \mathcal{H}_e(\lambda, z) + \mathcal{H}_m(xt, p_t, z) \\ &= W_{mag}(\lambda, z) + W_k(p_t) + W_p(x_t, z) \end{aligned} \tag{4.42}$$

Its port-Hamiltonian formulation is

$$\begin{bmatrix} \dot{\lambda} \\ \dot{z} \\ \dot{x}_t \\ \dot{p}_t \end{bmatrix} = \begin{bmatrix} -r & 0 & 0 & 0 \\ 0 & g(.) & 0 & 0 \\ 0 & 0 & 0 & 1 \\ 0 & 0 & -1 & -b \end{bmatrix} \begin{pmatrix} \frac{\partial \mathcal{H}}{\partial \lambda} \\ \frac{\partial \mathcal{H}}{\partial z} \\ \frac{\partial \mathcal{H}}{\partial x_t} \\ \frac{\partial \mathcal{H}}{\partial p_t} \end{pmatrix} + \begin{bmatrix} 1 & 0 \\ 0 & 0 \\ 0 & 0 \\ 0 & 1 \end{bmatrix} \begin{pmatrix} u = u_{ext} \\ mg = F_{ext} \end{pmatrix} \tag{4.43}$$

with output

$$\mathbf{y} = \begin{bmatrix} 1 & 0 & 0 & 0 \\ 0 & 0 & 0 & 1 \end{bmatrix} \begin{pmatrix} \frac{\partial \mathcal{H}}{\partial \lambda} \\ \frac{\partial \mathcal{H}}{\partial z} \\ \frac{\partial \mathcal{H}}{\partial x_t} \\ \frac{\partial \mathcal{H}}{\partial p_t} \end{pmatrix} = \begin{bmatrix} i \\ \dot{x}_t \end{bmatrix} \tag{4.44}$$

where $g(.)$ represents hysteresis. We now proceed to understand and detail the hysteresis part and propose a way to include it in a port-Hamiltonian framework.

4.5.4 Hysteresis in MSMA

Hysteretic behaviour is very problematic from a control point of view. Usually hysteresis is modelled as an input/output map. This view is not consistent with energy formulation as discussed in Goldfarb and Celanovic [22] and Karnopp [33]. In this section, an energy consistent formulation is made which can then be incorporated in the port-Hamiltonian framework.

Figure 4.21 shows a typical hysteretic curve of the MSMA. For increasing values of f and decreasing values of f, the path taken by the system is not the same. Hence it is a multi-valued function and the actual value of the output depends on the whole history of the material. Also the energy loss of the system in 1 cycle is given by

$$Q_{hyst} = \oint f dz \tag{4.45}$$

Therefore in the process of hysteresis, a part of energy is dissipated and a part of energy is conserved. The dissipative part is modelled using an R-element whereas the conservative part is modelled using a C-element.

The values of f_{cr}^{+} and f_{cr}^{-} shown in figure 4.21, usually called critical values, for the Magnetic Shape Memory alloy are those values below which determine whether reorientation can take place. These values depend on the current, i, and the load (stress) applied to the material. Once f_{cr}^{+} is exceeded while the material is taking the ascending path, reorientation starts to take place and elongation occurs. The reverse occurs when the material is taking the descending path. Once the value of the thermodynamic force becomes lower than f_{cr}^{-}, the material starts to shorten.

From these considerations, the R-element (damper) should be non-linear with a dead zone between f_{cr}^{+} and f_{cr}^{-}. The constitutive equation for the C-element need not necessarily be non-linear, it can be linear. The particular choice depends on the complexity required [33]. For our purposes, we choose a simple linear law. These two elements are connected in parallel to make one hysteron-a basic unit of hysteresis- because they experience the same force. Figure 4.22a shows the schematic of the elements whereas figure 4.22b

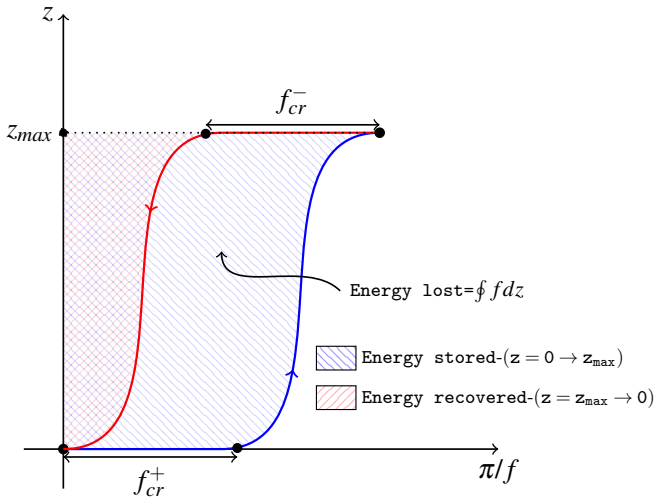

Figure 4.21: A typical hysteresis curve for MSMA.

shows the associated bond graph when the hysteresis is model with only one hysteron.

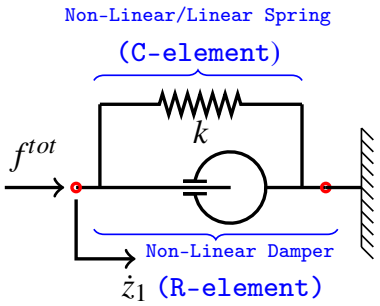

(a) Schematic of R-element in parallel with C-element. z=z_1 when only one hysteron is used.

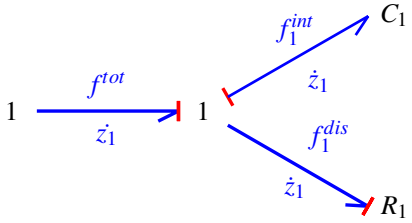

(b) Bond Graph of basic hysteretic R-C element.

Figure 4.22: Basic Hysteretic elements.

From the bond graph, looking at the causality strokes, we find that the effort, f^{tot} is the input to the system whereas $\dot{z}_1$ is the output. On the other hand, the C-element, takes as input $\dot{z}_1$ and gives the effort, f^{int} whereas the R-element takes in an effort, f^{dis} and gives back $\dot{z}_1$. The R-element therefore sets the $\dot{z}_1$ of the element. The continuity equation gives

$$f^{tot} = f_1^{int} + f^{dis} \tag{4.46}$$

whereas all the element share the same $\dot{z}$.

Taking the capacitive element as linear with a stiffness coefficient of k_{h1} we have the following constitutive equations

$$f_1^{int} = k_{h1} z_1 \quad , z_1 \text{ is the input} \tag{4.47}$$

and for the R-element, we have

$$\dot{z_1} = g_1(f_1^{dis}) \tag{4.48}$$

where $g_1(.)$ is the relationship between $\dot{z}$ and f^{dis} similar to an electrical resistance where $v = R\dot{q}$ for the linear case or $v = f(\dot{q})$ for the non-linear case. A very simple constitutive equation for the damper is given in figure 4.23. It shows that $\dot{z}$ does not start to change until the threshold critical

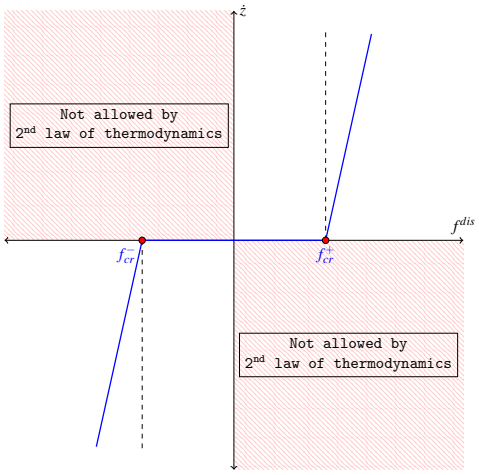

Figure 4.23: Constitutive Equation for Damper (R-element).

values are reached. Also, according to the second law of thermodynamics, $\dot{Q}_{hyst} \geq 0$ which forbids the constitutive equation for the R-element to be in the 2^{nd} and 4^{th} quadrant. The losses according to figure 4.21 can be more explicitly written as

$$Q_{hyst} = \oint f^{tot}\, dz = \underbrace{\oint f_1^{int}\, dz}_{=0 \text{ (conservative)}} + \underbrace{\oint f_1^{dis}\, dz}_{\neq 0 \text{ (dissipative)}} \tag{4.49}$$

Also, the slope of the line should be adjusted according to experimental data. Being a constitutive relationship it is therefore rate-independent. Such a formulation of hysteresis allows us to include it into the port-Hamiltonian formulation. To calculate, $\dot{z}_1$, we make use of the bond graph to obtain

$$\begin{aligned} \dot{z}_1 &= g_1(f^{dis}) \\ &= g_1(f^{tot} - f^{int}(z)) \\ &= g_1(f^{tot} - k_{h1} z_1) \end{aligned}$$

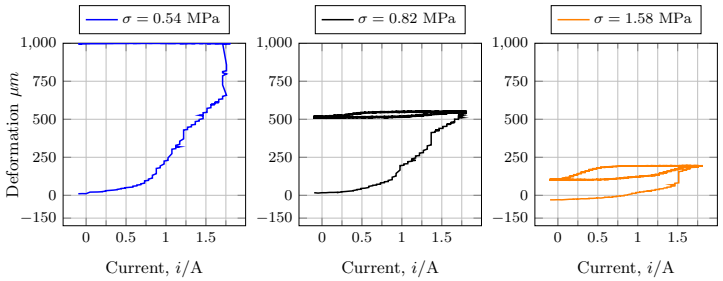

(a) Experiment showing hysteresis between deformation and current.

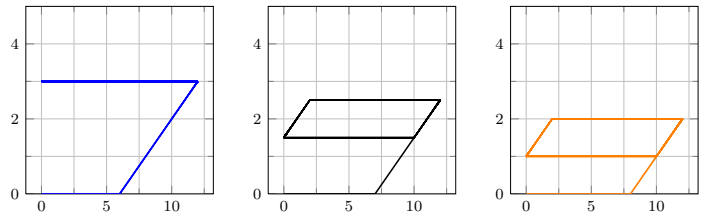

(b) Rough Simulation of one hysteretic Element. These curves were obtained by just varying the critical values.

Figure 4.24: Simulation of one hysteron to show it has the same shape (approximate) as experimental curves.

Using these relationship, a very basic simulation was performed where a sinusoidal input was applied to one hysteron (f^{tot} is the sine wave as it is the input to a hysteron). Figure 4.24 shows a comparison between the shape of experimental value (figure 4.24a) obtained with our the experimental setup and one the simulation (figure 4.24b).

Though very crude, this figure 4.24 gives us some insight into the workings of the actuator. It tells us that the values f_{cr}^{+} and f_{cr}^{+} changes with applied load. Also, as seen with one hysteretic element the simulation result are not very smooth. To palliate this problem, just like in the Preisach case, more than one of basic hysterons units should be used depending on the accuracy needed.

This is done by taking a number of hysterons and joining them in series as in Figure 4.25a. Each hysteron should be subjected to the same force hence the series connection.

Depending on this force, they will all switch according to their constitutive equations. All those hysterons (characterised by different critical values (f_{cr}^{+} and f_{cr}^{-}) and different spring stiffness (k_{hn})) depending on their state will contribute to a fraction of z. The bond graph in figure 4.25b also has the advantage that any number of hysterons can be added and the bond graph

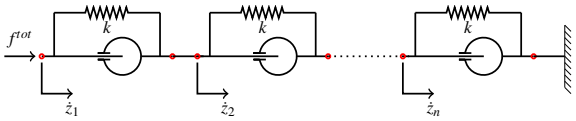

(a) Mechanical analogy of n-hysterons to model hysteresis more precisely.

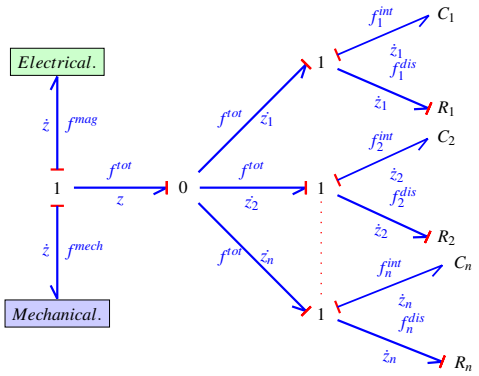

(b) Associated Bond Graph. The different z_n values sum at the '0' junction to give the final z.

Figure 4.25: Bond Graph for multiple hysterons.

will still be causal. And finally, the dynamic equation for each hysteron is

$$\begin{aligned}
\dot{z}_1 &= g_1(f_1^{dis}) = g_1(f^{total} - f_1^{int}(z_1)) \\
\dot{z}_2 &= g_2(f_2^{dis}) = g_2(f^{total} - f_2^{int}(z_2)) \\
&\vdots \\
\dot{z}_n &= g_n(f_n^{dis}) = g_n(f^{total} - f_n^{int}(z_n))
\end{aligned}$$

As each hysteron contribute to the final value of z as follows

$$z = z_1 + z_2 + \cdots + z_n \tag{4.50}$$

The Hamiltonian of the whole system becomes

$$\begin{aligned}
\mathcal{H}(\lambda, x_t, p_t, z_1, z_2, \cdots, z_n) =& W_{mag}(\lambda, z_1, z_2, \cdots, z_n) + W_k(p_t) \\
&+ W_p(x_t, z_1, z_2, \cdots, z_n) \\
&+ W_{h1}(z_1) + W_{h2}(z_2) + \cdots + W_{hn}(z_n)
\end{aligned} \tag{4.51}$$

where $W_{hn} = \frac{1}{2}k_{hn}z^2$ is similar to the energy stored in a linear spring. The

port-Hamiltonian model can then be written as:

$$\begin{bmatrix} \dot{\lambda} \\ \dot{z_1} \\ \dot{z_2} \\ \vdots \\ \dot{z_n} \\ \dot{x_t} \\ \dot{p_t} \end{bmatrix} = \begin{bmatrix} -r & 0 & 0 & 0 & 0 & 0 & 0 \\ 0 & g_1(.) & 0 & 0 & 0 & 0 & 0 \\ 0 & 0 & g_2(.) & 0 & 0 & 0 & 0 \\ 0 & 0 & 0 & \ddots & 0 & 0 & 0 \\ 0 & 0 & 0 & 0 & g_n(.) & 0 & 0 \\ 0 & 0 & 0 & 0 & 0 & 0 & 1 \\ 0 & 0 & 0 & 0 & 0 & -1 & -f \end{bmatrix} \begin{pmatrix} \frac{\partial \mathcal{H}}{\partial \lambda} \\ \frac{\partial \mathcal{H}}{\partial z_1} \\ \frac{\partial \mathcal{H}}{\partial z_2} \\ \vdots \\ \frac{\partial \mathcal{H}}{\partial z_n} \\ \frac{\partial \mathcal{H}}{\partial x_t} \\ \frac{\partial \mathcal{H}}{\partial p_t} \end{pmatrix} + \begin{bmatrix} 1 & 0 \\ 0 & 0 \\ 0 & 0 \\ \vdots & \vdots \\ 0 & 0 \\ 0 & 0 \\ 0 & 1 \end{bmatrix} \begin{pmatrix} u \\ mg \end{pmatrix} \tag{4.52}$$

with output

$$y = \begin{bmatrix} 1 & 0 & 0 & \cdots & 0 & 0 & 0 \\ 0 & 0 & 0 & \cdots & 0 & 0 & 1 \end{bmatrix} \begin{pmatrix} \frac{\partial \mathcal{H}}{\partial \lambda} \\ \frac{\partial \mathcal{H}}{\partial z_1} \\ \frac{\partial \mathcal{H}}{\partial z_2} \\ \vdots \\ \frac{\partial \mathcal{H}}{\partial z_n} \\ \frac{\partial \mathcal{H}}{\partial x_t} \\ \frac{\partial \mathcal{H}}{\partial p_t} \end{pmatrix} \tag{4.53}$$

4.6 Discussion

In this chapter, using energy methods we have obtained a coherent port Hamiltonian model of our system. Bond graph methodology was presented and used to model the system. The dynamics on the $\dot{z}$ variable which was missing from [18] and [8] is seen to come from the dissipative nature of hysteresis.

This model also has all its causality respected, therefore use of Lagrange multipliers or differential causality has not been necessary. It has also allowed us to view the energy flow throughout the MSMA actuator.

Though this bond graph has been done for an actuator, it can be readily extended to a sensor just by reversing the direction of power of a few arrows. The push-pull actuator can also be represented by using this bond graph and its mirror image and connecting them together through the external mechanical port. Causality should be reassigned while doing so. Furthermore, this actuator is actually voltage controlled. It would be interesting to replace the

voltage input with a current input in the actuator's bond graph and see the differences and difficulties that arise.

It has also been shown in this chapter that hysteresis can be included into the port Hamiltonian framework in an energetically coherent manner. This has many advantages as regards to the understanding and control of the material. Also, many possibilities open up such as how much energy can be recuperated in one hysteresis loop as well as how much is dissipated. This quantification can be really important in applications like energy harvesting.

On a final note, the interaction energy $K_{12}z(1-z)$ present in Chapter 3 can now be explained. This term was added to account for the hysteresis of the material. As seen in this chapter, hysteresis stores energy in a C-element. Hence there exists a constitutive relationship between f and z of the type $f = kz$ where f is an effort and z is an integrated flow.

Having our model, we now turn to some basic experimental results we performed on a test bed and the subsequent control of the actuator.

Chapter 5

Basic Experimental Validation and Control Perspectives

5.1 Introduction

This chapter is divided into 2 parts. In the first part, we detail the experimental setup to see the general behaviour of the material and the associated problems which might arise. In the second part, we show the first steps in designing a port Hamiltonian control law for the material. Both parts represent the first steps towards implementation of a working control law in a real time testbed.

5.2 Experimental Setup

An experimental testbed has been designed and built to investigate the behavior of the material, the MSMA actuator, to validate proposed model, to identify model parameters and finally to test possible control laws. The experimental setup consists of two main parts; an electrical part and a mechanical part. The electrical part is used to generate the high magnetic fields needed whereas the mechanical part is used to apply stress to the material as well to measure the deformation of the material.

Figure 5.1 shows a block diagram representing schematically the different parts of the data acquisition procedure. A PC connected to a *dSPACE 1104 R&D Controller board* which contains the necessary ADC and DAC channels is used for signal acquisition and processing. It has a real time interface which can easily be connected to *Simulink*. Programs/block diagrams made in Simulink can then be downloaded to the dSPACE processor using the provided dSPACE software. The lowest sample time which can be achieved with this processor is around 0.05 ms. As shown in Figure 5.1, a signal be-

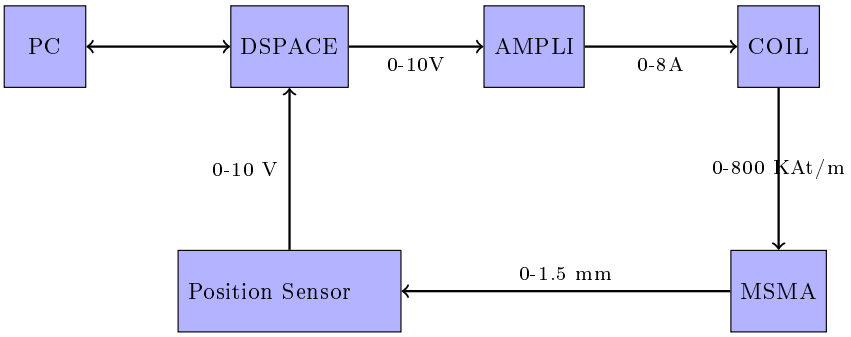

Figure 5.1: Block diagram of the experimental test bench.

tween $0-10V$[1] is sent from the controller to the power amplifier. This signal is amplified so as to provide a magnetic field which varies between 0 and a maximum value which causes the magnetization of the MSMA to saturate. This forms the electrical part of the experimental setup. On application of the magnetic field, the deformation, which depends on the stress applied to the material, is measured using a laser sensor. To measure the position and to apply a stress, a movable mechanical structure has been designed.

The main purpose of the electrical part is to be able to generate a variable magnetic field. The maximum value of the magnetic field should be enough so as to saturate the MSMA. This value is around $0.65T$. An electromagnet is therefore required to generate such a high magnetic field. The electromagnet consists of a ferromagnetic core with an air gap where the MSMA is inserted. The constraints that should be taken into consideration are the size of the MSMA which is $3mm \times 5mm \times 20mm$. The built electromagnet, has a value of $l_n = 350mm$ and $l_e = 5mm$. Its cross-sectional area is $30mm \times 47mm$. Figure 5.2 shows a schematic of the electromagnet with related dimensions as well as the built electromagnet. Furthermore, the electromagnet requires a very high power supply as the coil shown in the figure has a resistance of around 8Ω, and a current of around $8A$ is required to saturate the material.

As for the mechanical part, its main purpose is to apply a stress as well as to help measure the position. To achieve such a purpose, a structure as shown in Figure 5.3 is constructed.

It consists of an MSMA holder and a movable platform. The holder fixes the MSMA in an upright position. The movable platform fixed on rollers then applies a stress on the material by means of dead weights placed on top of it. In the presence of a magnetic field, the MSMA deforms which in turns moves the platform. A laser displacement sensor then measures the displacement of the platform from which the deformation of the MSMA is deduced.

[1] We have only used the positive values 0-10V but the device can be used in the -10 to +10V range

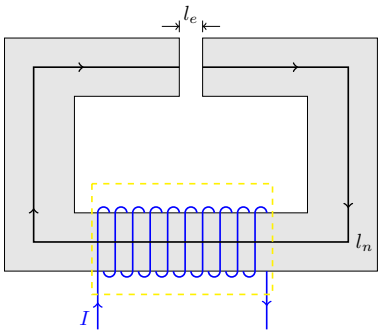

(a) Core+Solenoid+Air gap

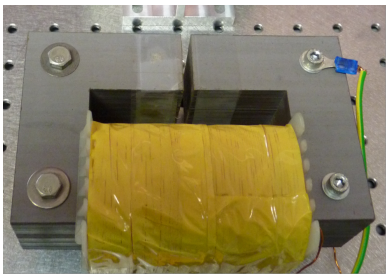

(b) Electromagnet used for experiments.

Figure 5.2: Electromagnet used to generate magnetic field.

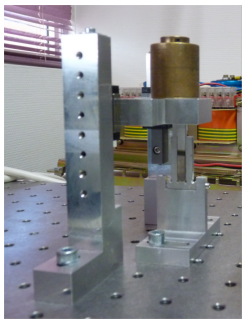

(a) Structure used to apply stress and measure displacement.

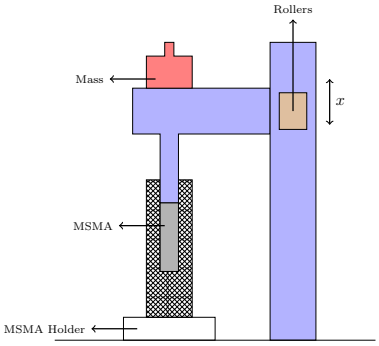

(b) Schematic of the structure.

Figure 5.3: Mechanical structure.

Figure 5.4 shows the assembled setup to make a very basic actuator. Various tests have been performed using this setup. To investigate the hysteretic nature of the material, a sinusoidal input has been applied to the electromagnet and the position was recorded. This was done for different values of stress and the results are shown in figure 5.5.

As seen in figure 5.5b, for a value of 0.54 MPa the actuator does not return back to any position even when the magnetic field is zero. This is typical of a dissipative material. Also for a few other values of stress, the material starts from a zero deformation goes to a certain maximum deformation but does not return back to the zero value. It oscillates about some other position. As expected from the theory, the weight (load) applied to the MSMA greatly influences its response.

Furthermore, the magnetic field produced in the air gap (where the material is located) is dependent on the current not the voltage (a certain

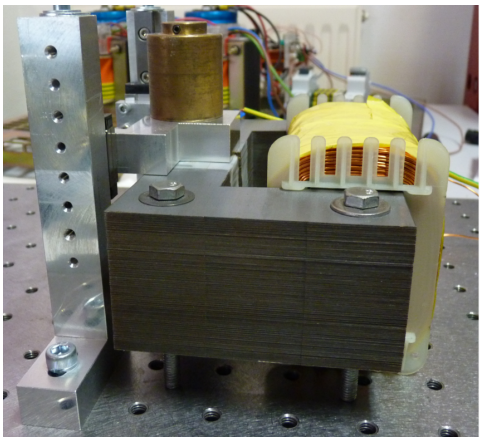

Figure 5.4: Assembled electric circuit and mechanical structure to make a crude actuator.

dynamics exists between the voltage and the current since in addition to resistance of the coil, inductance of the electromagnet core also influences it.). The relationship between current and position was therefore measured and figure 5.6 shows the hysteresis of the material only. An important information which can be inferred from the figure is that there is a certain critical value which must be reached before any positive or negative deformation takes place in addition to different paths taken while ascending and descending.

A first model of hysteresis using preisach was formulated and the algorithm implemented as discussed in [73]. It is seen that the preisach model can model hysteresis very precisely but unfortunately it is usually an input-output model. Without some kind of modifications, it cannot be used in our energetic framework. But on the other hand, it gives us some ideas about how to proceed with our hysteretic model.

The preisach plane Tan and Iyer [73], Iyer and Tan [29] which is a description of all possible hysterons in a plane also has some nice properties. Figure 5.9 shows the preisach plane and how it moves. All the hysterons used to model a system makes up the preisach plane. They are characterised by their switching values r and s. The preisach boundary which is the line seperating hysterons which are on and those which are off. This boundary has been shown to be passive in Gorbet et al. [23]. Passivity is very important for the control of port Hamiltonian systems as will be seen later. This area should be further investigated.

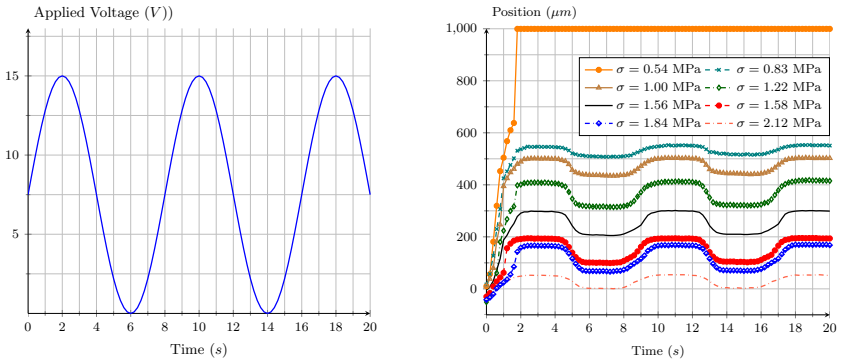

(a) Input waveform to coil.

(b) Position for different applied stresses.

Figure 5.5: Response of actuator to different stresses with an applied sinusoidal input.

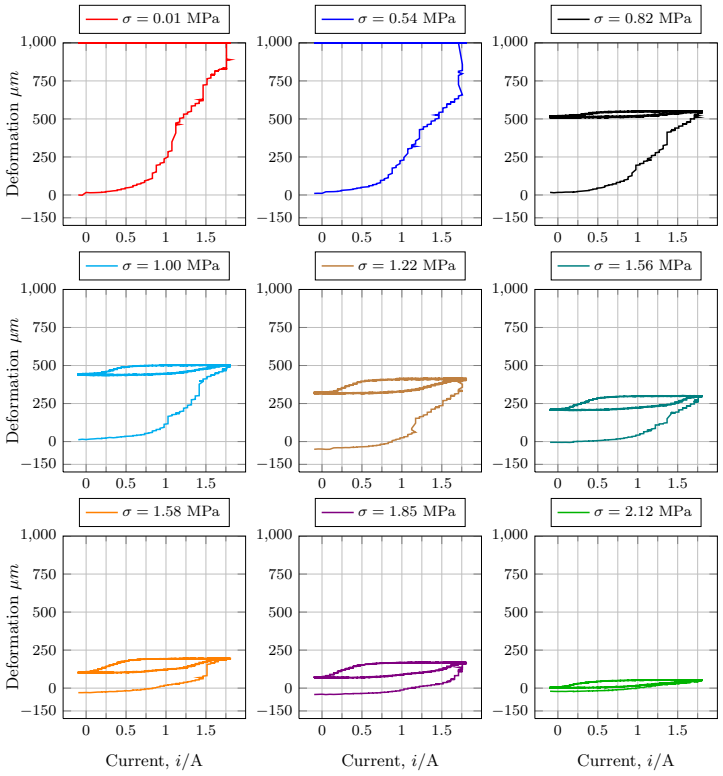

Figure 5.6: Hysteresis of actuator between current and position.

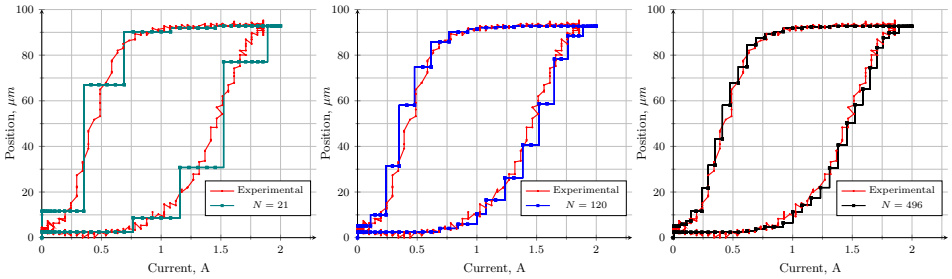

(a) N=21. (b) N=120. (c) N=496.

Figure 5.7: Preisach Model with different number of hysterons to model experimental curve. N is the number of hysterons.

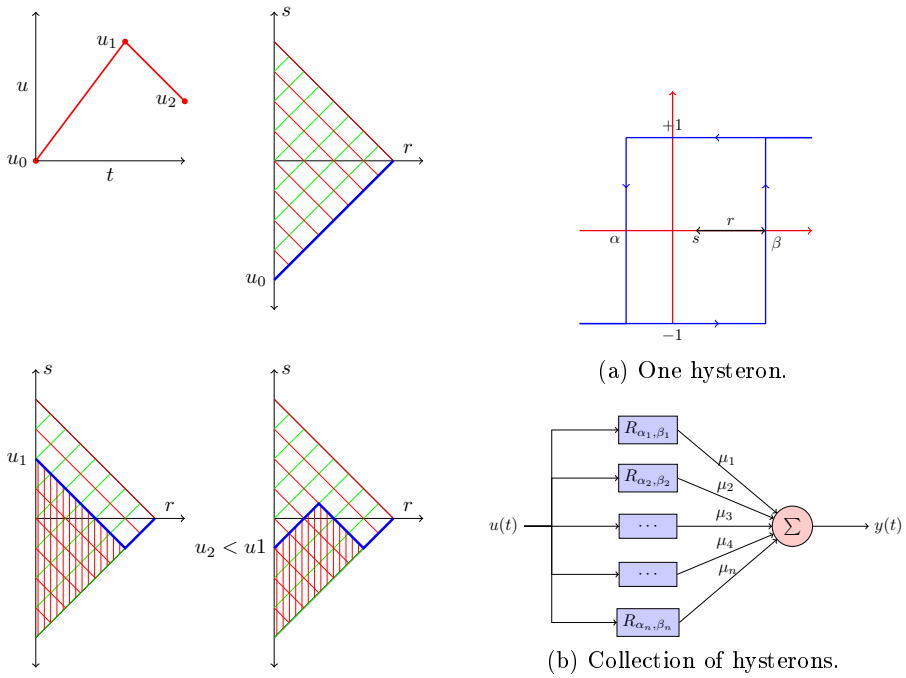

(a) One hysteron.

(b) Collection of hysterons.

Figure 5.8: Illustration of the preisach plane

Figure 5.9: Movement of Preisach plane

5.3 Control Perspectives

In an engineering context, to control means to make a system behave in a desired manner. In a more precise engineering definition it may be defined "to stabilise a system in a desired equilibrium point or trajectory". For linear systems, many techniques are available. They are described in [15, 14, 40] whereas the control of non-linear systems [76] revolves around Lyapunov's methods [35] and its variants. Lyapunov technique was originally used as an analysis tool but over time became useful technique for feedback control design.

Stability in the sense of Lyapunov is concerned with trajectories of a system when the initial state is near an equilibrium point. Roughly speaking, there are 3 types basic concepts: local stability, asymptotic stability and global stability. Local stability corresponds to the system trajectories staying continuously near the initial state. Asymptotic stability corresponds to trajectories starting sufficiently close to an equilibrium point actually converging to an equilibrium state as $t \to \infty$. Global asymptotic stability corresponds to *every* trajectory approaching a unique equilibrium point as $t \to \infty$.

Lyapunov-based control is a quite difficult task which involves the construction of a suitable Lyapunov function. The philosophy behind finding such a function derives from a physical observation: if the total energy of a mechanical (or electrical) system is continuously dissipated, then the system, *whether linear or nonlinear*, must eventually settle down to an equilibrium position [69]. Hence, stability may be concluded by examining the variation of a single *scalar* like function. This function is alike to the energy (or storage [79]) function. The main difference between many nonlinear control techniques is the way in which the Lyapunov method is constructed. This has given rise to many different nonlinear control schemes such as backstepping, adaptive [69] or Sliding Mode Control [35].

Passivity-based Control [49] is based on the fact that nonlinear systems are described by a storage function (which is a proper Lyapunov function). The goal then is to reshape the original energy function by means of a controller to achieve the control requirements (stability and/or tracking). The IDA-PBC (Interconnection and Damping Assignment-Passivity-based Control technique), uses the passivity properties of port Hamitonian systems,[49, 72] to modify the energy function such that it has a minimum at the *desired* equilibrium position.

5.3.1 Passivity Based Control

In the linear domain, most control problems have been solved using a signal processing point of view as for linear time-invariant systems, signals can be discriminated via filtering. The frequency domain can thus be used to design

control laws as exemplified by the robust control framework[67, 15]. However for nonlinear systems, frequency mixing makes this approach impossible as computations are far from obvious and very complex controls using very high gains are needed to minimise a large number of undesirable signals.

Most of the problem lies in the fact that no information about the structure is used. A shift in control paradigm is needed and this can be summarised in the catch phrase "control as energy exchanging entities". A detailed presentation of this energy-based approach is given in [52], [53] and [72].

Passivity can be defined as follows:

Definition 5.3.1. *The map $u \to y$ is passive if there exists a state functon $H(x)$, bounded from below, and a nonnegative function $d(t) > 0$ such that*

$$\underbrace{\int_0^t u^T(s)y(s)ds}_{\text{energy supplied to system}} = \underbrace{H(x(t)) - H(x(0))}_{\text{energy stored}} + \underbrace{d(t)}_{\text{dissipated energy}} \tag{5.1}$$

A very good example of a passive system is the mass spring damper. Consider such a system shown in Figure 5.10. It has an external force F applied to it which results in a displacement given by x. It also has a mass m, a spring constant, k and a coefficient of damping b.

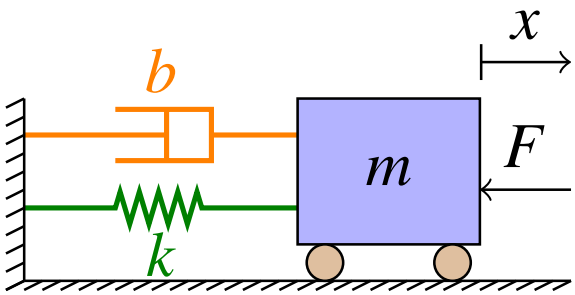

Figure 5.10: Example of a mechanical passive system.

If the velocity is taken as $v = \dot{x}$, we have

$$\begin{aligned}\int_0^t F(s)v(s)ds &= \int_0^t (m\dot{v} + kx(s) + bv(s))v(s)ds \\ &= \left(\frac{1}{2}mv^2(s) + \frac{1}{2}kx^2(s)\right)\Big|_0^t + b\int_0^t v^2(s)ds \\ &= H(x(t)) - H(x(0)) + b\int_0^t v^2(s)ds\end{aligned}$$

Since $d(t) > 0$ and there exists a function $H(x)$, the system is passive. Then if x^* is a global minimum of $H(x))$, with no input $u = F$, the system will

reach x^* asymptotically. This rate can be increased by setting the input u to

$$u = -K_{di}y \tag{5.2}$$

with $K_{di}^T = K_{di} > 0$.

This is the key idea behind passivity based control: use feedback.

$$u(t) = \beta(x(t)) \tag{5.3}$$

where $\beta(x)$ is a function of the states, so that the closed loop system is again a passive system with respect to the map $\beta \to y$. The closed loop energy $H(d)$, is then a global minimum at the desired point.

With (5.3), $\mathcal{H}_a$ the energy supplied to the system (minus) is

$$\mathcal{H}_a = -\int_0^t \beta^T(x(s))y(s) \tag{5.4}$$

then the closed loop energy is given by

$$\mathcal{H}_d(x(t)) = \mathcal{H}(x(t)) - \int_0^t \beta^T(x(s))y(s) = \mathcal{H}(x(t)) + \mathcal{H}_a(x(t)) \tag{5.5}$$

Most control strategies in the port Hamiltonian framework tries to change the original energy function $\mathcal{H}$ to a desired one $\mathcal{H}_d$ that has a minimum at the desired equilibrium. These techniques have been called IDA-PBC.

5.3.2 IDA-PBC Technique

The main idea behind the IDA-PBC technique [52] is to change the matrices J and R as well as the energy function H to achieve control objectives. Usually given a port Hamiltonian system, one aims at a closed loop Hamiltonian system such as

$$\dot{x} = (J_d(x) - R_d(x))\frac{\partial \mathcal{H}_d}{\partial x} \tag{5.6}$$

where $J_d = -J_d^T$ is the desired structure matrix, $R_d = R_d^T$ is the desired dissipation matrix and H_d is the desired Hamiltonian.

Propositioin 5.3.1. *Consider the system*

$$\dot{x} = f(x) + g(x)u \tag{5.7}$$

Assume there are matrices $J_d = -J_d^T$, $R_d = R_d^T > 0$ and a smooth function H_d that verify the so-called matching equation

$$f(x) + g(x)u = (J_d(x) - R_d(x))\frac{\partial \mathcal{H}_d}{\partial x} \tag{5.8}$$

Then the closed-loop with control $u = \beta(x)$,

$$\beta(x) = (g^T(x)g(x))^{-1}g^T(x)((J_d(x) - R_d(x))\frac{\partial \mathcal{H}_d}{\partial x} - f(x)) \tag{5.9}$$

is asymtotically stable.

Most of IDA-PBC relies on solving the matching equation (5.9) in one form or the other. The freedom in choosing J_d ,R_d and H_d has given rise to many variations of IDA-PBC (see [50, 52, 72]) for more details). Some are given below.

- In **Non-Parametrized IDA**, the structure and damping matrices are fixed, the matching equation is pre-multiplied by a left annihilator of $g(x)$ and the resulting PDE in H_d is solved.

- In **Algebraic IDA**, the desired Hamiltonian function H_d is first selected and then the resulting algebraic equations are solved for J_d and R_d.

- In **Parametrized IDA**, applicable mainly to underactuated mechanical systems, the knowledge of a priori structure of the desired Hamiltonian is used to obtain a more easy to solve PDE.

- In **Interlaced Algebraic-Parametrized IDA**, the PDE is evaluated in some subspace (where solution can be easily computed) and then matrices J_d, R_d are found to ensure valid solution of the matching equation.

One of the way to solve the matching equation which belong to the class of *non-parametrized IDA* is to introduce new matrices J_a, R_a and an energy function H_a. Then the matching equation to solve is:

$$[J(x) + J_a(x) - R(x) - R_a(x)]\frac{\partial \mathcal{H}_a}{\partial x} = -[J_a - R_a]\frac{\partial \mathcal{H}}{\partial x} + g(x)\beta(x) \quad (5.10)$$

where

$$J_a(x) = J_d(x) - J(x) \qquad R_a = R_d(x) - R(x) \quad (5.11)$$

and

$$\mathcal{H}_a(x) = \mathcal{H}_d(x) - \mathcal{H}(x) \quad (5.12)$$

The closed loop representation of the port-Hamiltonian is then given by:

$$\dot{x} = [J_d - R_d]\frac{\partial \mathcal{H}_d}{\partial x} \quad (5.13)$$

where $J_d = -J_d^T$ and $R_d = R_d^T \geq 0$ are the new interconnection and damping matrices. $\mathcal{H}_d$ is the new energy function.

We will apply this technique to both a magnetic levitation system and the MSMA actuator. Also, for the MSMA we will try an *algebraic IDA*.

Table 5.1: Identified Values

k	0.7107	Hm
a	0.5	m

5.3.3 Magnetic Levitation Example

Magnetic levitation presents a very interesting problem from the Port-Hamiltonian control point of view as the constitutive laws are not linear and there is an electro-mechanical coupling which should be taken into consideration while designing the control law. This model has been extensively studied and the results are published in [52, 72, 52]. We take this example here due to the similarity between the model and our MSMA actuator as seen from their bond graphs. They both contain magnetic circuit, a variable inductance and an energy field with 2 constitutive equations. We first work out the control law for this system using IDA-PBC techniques to get the basics right. This allows us to draw some parallel between the 2 systems.

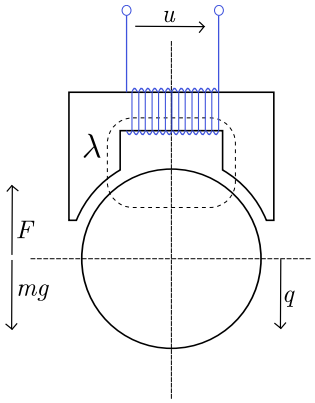

Figure 5.11: Magnetic Levitation System

Figure 5.11 shows the system we studied in bond graph. The position q is measured position from a datum line and λ is the flux linkage. The latter changes when q changes-$\lambda = L(q)i$. Usually for such systems, the inductance, L, varies with distance q. When $q = 0$ corresponds to the postion where the ball is fully in contact with the magnetic core. Then the inductance constitutive law can be taken as follows:

$$L = \frac{k}{a+q} \tag{5.14}$$

The identified values are given in table 5.1: And hence, the constitutive law relating i and λ is:

$$\lambda = L(q)i \tag{5.15}$$

For simulation purposes , we use the following values: the resistance of the coil is taken to be $R = 5\Omega$, the number of turns $N = 40$, gravitational acceleration is taken as $g = 9.81ms^{-2}$, the mass of the ball is $m = 0.05kg$, constants $k = 0.7107Hm$ and finally $a = 0.5m$.

Port Hamiltonian Model.

Using the model derived earlier, the equations of motion for the system are:

$$\begin{aligned} \dot{\lambda} &= -Ri + u \\ \dot{q} &= v \\ m\dot{v} &= F + mg \end{aligned}$$

Taking $x_1 = \lambda$, $x_2 = q$ and $x_3 = mv = p$, the Port Hamiltonian model can be written as:

$$\begin{aligned} \dot{x} &= \left[\underbrace{\begin{pmatrix} 0 & 0 & 0 \\ 0 & 0 & 1 \\ 0 & -1 & 0 \end{pmatrix}}_{\mathbf{J}} - \underbrace{\begin{pmatrix} R & 0 & 0 \\ 0 & 0 & 0 \\ 0 & 0 & 0 \end{pmatrix}}_{\mathbf{R}} \right] \frac{\partial \mathcal{H}}{\partial x} + \begin{bmatrix} 1 \\ 0 \\ 0 \end{bmatrix} u \\ y &= \begin{bmatrix} 1 & 0 & 0 \end{bmatrix} \frac{\partial \mathcal{H}}{\partial x} \end{aligned} \tag{5.16}$$

with $\mathcal{H}$ being the Hamiltonian of the system.

$$\mathcal{H}(\lambda, q, p) = \frac{x_1^2.(a + x_2)}{2k} - mgx_2 + \frac{x_3^2}{2m} \tag{5.17}$$

As a first design, we take $J_a = 0$ and $R_a = 0$, we see that equation (5.10) reduces to

$$[J - R]K(x) = G\beta(x) \begin{cases} -RK_1(x) = \beta(x) \\ K_2(x) = 0 \\ K_3(x) = 0 \end{cases} \tag{5.18}$$

and, consequently, H_a depends only on x_1 with resulting energy function

$$\mathcal{H}_d = \frac{x_1^2.(a + x_2)}{2k} - mgx_2 + \frac{x_3^2}{2m} + \mathcal{H}_a(x_1) \tag{5.19}$$

and Hessian

$$\begin{bmatrix} \frac{a+x2}{k} + \frac{d^2}{dx1^2} Ha\,(x1) & \frac{x1}{k} & 0 \\ \frac{x1}{k} & 0 & 0 \\ 0 & 0 & \frac{1}{m} \end{bmatrix} \tag{5.20}$$

Using software like $Maple^{©}$, it can be shown that the hessian has at least one negative eigenvalue (not positive definite) for whatever value of

$\mathcal{H}_a$. Hence though an equilibrium point x_2^* can be assigned, its asymptotic stability cannot be guaranteed.

The problem lies in the lack of coupling between mechanical and electrical domain. Therefore, we choose a J_a such that

$$J_a = \begin{bmatrix} 0 & 0 & -\alpha \\ 0 & 0 & 0 \\ \alpha & 0 & 0 \end{bmatrix} \tag{5.21}$$

which adds the required coupling and $R_a = 0$. Eq (5.10) then reduces to

$$-RK_1 - \alpha K_3 = \frac{\alpha x_3}{m} + \beta(x) \tag{5.22}$$

$$K_3 = 0 \tag{5.23}$$

$$\alpha K_1 - K_2 = -\frac{\alpha x_1 (a + x_2)}{k} \tag{5.24}$$

which after solving (5.24) gives the required H_a

$$\mathcal{H}_a = -\frac{x_1^3}{6k\alpha} - \frac{x_1^2(a + x_2)}{2k} + \Phi(\frac{x1}{\alpha} + x_2) \tag{5.25}$$

where Φ is an arbitrary function which can be used for equilibrium assignment and to assure stability of the closed loop Hamiltonian.

If $\tilde{x} = x - x^*$, α and $b > 0$ then a possible choice for Φ is:

$$\Phi(\frac{x1}{\alpha} + x_2) = mg \left[\left(\tilde{x_2} + \frac{\tilde{x_1}}{\alpha} \right) + \frac{b}{2} \left(\tilde{x_2} + \frac{\tilde{x_1}}{\alpha} \right)^2 \right] \tag{5.26}$$

where b is used to control the rate of convergence.

Then using (5.22), the control law is given by

$$\beta(x) = -R\frac{\partial H_a}{\partial x_1} - \frac{\alpha x_3}{m} \tag{5.27}$$

$$= \frac{R}{\alpha} \left[\frac{x_1^2}{2k} - mg \right] + \frac{Rx_1(a + x_2)}{k} - \frac{Rmgb}{\alpha} \left(\tilde{x_2} + \frac{\tilde{x_1}}{\alpha} \right) - \frac{\alpha x_3}{m} \tag{5.28}$$

$$= \frac{R}{\alpha} \left[\frac{x_1^2}{2k} - mg \right] + \frac{Rx_1(a + x_2)}{k} - K_p \left(\tilde{x_2} + \frac{\tilde{x_1}}{\alpha} \right) - \frac{\alpha x_3}{m} \tag{5.29}$$

The new energy function H_d then becomes

$$\mathcal{H}_d = -\frac{x_1^3}{6k\alpha} - mgx_2 + \frac{p^2}{2m} + mg \left[\left(\tilde{x_2} + \frac{\tilde{x_1}}{\alpha} \right) + \frac{b}{2} \left(\tilde{x_2} + \frac{\tilde{x_1}}{\alpha} \right)^2 \right] \tag{5.30}$$

With Hessian

$$\begin{bmatrix} \frac{-x_1}{k\alpha} + \frac{mgb}{\alpha^2} & \frac{mgb}{\alpha} & 0 \\ \frac{mgb}{\alpha} & mgb & 0 \\ 0 & 0 & \frac{1}{m} \end{bmatrix} \tag{5.31}$$

its eigenvalues are

$$\begin{bmatrix} \frac{1}{m} \\ \frac{1}{2}\,\frac{2\,mgk-x1+\sqrt{4\,m^2g^2k^2+x1^2}}{k} \\ -\frac{1}{2}\,\frac{-2\,mgk+x1+\sqrt{4\,m^2g^2k^2+x1^2}}{k} \end{bmatrix} \tag{5.32}$$

which are all positive for $x_1 < 0$ and $\alpha = 1$. In fact for positive value of x_1* the eigenvalues are

$$\begin{bmatrix} 20 \\ 0.688 \\ -0.8622 \end{bmatrix} \tag{5.33}$$

and for a negative value of x_1^*, they are

$$\begin{bmatrix} 20 \\ 1.84 \\ 0.31 \end{bmatrix} \tag{5.34}$$

b was taken as 1. Hence asymtotic stability can be assured for $x_1 < 0$. Since $x_1^* = \sqrt{2kmg}$, we take the negative value of it.

Taking a look at the open loop energy and the closed loop energy in figure 5.12, we see clearly that the shape of the hamiltonian has changed to have a minimum at the desired position.

Figure 5.13 show the result obtained when applying the control law above. It can be seen that the response is very oscillatory in nature.

Damping

Although our system is stable and we do reach the equilibrium point, the oscillatory response is very unsatisfactory. In practice, such large overshoots will make the ball either stick to the electromagnet or fall.

To remedy this situation, damping should be added. This is done by changing the structure of matrix R_a which was previously taken to be 0. The J_a matrix remains the same. We remove the damping from the electrical part (x_1) and adds it to the position (x_2) Our new $J_a - R_a$ matrix therefore becomes:

$$J_a - R_a = \begin{bmatrix} R & 0 & -\alpha \\ 0 & -R_\alpha & 0 \\ \alpha & 0 & 0 \end{bmatrix} \tag{5.35}$$

and

$$J_d - R_d = \begin{bmatrix} 0 & 0 & -\alpha \\ 0 & -R_\alpha & 1 \\ \alpha & -1 & 0 \end{bmatrix} \tag{5.36}$$

Using (5.10), the new set of PDEs to solve then are:

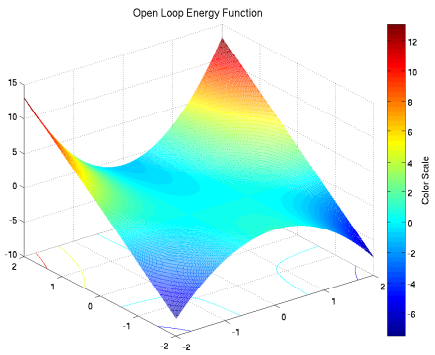

(a) 3D plot of Open loop energy function.

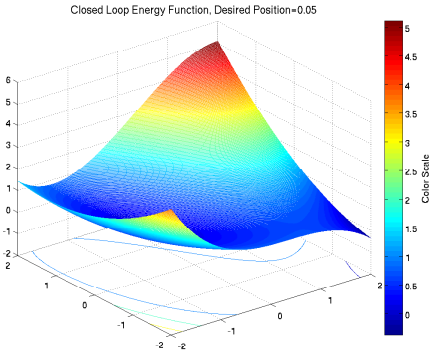

(b) 3D plot of Closedloop energy function.

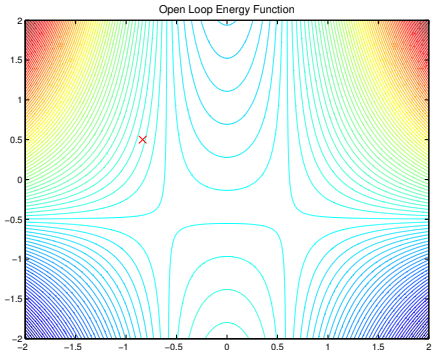

(c) Contour plot of Open Loop Energy Function

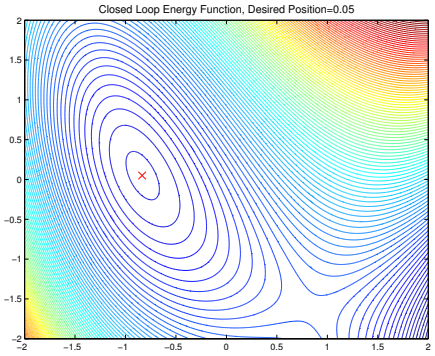

(d) Contour plot Closed loop Energy Function

Figure 5.12: Open Loop and Closed loop of H_d.Desired Position=0.05

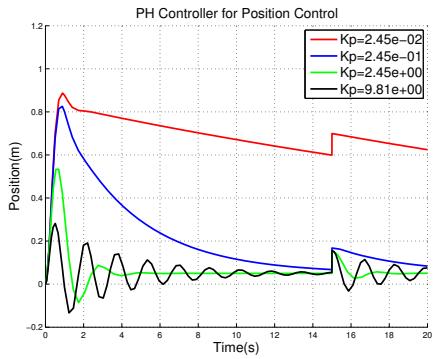

(a) Position Control of ball

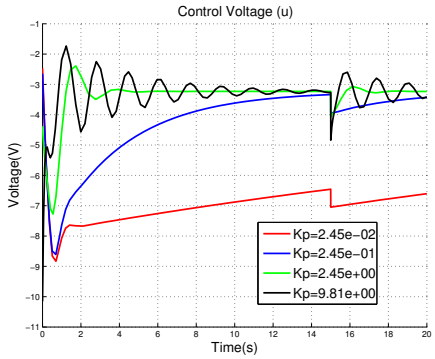

(b) Control Voltage u.

Figure 5.13: Postion Control and Control voltage when the designed control law is applied.

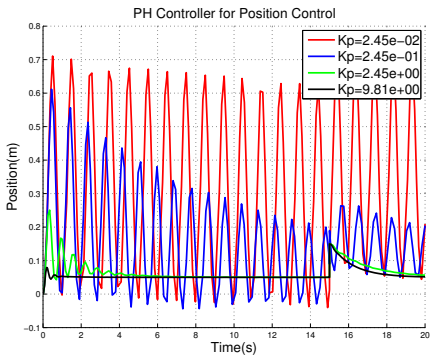

(a) Position Control of ball with damping.

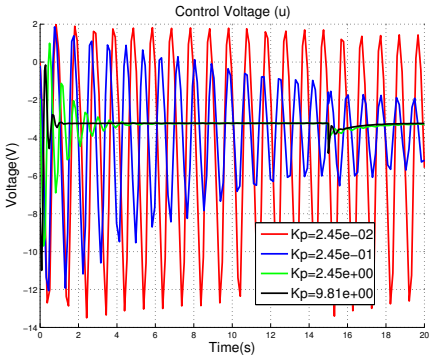

(b) Control Voltage u with damping.

Figure 5.14: Postion Control and Control voltage when damping is added to the sytem.

$$-\alpha K_3 = \frac{-Rx_1(a+x_2)}{k} + \frac{\alpha x_3}{m} + \beta(x) \tag{5.37}$$

$$-R_\alpha K_2 + K_3 = R_\alpha(\frac{\lambda^2}{2k} - mg) \tag{5.38}$$

$$\alpha K_1 - K_2 = -\frac{\alpha x_1(a+x_2)}{k} \tag{5.39}$$

Resolving 5.39, we get the following control law:

$$\beta(x) = \underbrace{\frac{Rx_1(a+x_2)}{k}}_{i} - Kp\left(\frac{\tilde{x_1}}{\alpha} + \tilde{x_2}\right) - \frac{\alpha x_3}{m} - (\frac{\alpha}{m} + KpR_\alpha)x_3 \tag{5.40}$$

which we apply to our simulation.

Figures 5.14 and shows we have drastically reduced the oscillations for gain values above 3. The control voltage maximum also is comparable to the our previous results. Also, disturbance rejection is also much improved.

This controller has the added advantage that instead of measuring the flux, we can use the current, i, directly.

Discussion

The control law seem to be working correctly in simulation. It should be noted that with an increase in value of K_p, we have smaller overshoot but unfortunately oscillation increases. Also, our open loop dynamics is given

by

$$\dot{\lambda} = \frac{-R\lambda(a+q)}{k}$$
$$\dot{q} = \frac{p}{m}$$
$$\dot{p} = mg - \frac{\lambda^2}{2k}$$

The equilibrim points ($\dot{x} = 0$) for $\lambda_d = x_1^* = \sqrt{2mgk}$ whatever the value of desired position $q_d = x_2^*$. In our simulation if we take a positive value for λ_d, we do obtain a stable system but then x_2 is not equal to x_2*. Only with a negative value of λ_d do we obtain the required result. This point should be further investigated. Having most of the basics we can now embark on the design of a control law for the MSMA actuator.

5.3.4 Control of MSMA Actuator

In this section, we detail a control strategy for the MSMA actuator using the previous concepts. It is assumed that all the parameters are known precisely. We will use the *non-parametrized* IDA-PBC technique and the *algebraic* IDA-PBC to give some possible ways of designing the control law of the MSMA Actuator. For simplicity, we will use a model consisting of one hysteron only therefore $z = z_1$. We will use a slightly different model as we will lump the force due to gravity mg with the potential energy of the material such that our matrix u depends only on the input voltage.

$$W_p(x_t, z) = \frac{1}{2}k(x_t - \gamma z l)^2 + mgx_t \tag{5.41}$$

Starting from the Hamiltonian

$$\begin{aligned}\mathcal{H}(\lambda, x_t, p_t, z) &= \mathcal{H}_e(\lambda, z) + \mathcal{H}_m(xt, p_t, z) \\ &= W_{mag}(\lambda, z) + W_k(p_t) + W_p(x_t, z) + W_h(z)\end{aligned} \tag{5.42}$$

where

- W_{mag} is the magnetic energy stored in the actuator.
- W_k is the kinetic energy of the mass.
- W_p is the potential energy of the mass.
- W_h is the energy stored in the equivalent capacitor of the hysteron.

The port Hamiltonian model with state variables $\mathbf{x} = \begin{bmatrix}\lambda & z & x_t & p_t\end{bmatrix}$ is then given by

$$\begin{bmatrix}\dot{\lambda}\\ \dot{z}\\ \dot{x}_t\\ \dot{p}_t\end{bmatrix} = \begin{bmatrix}-r & 0 & 0 & 0\\ 0 & g(.) & 0 & 0\\ 0 & 0 & 0 & 1\\ 0 & 0 & -1 & -b\end{bmatrix}\begin{pmatrix}\frac{\partial \mathcal{H}}{\partial \lambda}\\ \frac{\partial \mathcal{H}}{\partial z}\\ \frac{\partial \mathcal{H}}{\partial x_t}\\ \frac{\partial \mathcal{H}}{\partial p_t}\end{pmatrix} + \begin{bmatrix}1\\0\\0\\0\end{bmatrix}\Big(u\Big)$$

$$y = \begin{bmatrix}1 & 0 & 0 & 0\end{bmatrix}\begin{pmatrix}\frac{\partial \mathcal{H}}{\partial \lambda}\\ \frac{\partial \mathcal{H}}{\partial z}\\ \frac{\partial \mathcal{H}}{\partial x_t}\\ \frac{\partial \mathcal{H}}{\partial p_t}\end{pmatrix} = \begin{bmatrix}i\end{bmatrix} \tag{5.43}$$

At equilibrium, $\dot{\mathbf{x}} = 0$ we have:

$$u = r\frac{\partial \mathcal{H}}{\partial \lambda} \tag{5.44}$$

$$g\left(\frac{\partial W_{mag}}{\partial z} + \frac{\partial W_p}{\partial z} - \frac{\partial W_h}{\partial z}\right) = 0 \tag{5.45}$$

$$\frac{\partial \mathcal{H}}{\partial p_t} = 0 \tag{5.46}$$

$$-\frac{\partial \mathcal{H}}{\partial x_t} - b\frac{\partial \mathcal{H}}{\partial p_t} = -k(x_t - \gamma z l) - mg = 0 \implies z = \frac{1}{\gamma l}\left(x_t + \frac{mg}{k}\right) \tag{5.47}$$

From (5.47), we see that setting a desired x_t^*, a desired z^* is automatically set. Then (5.45) tells us that the expression within bracket should lie between the critical values for the hysteron:

$$f_{cr}^- \leq -\frac{1}{2}\frac{\lambda^2 K_1(\chi_a - \chi_t)}{(K_0 + K_1(\chi_a z^* + \chi_t(1 - z^*)))^2} + k(x_t^* - \gamma z^* l) + mg - k_h z^* \leq f_{cr}^+ \tag{5.48}$$

which in terms of current $i = \frac{\partial \mathcal{H}}{\partial \lambda}$ is equivalent to

$$-f_{cr}^- \leq -\frac{1}{2}K_1 i^2(\chi_a - \chi_t) + k(x_t^* - \gamma z^* l) + mg - k_h z^* \leq f_{cr}^+ \tag{5.49}$$

From (5.49), we see that we have some liberty in choosing i^* or λ^*. We can set it to '0' (we know the range must necessarily include zero as the critical values lies only in the first and third quadrant) to make calculations easier or choose it such that i is minimum and hence the power delivered to the actuator is minimised.

Using IDA-PBC technique as above we will try a simple feedback of the type $u = \beta(x)$ and we set $J_a = 0$ and $R_a = 0$. Applying equation 5.10, we

have

$$\begin{bmatrix} -r & 0 & 0 & 0 \\ 0 & g(.) & 0 & 0 \\ 0 & 0 & 0 & 1 \\ 0 & 0 & -1 & -b \end{bmatrix} \begin{pmatrix} K_1 \\ K_2 \\ K_3 \\ K_4 \end{pmatrix} = \begin{bmatrix} 1 \\ 0 \\ 0 \\ 0 \end{bmatrix} \beta(\mathbf{x}) \tag{5.50}$$

which gives

$$\begin{aligned} -rK_1(\mathbf{x}) =& \beta(\mathbf{x}) && (5.51)\\ g(.) =& 0; && (5.52)\\ K_3(\mathbf{x}) =& 0 && (5.53)\\ -K_3(\mathbf{x}) - bK_4(\mathbf{x}) =& 0 && (5.54) \end{aligned}$$

The system of equation above, wont yield a proper control as it depends only on λ

$$K_1(x) = \frac{\partial H_a}{\partial \lambda} \tag{5.55}$$

To remedy this problem we choose

$$J_a = \begin{bmatrix} 0 & \alpha & 0 & 0 \\ -\alpha & 0 & 0 & \beta \\ 0 & 0 & 0 & 0 \\ 0 & -\beta & 0 & 0 \end{bmatrix} \quad R_a = \begin{bmatrix} 0 & 0 & 0 & 0 \\ 0 & R_z - g(.) & 0 & 0 \\ 0 & 0 & 0 & 0 \\ 0 & 0 & 0 & 0 \end{bmatrix} \tag{5.56}$$

We thus add a coupling between z and λ as well as between z and p_t. To remove hysteresis and add a viscous damping to z, we add the term $R_z - g(.)$ to the dissipation matrix. The equation to resolve then become

$$\begin{bmatrix} -r & \alpha & 0 & 0 \\ -\alpha & -R_z & 0 & \beta \\ 0 & 0 & 0 & 1 \\ 0 & -\beta & -1 & -b \end{bmatrix} \begin{pmatrix} \frac{\partial \mathcal{H}_a}{\partial \lambda} = K_1 \\ \frac{\partial \mathcal{H}_a}{\partial z} = K_2 \\ \frac{\partial \mathcal{H}_a}{\partial x_t} = K_3 \\ \frac{\partial \mathcal{H}_a}{\partial p_t} = K_4 \end{pmatrix} = \begin{bmatrix} 0 & \alpha & 0 & 0 \\ -\alpha & -R_z + g(.) & 0 & \beta \\ 0 & 0 & 0 & 0 \\ 0 & -\beta & 0 & 0 \end{bmatrix} \begin{pmatrix} \frac{\partial \mathcal{H}}{\partial \lambda} \\ \frac{\partial \mathcal{H}}{\partial z} \\ \frac{\partial \mathcal{H}}{\partial x_t} \\ \frac{\partial \mathcal{H}}{\partial p_t} \end{pmatrix} + \begin{bmatrix} 1 \\ 0 \\ 0 \\ 0 \end{bmatrix} u(\mathbf{x}) \tag{5.57}$$

$$-rK_1 + \alpha K_2 = \alpha \frac{\partial \mathcal{H}}{\partial z} + u(x) \tag{5.58}$$

$$-\alpha K_1 - R_z K_2 + \beta K_4 = -\alpha \frac{\partial \mathcal{H}}{\partial \lambda} - R_z \frac{\partial \mathcal{H}}{\partial z} + g(.) + \beta \frac{p_t}{m} \tag{5.59}$$

$$-\beta K_1 - K_3 = \beta k(x_t - \gamma z l) \tag{5.60}$$

The above set of PDEs should be resolved to get $\mathcal{H}_a$ and then calculate the resulting $\mathcal{H}_d = \mathcal{H} + \mathcal{H}_a$. It will be one of the future works in this thesis. We now use an easier method, the *algebraic IDA* to find a control law.

Algebraic IDA

To apply the *algebraic* IDA-PBC technique, we fix a desired Hamitonian, $\mathcal{H}_d$ as follows

$$\mathcal{H}_d = \frac{1}{2C_1}(\lambda - \lambda^*)^2 + \frac{1}{2}C_2(z - z^*)^2 + \frac{1}{2}C_3(x_t - x_t^*)^2 + \frac{p_t^2}{2m} \tag{5.61}$$

This function being quadratic in the terms will have a minimum at the equilibrium values. The C_ns' determine the rate of convergence towards the minimum of the desired function. The desired interconnection matrix J_d couples z and p_t as well as λ and z. We also wish to remove hysteresis and replace it with a dissipation of viscous type which is done by changing the R_d matrix. The matching equation then becomes taking into account that

$$\frac{\partial \mathcal{H}_d}{\partial \lambda} = i - i^* \tag{5.62}$$

we have

$$\begin{bmatrix} -r & \alpha & 0 & 0 \\ -\alpha & -R_z & 0 & \beta \\ 0 & 0 & 0 & 1 \\ 0 & -\beta & -1 & -b \end{bmatrix} \begin{pmatrix} (i - i^*) \\ C_2(z - z^*) \\ C_3(x_t - x_t^*) \\ \frac{p_t}{m} \end{pmatrix} = \begin{bmatrix} -r & 0 & 0 & 0 \\ 0 & g(.) & 0 & 0 \\ 0 & 0 & 0 & 1 \\ 0 & 0 & -1 & -b \end{bmatrix} \begin{pmatrix} \frac{\partial \mathcal{H}}{\partial \lambda} \\ \frac{\partial \mathcal{H}}{\partial z} \\ \frac{\partial \mathcal{H}}{\partial x_t} \\ \frac{\partial \mathcal{H}}{\partial p_t} \end{pmatrix} + \begin{bmatrix} 1 \\ 0 \\ 0 \\ 0 \end{bmatrix} u(\mathbf{x}) \tag{5.63}$$

$$-r(i - i^*) + \alpha C_2(z - z^*) = -ri + u(\mathbf{x}) \tag{5.64}$$

$$-\alpha C_1(i - i^*) - R_z C_2(z - z^*) + \beta \frac{p_t}{m} = g\big(\frac{\partial W_{mag}}{\partial z} + \frac{\partial W_p}{\partial z} - \frac{\partial W_h}{\partial z}\big) \tag{5.65}$$

$$-\beta C_2(z - z^*) - C_3(x_t - x_t^*) - b\frac{p_t}{m} = -k(x_t - \gamma z l) - b\frac{p_t}{m} \tag{5.66}$$

In (5.66), if we set $C_3 = k$, we have $\beta = -\frac{\gamma l}{C_2}$. Substituting for β in (5.65) we have,

$$\alpha = -\frac{1}{(i - i^*)}\left(g(.) + R_z k(z - z^*) + \frac{\gamma l}{C_2}\frac{p_t}{m}\right) \tag{5.67}$$

And finally substituting for α in (5.64) we get for the control voltage $u(\mathbf{x})$:

$$u(\mathbf{x}) = ri^* - \frac{k(z - z^*)}{(i - i^*)}\left(g(.) + R_z k(z - z^*) + \frac{\gamma l}{C_2}\frac{p_t}{m}\right) \tag{5.68}$$

Eq (5.68) is the control action which modifies our enegy function such that it is as desired. The parameter R_z is the amount of damping or dissipation on z we can remove it all together which will result in a pure conversion of energy between the electrical part and the mechanical part just by setting $R_z = 0$.

5.4 Discussion

In this chapter, we detailed our experimental setup and gave some basic experimental results. This setup was used to test the behaviour of the material. During our experiment, we discovered that we could not find any difference in the value of magnetic field whether the material is present or no. This is unusual as the material modifies the reluctance of the circuit. The problem lies in the fact that we built an air gap with an area which is approximately 5 times more than the area of the MSMA. As the permeability of the MSMA is between 2 and 65, the changes it caused to the magnetic field in the air were not discernible. This parameter is essential for the identification of λ and therefore we could not measure the inductance of the MSMA when its length changes. One possible solution would be to follow the model and built a setup which has an air gap just $2-3\%$ bigger than the area of the MSMA.

In the control section, we saw that the port-Hamiltonian framework provides a way to incorporate knowledge and structure into the design of the controller. Depending on how we want our system to behave we can modify the interconnection matrix and the dissipation matrix. The resulting control laws are very tedious to calculate but the magnetic levitation has shown that the performances are very good. So if proper design of the control law is done for the MSMA, we can expect similar results. Furthermore, we have seen a way to exploit hysteresis in our controller, it has a degree of freedom in the dead zone, where a range of values exist for which the dynamics on z is 0. This can be exploited to either use a control input which minimises energy or make calculations easier. Another interesting feature which appeared in our control is that it seems we need not invert hysteresis. This needs more investigation. And finally this first control law need to be implemented to validate its value.

Chapter 6

Conclusion

General Conclusions

Magnetic Shape Memory Alloys (MSMA) promises to enhance and add to the different types of smart materials already available. In doing so, it can only further increase the number of applications of the smart material family. MSMA present some advantages that can be exploited in new areas, including actuation, energy harvesting or sensor applications. For example and contrary to other smart materials, which needs an energy source to bias them, MSMA only require a pair of magnets (magnetic field-'free of cost') and some wires to make a coil around it. Then by Faraday's law, every time the material is compressed or extended by an external mechanical force, a voltage is induced in the coil which can be recuperated.

The characteristics and properties of MSMA are nevertheless unusual and only a good understanding of their physics seems adequate to use them smartly. From our point of view, simple control laws and linear models miss out completely on their main possibilities and potential applications.

The objective of this thesis was to confront the true characteristics of Magnetic Shape Memory Alloys without skipping its non-linear and hysteretic behaviour. As this thesis has shown a deep understanding of its physics is needed for both its modelling and control. Understanding the material is not only needed to design the actuator but also to design control laws which can work in an optimum fashion. Moreover, such control laws must be compatible with the thermodynamics of irreversible processes to take advantages of non-linearity and hysteresis phenomena.

Several goals were targeted during in this thesis. The first one was to continue the work of previous thesis conducted at the FEMTO-ST Institute by J. Y. Gauthier. The perspectives outlined in his thesis were investigated in Chapter 2. Simulation problems encountered in his thesis were pinned down to the non-minimal dynamical systems, causality problems and kinematics constraints which gave rise to DAE (Differential-Algebro equations)

which resulted in algebraic loops. We proposed a reduction method to obtain a minimal dynamical system and to remove the constraints from the state variables. The promising work of Gauthier on "canonical" Hamiltonian modelling was also cast into the "true" port-Hamiltonian framework, that allows an easy interconnection between subsystems. Chapter 2 also revealed some inconsistencies in the way the hysteresis phenomena and dissipation in the materials were taken into account.

Chapter 3 was devoted to the in depth understanding of the MSMA using thermodynamics. From a distributed parameters system the modelling of the actuator was transformed into a lumped parameter system. Energetic consideration were studied and "piece wise" non-linear constitutive behaviour laws were proposed. The construction of the lumped parameter model was motivated by its subsequent use for control. The use of thermodynamic internal variables, such as z proposed by Gauthier, were used all around the chapter. Two important things to retain from this chapter are the derivation of the thermodynamics driving force f for lumped parameter and π for distributed parameter as well as the derivation of the total strain. Also, the total magnetic energy and mechanical energy taking into account saturation and non-linearities of the material were derived. This paved the way for a more consistent energetic representation than was available until now.

From previous chapters, it was seen that thermodynamics was not sufficient to derive the dynamics of the systems. Notably that thermodynamics is a static theory. So Chapter 4 was then devoted to derive the dynamics. As a system always consists of 2 parts, the structure which is how its elements are connected and the physics (constitutive relation), a bond graph approach was adopted which combines both in one theory. It has provided great insight into how and where each element go and how they must be related to each other. In addition to providing a better understanding of the material and the actuator, it has been a great help in understanding where hysteresis goes and how to approach it from an energetic point of view. As we were already using an internal variable z which has a power conjugated effort variable, it was only natural that the hysteresis resides in what we call the 'MSMA' domain. And it has come to light that the dynamics on the z variable is greatly governed by the hysteresis. We then formulated it as having both a conservative and a dissipative part modelled with simple elements-a generalised capacitor and a non linear generalised resistor. We thus were able to formulate it energetically. From there on, it was simple to put it into the port-Hamiltonian framework as both bond graphs and port Hamiltonian employ the energy/co-energy variables. The corresponding results are of great interest to the port-Hamiltonian community as it is a theory proposed mainly for conservative systems. Very few works in this community has been done regarding complex type dissipation. Most of time

simple dissipative phenomena were treated like viscous quadratic dissipative potential. Furthermore, the bond graph representation is not limited to the actuator. With some modifications it can be used for sensor applications, for the push-pull actuator as well as for energy harvesters.

The goal of Chapter 5 was to set the basics for control and experimental validation. We showed some experimental results and have discussed some limitations of the setup. Furthermore some preliminary work on the preisach operator was done. As the preisach has been studied extensively, we intended to learn from it so as to propose our own hysteresis model. Our model of hysteresis is seen to have the same form as the hysteresis present in the material. Unlike the preisach which with one hysteron can model only 2 values, our model with one hysteron is continuous. But to approximate the real hysteresis, we also need a number of hysterons but we believe it will be lower than for a preisach model. For control purposes, we studied a magnetic levitation actuator which is very common in port Hamiltonian literature. Its structure and dynamics is similar to our MSMA actuator and thus we derived some important understandting to design our control law. An *algebraic IDA* method has yielded a first controller which needs to be tested. One interesting feature has appeared while designing the controller. Hysteresis can be positively used as it provides a dead zone where we have a choice of values for our control input.

Perspectives and Future Works

The main perspective of this work should be in refining the model to take into account the temperature. Hysteresis dissipates heat and from the experimental data we see that we have a hysteresis curve with a large width. This implies that much heat is produced. Its effects should be taken into account through thermodynamics.

Secondly, more detailed investigation both qualitative and quantitative of the hysteresis is needed. One direction could be the identification of the critical values of our hysterons and their spring constants. In classic hysteresis, it is a static curve that is identified or fitted. In our case, the identifcation need to be perfomed on a dynamic curve. A preisach-like plane and boundary should be developed to characterise a distribution of hysterons.

Thirdly, the port Hamiltonian seems to be the appropriate framework to deal with hysteresis. Since hysteresis involve the creation of entropy, a perspective would be to reformulate it into the irreversible port-Hamiltonian framework [58] and use thermodynamic availability as a Lyapunov function.

Also, a better experimental testbed should be used and nowadays better MSMA material are on the market. The one we used in our experiments required a very high magnetic field of around 0.65 T which is not trivial

for the electronics involved. The material on the market now have a saturation value of 0.3 T which greatly reduces the complexity and cost of the electronics.

Finally for the control part, various forms of IDA-PBC should be tried with different energy function to yield the best results. One thing to consider is the path dependence. In hysteretic material, many paths exists to reach the same point. One control strategy could be to take the path which require minimum energy or which maximises output.

Appendix A

Linear Graph Theory in Brief

A.1 Linear Graphs

To characterize any system, the topology as well as the constitutive equations are required. In this section we present the graph theory approach and we show how the topology of the circuit can be derived. We will adopt an electrical terminology such as branch current and branch voltage and later we will generalise to other domains. Figure A.1 shows a two terminal lumped element and its associated linear graph. Usually, we associate a reference direction for the branch voltage and the branch current. We usually take a current as positive when it enters a branch through the positive terminal and leaves the branch through the negative.

Figure A.2 shows the linear graph of an RLC circuit. The graph consists of nodes (circles) and branches (lines). Branches originate and terminate at nodes. Branches also have a direction associated with them and hence this type of graph is called an oriented graph or digraph (directed graph).

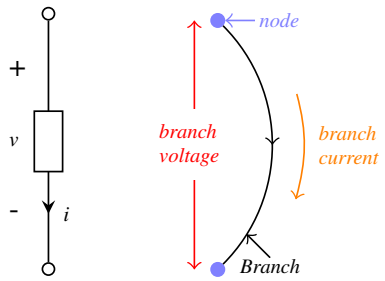

Figure A.1: Two terminal lumped element and its associated linear graph.

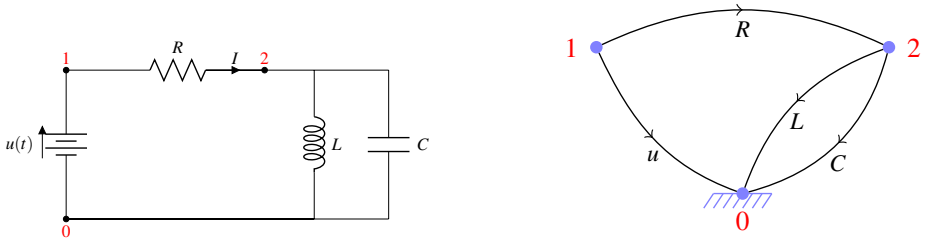

(a) RLC circuit (b) Linear graph

Figure A.2: Linear graph example.

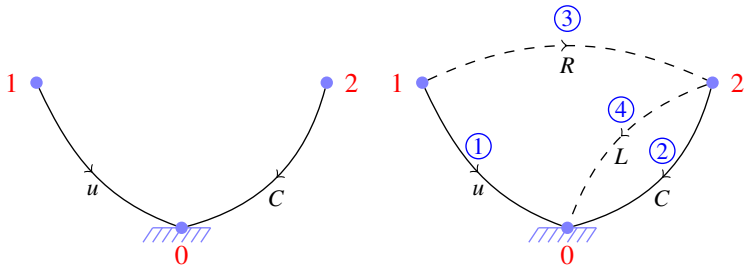

Figure A.3: The tree is on the left whereas the remaining branches added to the tree are called links are on the right.

A.2 Trees and links

To derive the topology, we introduce the concept of *trees* and *links*. A tree is defined as the path through all nodes without making a loop and the links are the remaining branches. Consider the graph in A.3, it has $n_t = 3$ nodes and $b = 4$ branches. Then the tree consists of $n = n_t - 1 = 2$ branches known as *tree branches* and $l = b - n_t = 2$ links. In [26], it is shown that the link currents fix all the current values in the circuit whereas the tree voltages fix all the voltages in the circuit. Hence by either tree voltages or branch currents can be used to completely characterize the network behaviour. Loop-sets and cut-sets are the tools for doing so.

A.3 Loop Set and Cut Set

A loop set is the set of loops obtained by adding one link at a time to a tree. These loops are called fundamental loops. They are the minimum number of loops required to express the dependent voltages (link voltages) in terms of independent voltages (tree branch voltage). To each fundamental loop, KVL is applied to obtain the necessary relationships. While traversing the loop, the direction of the link voltage is taken as positive. A closer look at the

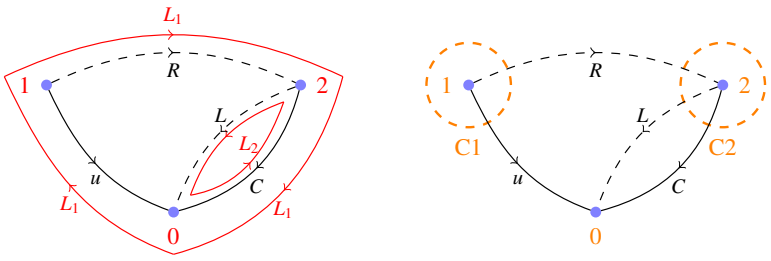

Figure A.4: A loop set(left) contains only 1 link whereas a cut set(right) cuts only 1 tree branch.

loop-set of figure A.4 also reveals that the branch currents can be expressed as the link currents.

The loop sets then give the following equations if taking the only link current of a loop as the positive direction.

	u	v_C	v_R	v_L
	A_1	A_2	A_3	A_4
L_1	-1	1	1	0
L_2	0	-1	0	1

which reduced to

$$\underbrace{\begin{bmatrix} -1 & 1 & 1 & 0 \\ 0 & -1 & 0 & 1 \end{bmatrix}}_{B} \begin{bmatrix} u \\ v_C \\ v_R \\ v_L \end{bmatrix} = \begin{bmatrix} 0 \\ 0 \\ 0 \\ 0 \end{bmatrix} \tag{A.1}$$

For the tree branch current, it is clearly seen that

$$i_C = i_R - i_L$$
$$i_u = -i_R$$

which can be written as

$$\underbrace{\begin{bmatrix} i_u \\ i_C \\ i_R \\ i_L \end{bmatrix}}_{j} = \underbrace{\begin{bmatrix} -1 & 0 \\ 1 & -1 \\ 1 & 0 \\ 0 & 1 \end{bmatrix}}_{B^T} \underbrace{\begin{bmatrix} i_R \\ i_L \end{bmatrix}}_{i} \tag{A.2}$$

Hence in a loop set, we have $Bv = 0$ and $j = B^T i$ where j is the currents in the circuit and i are the loop currents (same as link currents).

A cut set is a set obtained by splitting a graph into 2 separate graphs by removing one of the tree branches. These cut sets are called fundamental cut set. They are the minimum amount of cut set needed to express the dependent current (tree branch) currents in terms of the independent currents (link currents). To each cutset, KCL is then applied to obtain:

	i_u	i_C	i_R	i_L
	A_1	A_2	A_3	A_4
C_1	1	0	1	0
C_2	0	1	-1	1

$$\underbrace{\begin{bmatrix} 1 & 0 & 1 & 0 \\ 0 & 1 & -1 & 1 \end{bmatrix}}_{Q} \begin{bmatrix} i_u \\ i_C \\ i_R \\ i_L \end{bmatrix} = 0 \tag{A.3}$$

Looking now at each cut-set, we notice that each voltage can be express as a linear combination of tree-branch voltages.

$$\underbrace{\begin{bmatrix} u \\ v_C \\ v_R \\ v_L \end{bmatrix}}_{v} = \underbrace{\begin{bmatrix} 1 & 0 \\ 0 & 1 \\ 1 & -1 \\ 0 & 1 \end{bmatrix}}_{Q^T} \underbrace{\begin{bmatrix} u \\ v_C \end{bmatrix}}_{e} \tag{A.4}$$

Loop sets and cut sets can be used alone to establish circuit topology. To give the topology in terms of currents, loop set is used whereas cut sets are used to give the topology in terms of voltages.

As long as there is an algebraic relationship between the branch voltage and the branch current, any one of them is suitable. But for networks, containing inductors or capacitors where this relationship is a differential equation usually of type

$$v_L = L\frac{di_L}{dt} \tag{A.5}$$

$$i_C = C\frac{dv_C}{dt} \tag{A.6}$$

using loop set alone or cut set alone is not sufficient. This is due to the causality of these elements which will be discussed shortly. Hence a mixture of cut set and loop set should be used to model the circuit.

A.4 State-Space formulation of Linear Graph Network

A state space formulation requires that the model be in the form

$$\dot{x} = f(x, u, t) \tag{A.7}$$

Hence for capacitors, the state variable would be v_c and for inductors it would be i_L. To evaluate $C\frac{dv_C}{dt}$, we will need the state variables and possibly the inputs. Therefore, a cut-set equation will give the necessary equation. Similarly, to find $L\frac{di_L}{dt}$, a loop equation is needed.

Referring to figure A.2, the cut-set equation is:

$$C\frac{dv_C}{dt} + i_L - i_R = 0 \tag{A.8}$$

$$C\frac{dv_C}{dt} + i_L - \frac{u - v_C}{R} = 0 \tag{A.9}$$

$$\frac{dv_C}{dt} = -\frac{i_L}{C} - \frac{v_C}{RC} + \frac{u}{RC} \tag{A.10}$$

$$\tag{A.11}$$

the loop-set equation becomes

$$L\frac{di_L}{dt} - v_C = 0$$

$$L\frac{di_L}{dt} = v_C$$

$$\frac{di_L}{dt} = \frac{v_C}{L}$$

And the state space equation is obtained as:

$$\begin{bmatrix} \frac{dv_C}{dt} \\ \\ \frac{di_L}{dt} \end{bmatrix} = \begin{bmatrix} -\frac{1}{RC} & -\frac{1}{C} \\ \\ \frac{1}{L} & 0 \end{bmatrix} \begin{bmatrix} v_C \\ \\ i_L \end{bmatrix} + \begin{bmatrix} \frac{1}{RC} \\ \\ 0 \end{bmatrix} u \tag{A.12}$$

In [39], a systematic procedure is given to find the state space equations which is as follows:

1. Find a tree with all voltage sources and capacitors and possibly resistors.

2. Put all inductances in the links or co-tree and remaining resistors.

3. Use tree branch capacitor voltages and link inductor currents as state variables.

4. Write a fundamental cut set equation for each capacitor and a fundamental loop equation for each inductor and express everything in terms of the state variables and inputs.

The choice of state variables is not fixed to inductor currents and capacitor voltages. *Inductor fluxes* and *capacitor charges* are also an appropriate choice for state variables. In fact, from an energetic point of view, these variables are much more significant. Using $\phi(t) = Li(t)$ and $q(t) = Cv(t)$ for fluxes and charges respectively, the cut-set equation becomes

$$\dot{q} = -\frac{\phi}{L} + \frac{u}{R} - \frac{q}{CR} \tag{A.13}$$

and the loop-set equation becomes

$$\dot{\phi} = \frac{q}{C} \tag{A.14}$$

then the state space representation is given as:

$$\begin{bmatrix} \dot{q} \\ \dot{\phi} \end{bmatrix} = \begin{bmatrix} -\frac{1}{CR} & -\frac{1}{L} \\ \frac{1}{C} & 0 \end{bmatrix} \begin{bmatrix} q \\ \phi \end{bmatrix} + \begin{bmatrix} \frac{1}{R} \\ 0 \end{bmatrix} u \tag{A.15}$$

which, if we choose $\frac{q}{C}$ and $\frac{\phi}{L}$ as state variables, can be rewritten as

$$\begin{bmatrix} \dot{q} \\ \dot{\phi} \end{bmatrix} = \begin{bmatrix} -\frac{1}{R} & -1 \\ 1 & 0 \end{bmatrix} \begin{bmatrix} \frac{q}{C} = v_C \\ \frac{\phi}{L} = i_L \end{bmatrix} + \begin{bmatrix} \frac{1}{R} \\ 0 \end{bmatrix} u \tag{A.16}$$

which is in fact the port-Hamiltonian [52] representation of the system if we take the output to be the dual of the input $\frac{1}{R} \cdot u = I(t)$, that is to say if we take the output as $y(t) = u(t)$.

In brief we see that any network consisting of b branches has $2b$ unknowns of which b are branch currents (through variable) and b branch voltages (across variables). If s branches are active sources, we are left with $2b - s$ unknowns. b equations are given by either cut set or loop set and the remaining $b - s$ equations can be obtained by the elemental – constitutive – equations relating the *across* variable to the *through* variable.

Appendix B

Magnetism theory in Brief

This section establishes the basics we will need to model complicated magnetic systems. Starting from Maxwell equations ("field equations"), we derive the necessary equations needed to model lumped parameter systems.

$$\nabla \cdot \mathbf{D} = \rho \tag{B.1}$$

$$\nabla \cdot \mathbf{B} = 0 \tag{B.2}$$

$$\nabla \times \mathbf{E} = -\frac{\partial \mathbf{B}}{\partial t} \tag{B.3}$$

$$\nabla \times \mathbf{H} = \mathbf{J} + \frac{\partial \mathbf{D}}{\partial t} \tag{B.4}$$

We use a quasistatic version of these laws, i.e we neglect the coupling terms between electric and magnetic field ($\frac{\partial \mathbf{D}}{\partial t} \approx 0$). Such an assumption allows us to determine electric and magnetic characteristics independently.

B.1 Magnetic Work

To study the magnetic properties of matter one requires the expression for the work done in magnetizing a material. We should exert some care in defining precisely the system under consideration since one can easily obtain different expressions for work. We will consider a process in which an initially unmagnetized sample of a material is magnetized. Such a change can be brought about by application of a magnetic field. The magnetic field can come from various sources such as solenoids, permanent magnets or electromagnets. In all such cases, the sample is situated in an *externally applied field*.

B.1.1 Magnetics in vacuum

Here we will consider the case where the material is magnetized by a solenoid as shown in figure B.1. The solenoid has N turns and a cross-sectional area

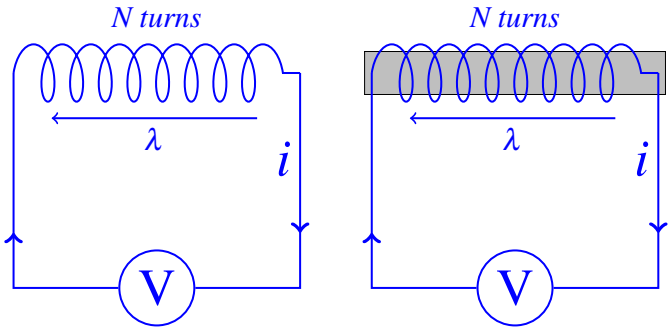

Figure B.1: Solenoid with and without material

A. $n = \frac{N}{l}$ is the number of turns per unit length if l is the length of the solenoid. A current in an *infinite length*[1] solenoid produces a magnetic field, H_0, parallel to the axis of the solenoid given by

$$H_0 = ni = \frac{N}{l}i \tag{B.5}$$

If B is the magnetic induction parallel to the axis of the solenoid the total magnetic flux through the solenoid is

$$\phi = BA \tag{B.6}$$

and the magnetic flux linkage through the solenoid is

$$\lambda = N\phi = NBA = (nl)BA \tag{B.7}$$

A change in flux induces an E.M.F by Faraday law in the electrical circuit equal to

$$v_{ind} = -N\frac{d\phi}{dt} = -\frac{d\lambda}{dt} = -(nl)A\frac{dB}{dt} \tag{B.8}$$

Hence for the battery V to keep the same current in the circuit, work has to be done against this induced E.M.F. Therefore the battery in a time interval of dt does work an amount of work equal to

$$dW_b = v_{ind} i\, dt \tag{B.9}$$

Replacing i and v_{ind} of (B.9) by (B.8) and (B.5), we get

$$dW_b = V H_0 . dB \tag{B.10}$$

where $V = Al$ is the volume of the solenoid.

[1] The hypothesis of *infinite length* is done here just to simplify the computation of the forth Maxwell equation (B.4) but it does not restrict the main ideas of this section.

B.1.2 Magnetization in matter

Now we consider the case where the material is inside the solenoid. Without the material the magnetic induction is $B = \mu_0 H_0$, whereas with the material, it becomes $B = \mu_0 \mu_r H_0$ which in terms of magnetization can be written as $B = \mu_0(M + H_0)$ where M is the magnetic moment per unit volume of the matter or more simply the magnetization of the matter. Replacing the latter relation in (B.10) we get

$$\begin{aligned} dW_b =& V H_0 \mu_0 dH_0 + V H_0 \mu_0 dM \\ dW_b =& d(V \frac{1}{2} \mu_0 H_0^2) + V \mu_0 H_0 dM \\ dW_b =& d\Big(\int \frac{1}{2} \mu_0 H_0^2 dV \Big) + \int (\mu_0 H_0 dM) dV \end{aligned}$$

Now the total magnetic moment is $m = \int M \, dV$ and hence the above equation becomes

$$dW_b = d\Big(\int \frac{1}{2} \mu_0 H_0^2 dV \Big) + \mu_0 H_0 dm \tag{B.11}$$

The first term on the right hand side of (B.11) is the magnetic energy stored in the empty solenoid and the second term is the work done on the matter specimen in changing its magnetization. W_b is therefore the sum of work done to create the magnetic field and to magnetize the material. Total work done to magnetize the material only, W_m can be written as

$$dW_m = \mu_0 H_0 dm \tag{B.12}$$

B.2 Magnetic Circuits

Another very useful way by which magnetic quantities may be quantified is by postulating the existence of magnetic monopoles. Though fictitious and hypothetical in nature, they are very useful and gives access to all the machinery of electric fields. Although not physical, calculation considering a pair of magnetic monopoles producing the same effect as a magnetic dipole, and then gives similar results. Hence just as in electrostatics, we will assume that the force derives from a scalar potential.

B.2.1 MMF, reluctance and scalar magnetic potential

When a current flows in the coil, a magnetic flux is produced around the circuit. In order to carry a unit magnetic pole around the circuit against the magnetic field, a certain amount of work is required. Analogue to electromotive force in electrostatics, this quantity is called the magnetomotive force (mmf).

If l is the mean path of the magnetic circuit and a current i flows into the circuit then the force acting inside the winding is the magnetic field

$$H = \frac{Ni}{l} \tag{B.13}$$

The mmf is therefore the work done, such that

$$\text{Work done=Force} \times \text{distance} \tag{B.14}$$

$$mmf = Hl = \frac{Ni}{l}l = Ni \tag{B.15}$$

Making use of the forth Maxwell equation (B.4) in integral form, it corresponds to:

$$mmf = \int_A \nabla \times \mathbf{H}\, dS = \oint_{\partial A=\Gamma} \mathbf{H}.dl = \int_A \mathbf{J} dS = Ni \tag{B.16}$$

An equivalent to *resistance* called **reluctance**,$\mathcal{R}$, can also be defined. The total magnetic flux, ϕ, is given by

$$\begin{aligned}\phi &= BA = \mu_r\mu_0 HA = \mu HA \\ &= \mu\frac{Ni}{l}A \\ &= \frac{Ni}{\frac{l}{A}\cdot\frac{1}{\mu}} \\ &= \frac{mmf}{\mathcal{R}}\end{aligned}$$

with $\mathcal{R} = \frac{l}{\mu A}$ the reluctance of the magnetic circuit. As compared to electric circuits, we can say that ϕ is equivalent to *current* and *reluctance* is equivalent to *resistance* while emf and mmf are analogous. These concepts are very useful to design circuits in the static case.

From (B.16), we see that the integration of H around a closed contour is equal to the net current crossing the surface enclosed by the contour. From this definition, we can define a scalar magnetic potential just as we define a scalar electric potential.

$$\int_a^b E\, dl = \varphi_e(a) - \varphi_e(b) = v_{e\,ab}, \text{ electric potential difference} \tag{B.17}$$

$$\int_a^b H\, dl = \varphi_m(a) - \varphi_m(b) = v_{m\,ab}, \text{ magnetic potential difference} \tag{B.18}$$

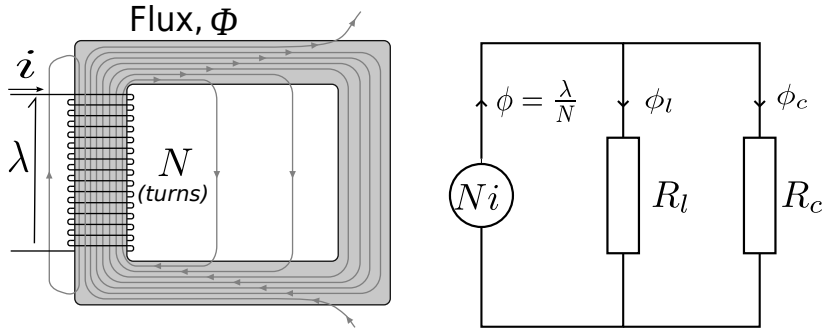

(a) Magnetic Field Lines. (b) Magnetic Circuit.

Figure B.2: Magnetic Circuit.

B.2.2 Application to a simple magnetic circuit

Consider the simple magnetic circuit of the figure B.2: a coil supplied by a cuurent i is wounded around a core made of magnetic material. The current generates magnetic field lines perpendicular to the core's cross-sectional area. These lines close on themselves as shown in figure B.2. The flux linkage, λ, and the current, i, form an external port which usually provides good results for simple cases (to design transducers or motors, a more detailed representation using magnetic circuits is nevertheless needed). The physical effects inside the core are completely ignored when everything is related to the electrical side, i.e to λ and i. Through measurement, the function relating λ to i can be retrieved and used. On the other hand, to get insight into the physics of magnetic circuit and the related energy issues, the concept of magnetic circuit, magnetomotive force (mmf) and reluctance should be used.

When a current flows into the circuit, magnetic flux is induced in the coil. This magnetic flux, ϕ, measured in *Webers*, is equivalent to *volt-second*. This magnetic field (the gray lines in Figure B.2a) can be described by the *magnetic flux vector density* B with units of *teslas*. It represents the amount of flux (number of lines) crossing a unit area perpendicular to the lines. As seen before, the magnetic flux linkage , λ, is related to the magnetic flux, ϕ, by the following equation

$$\lambda = N\phi \tag{B.19}$$

where N is the number of turns of the solenoid. Usually, as seen in figure B.2a, not all field lines pass through the core, there are some flux which leaks out of the coil.

The "driving force" which sets up ϕ in the core was defined as the magnetomotive force $mmf = Ni$ and the reluctance of the magnetic circuit was defined as $\mathcal{R} = \frac{l}{\mu_0 \mu_r A}$ where l is the mean magnetic path, A is the cross-sectional area of the core, μ_0 is the permeability of air and μ_r the relative

permeability of the core. Then the magnetic flux, ϕ, is given by

$$\phi = \frac{mmf}{reluctance} = \frac{Ni}{\mathcal{R}} \tag{B.20}$$

For the magnetic circuit with leakage given in figure B.2b, the total reluctance, $\mathcal{R}_t$, is given by

$$\mathcal{R}_t = \frac{\mathcal{R}_l \mathcal{R}_c}{\mathcal{R}_l + \mathcal{R}_c} \tag{B.21}$$

where $\mathcal{R}_l$ is the reluctance of the leakage flux and $\mathcal{R}_c$ is the reluctance of the core. Therefore the magnetic flux in the circuit is given by $\phi = \frac{Ni}{\mathcal{R}_t}$ and $\phi = \phi_l + \phi_c$.

In this regard, magnetic circuits can be considered to be analogous to electric circuit and reluctance is similar to electrical resistance. Unfortunately this analogy works well only in the static case (magnetostatics). A major difference is that a magnetic field stores energy whereas an electrical resistance dissipates energy. In this regard, reluctance is more like a non-linear capacitor which stores energy.

A more correct representation used in the Bond Graph analogy is to treat the magnetomotive force as an effort variable and instead of the magnetic flux, ϕ, it is $\dot{\phi}$ which becomes the flow variable. As there is a relationship between the integrated flow(ϕ) and the effort (mmf), magnetic circuit can be represented as a bond graph "C" element, i.e a generalized capacitance.

Moreover, it should be noted that two main kind of losses occur in the core. Firstly there are eddy current losses which are current induced in the core. Being conducting, these current experiences a resistance and hence heat dissipation occurs. Secondly the effects of hysteresis invariably leads to a loss in energy.

Appendix C

Thermodynamic theory in brief

Thermodynamics can be described as the science, more importantly, as an engineering tool used to describe processes that involve changes in temperature, transformation of energy, and the relationships between heat and work [9, 6, 59]. It is a phenomenological theory based on two laws usually called the *The First Law of Thermodynamics* and *The Second Law of Thermodynamics*. Whereas the former is a statement of the conservation of energy, the latter gives the direction of a process. In this sense, it is more an evolution law. This will be made clear in the following sections.

C.1 The First law of Thermodynamics

The first law of thermodynamics states that there is a state function which is extensive and conservative called *internal energy* and usually denoted by U which can only be changed by *work* or *heat*. Mathematically it is written as:

$$dU = đW + đQ \tag{C.1}$$

where $đW$ is the amount of work done by or on the system and $đQ$ is the amount of heat added or removed from the system.

To understand (C.1), three quantities need to be explained: namely extensive (intensive), conservative and state function.

In thermodynamics, we deal with two main types of variables intensive and extensive. Intensive variables are those variables which do not depend on size such as temperature and pressure. On the other hand, variables which depend on size such as mass and volume are called extensive quantities. We will exclusively talk of intensive and extensive quantities as duals in an energy formulation. That is in an elastic deformation, the force f, is the intensive quantity whereas the displacement l is extensive and their product fdl is the infinitesimal amount of work done. Similarly the work done by a battery is vdq, the intensive variable being the voltage v and the extensive being the charge q.

Conservative systems are those systems whose energy stays constant over time when left by themselves. A pendulum oscillating without damping will continue to do so indefinitely unless acted upon by an external force.

And finally, a state function is a function whose values depend only on the end-points, i.e initial and final values but not on the path taken. Suppose we have the internal energy of system which is a function of *entropy*, S, and *generalized displacements*, q, terms to be defined later. The internal energy can then be completely defined knowing the entropy and the generalized coordinates. If then the internal energy is changed by adding some heat and performing some work on the system, the new internal energy is only characterized by the values of entropy and generalized coordinates at the new point. It does not matter how much heat or how much work has been done provided their sum is the same. Hence this is called a state function and its value depend only on end points. Hence, in equation (C.1) dU is a state function whereas $đW$ and $đQ$ are not. Their value depend on the path taken. In mathematics, dU is called an exact differential whereas the other $đW$ and $đQ$ are called inexact differentials.

Most of the difficulty in thermodynamics lies in making the inexact differentials exact.

C.2 The Second law of Thermodynamics

The second law of thermodynamics stipulates that there exists a state function, S, which is extensive and *non-conservative* called *entropy* such that, in any *reversible* change,

$$dS = \frac{đQ}{T} \tag{C.2}$$

Futhermore, if the change is *irreversible*, then

$$dS > \frac{đQ}{T} \tag{C.3}$$

By *reversible*, we mean that the process after undergoing a change, is able to return back to its original configuration after the external agent causing the change is removed. An example would be the elastic deformation of a spring. A spring can be extended by application of a force and on removing the force, the spring returns to its original position. Conversely, in an *irreversible* process, after removal of the external agent, the process does not return to its original configuration. A compensating agent, which is reverse of the original force should be used to return it to its original position [6].

Furthermore, entropy can be broken down into two parts which are S_e and S_i. We will call S_e, exchange entropy and S_i, irreversible entropy created inside the system under consideration.

$$dS = đS_e + đS_i \tag{C.4}$$

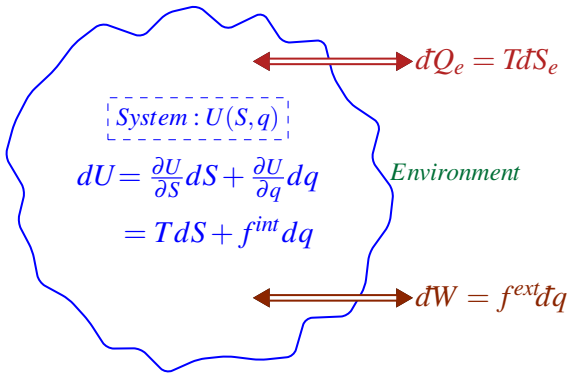

Figure C.1: Laws of Thermodynamics

S_e, being the exchange entropy, is related to the exchange of heat with the environment.

$$đQ_e = T.đS_e \tag{C.5}$$

whereas S_i is used to quantify the 'irreversibility' of the process and is always positive.

$$đS_i > 0 \tag{C.6}$$

C.3 Energy and Work.

The total energy of a system can be considered to be the sum of kinetic energy, potential energy (due to gravitational field) and internal energy. Whereas internal energy of a system concerns itself with what is happening inside the system, kinetic energy and potential energy on the hand considers the system as a bulk and its motion. Thus, magnetic energy, electrical energy, heat energy etc. are considered part of internal energy while the position and motion of the system as a bulk dictates its potential and kinetic energy respectively. Hence using $\mathcal{E}_T$ for total energy and $\mathcal{E}_K$, $\mathcal{E}_P$ and U for kinetic, potential and internal energy respectively we have

$$\mathcal{E}_T = \mathcal{E}_K + \mathcal{E}_P + U \tag{C.7}$$

Energy in whatever form can be thought of as the sum of infinitesimal work. The common terminology used for work are *generalized forces* and *generalized displacements*. The latter are the extensive variable whereas the former are intensive variables. In an elastic system, work can be defined as

$$W = \int_{q_1}^{q_2} f dq \tag{C.8}$$

where f is the applied force and dq is the displacement. In electric system, it takes the form of $dW = vdq$ whereas in magnetic systems it is $dW = id\lambda$.

Figure C.1 shows how the internal energy of system changes. Q_e is the heat added from outside. f^{ext} is the generalized external force. It is not necessarily equal to f^{int} except in equilibrium. Also as shown in the figure, dU, is an exact total differential.

C.4 Maximum Work

Suppose that a system is at rest and we can neglect the potential and kinetic energies, then the internal energy dU can be written as

$$dU = \underbrace{đQ_e}_{TđS_e} + đW = TdS - TđS_i + đW \tag{C.9}$$

Now at constant entropy, we have $dS = 0$, then the equation above reduces to

$$dU + TđS_i = đW \tag{C.10}$$

Now since $TđS_i > 0$, we get

$$dU \leq đW \tag{C.11}$$

This equation shows that the maximum work is only obtained in a reversible process otherwise it is not. If a system is described by (generalized) coordinates q_r and if the (generalized) force of external origin that tend to increase q_r is P_r, the rate of work done of these forces is $P_r\dot{q}_r$. The work by them in a small displacement dq_r is $P_r dq_r$.

U is the *internal energy*. The *second* law states that there is another function S, the entropy, such that, in any change, by suitable definition of the temperature (Kelvin) T,

$$đQ \leq TdS \tag{C.12}$$

the equality holds in the ideal limiting case of *reversible* process; the inequality holds in all other cases. On eliminating $đQ$, we get

$$dU \leq P_r dq_r + TdS \tag{C.13}$$

Note how the inexact differential have been converted to state function. A state function is one whose values do not depend on path. We can never say that a body contains a quantity of heat or a quantity of work as they are interchangeable but we can always say the amount of internal energy (to a constant) or the amount of entropy.

C.5 Equilibrium and Stability

In an equilibrium reversible process, at each stage we have

$$dU = P_r dq_r + TdS \tag{C.14}$$

U therefore is not a function of q_r alone, as in mechanics, but of S also and perhaps of other parameters which remain constant during the changes being considered. Knowing U as a function of q_r and S we can find the generalised forces P_r and the temperature by using the following relations

$$P_r = \frac{\partial U}{\partial q_r}, \qquad T = \frac{\partial U}{\partial S} \tag{C.15}$$

In particular, we seldom have such knowledge, we are most likely to know the temperature rather than the entropy. Then we make use of the *Legendre transform*, and write

$$F = U - TS \tag{C.16}$$

then in any reversible change we have

$$dF = dU - TdS - SdT = P_r dq_r - SdT \tag{C.17}$$

F is usually called the Helmholtz free energy. Then if we know F as a function of q_r and T, we can find P_r and S by using the following

$$P_r = \frac{\partial F}{\partial q_r}, \qquad S = -\frac{\partial F}{\partial T} \tag{C.18}$$

Often also, we wish to use the P_r rather than the q_r as independent variables. For this case we let

$$G = F - P_r q_r \tag{C.19}$$

then in any reversible change we have

$$dG = dF - P_r dq_r - q_r dP_r = -q_r dP_r - SdT \tag{C.20}$$

and then again knowing G, the Gibbs free energy, as a function of P_r and T, we can find q_r and S as above.

Sometimes we also wish to use a combination of P_r and q_r as independent variables, we extend the sum only over those r's for which the independent variable is P_r; thus for independent variables T, q_1 and P_2 the appropriate function is $F - P_2 q_2$, and its differential is $P_1 dq_1 - q_2 dP_2 + TdS$. Similarly, if the independent variables are S, q_1 and P_2, we use the function $U - P_2 q_2$. By such *Legendre transformation*, we can get the proper *thermodynamic potential* for any choice of independent variables; all the dependent variables can be found by differentiation of this one function.

Equa tion (C.1) helps us to derive relations between independent and dependent variables for a system in equilibrium but it does not say anything about stability of the equilibrium. To derive conditions for stability, we return to equation (C.13) which holds for most system i.e irreversible system

$$dU < P_r dq_r + TdS \tag{C.21}$$

This equations tells us that if we hold the coordinates and the entropy constant ($dq_r = 0$ and $dS = 0$), the internal energy U can only decrease and if we hold the energy and coordinates constant, the entropy can only increase. The condition for stable equilibrium therefore is that the energy be as small as possible the given coordinate and entropy, or that the entropy be already as large as possible for the given coordinate and energy. It should be noted in that in experiments only the second condition is possible by preventing heat flow and keeping the coordinates constant).

If instead we hold the coordinates constant as well as the temperature, the conditions for equilibrium becomes

$$d(U-TS) < 0$$
$$dF < 0$$

Hence we see that F should be a minimum for stable equilibrium at given coordinates and temperature. A similar reasoning for G also leads to a minimum $dG < 0$ for stable equilibrium.

C.6 Irreversible thermodynamics

From the first law of thermodynamics, we see that work done and heat both hold equal value in changing the internal energy. Hence mechanical energy can be converted to heat energy and heat energy can be converted to mechanical energy. But in practice one transformation is more feasible than the other and this direction is given by the second law.

The subject of irreversible thermodynamics deals mainly with the rate of production of entropy. And from such consideration, there is an inequality called Clausius-Duhem inequality.

Bibliography

[1] Jake J Abbott, Zoltan Nagy, Felix Beyeler, and Bradley J Nelson. Robotics in the small, part i: microbotics. *Robotics & Automation Magazine, IEEE*, 14(2):92–103, 2007.

[2] SH Birkett and PH Roe. The mathematical foundations of bond graphs—ii. duality. *Journal of the Franklin Institute*, 326(5):691–708, 1989.

[3] SH Birkett and PH Roe. The mathematical foundations of bond graphs—i. algebraic theory. *Journal of the Franklin Institute*, 326(3): 329–350, 1989.

[4] SH Birkett and PH Roe. The mathematical foundations of bond graphs—iii. matroid theory. *Journal of the Franklin Institute*, 327(1): 87–108, 1990.

[5] Anthony M Bloch, Naomi E Leonard, and Jerrold E Marsden. Controlled lagrangians and the stabilization of mechanical systems. i. the first matching theorem. *Automatic Control, IEEE Transactions on*, 45 (12):2253–2270, 2000.

[6] George Hartley Bryan. *Thermodynamics: An Introductory Treatise Dealing Mainley with First Principles and Their Direct Applications*, volume 21. BG Teubner, 1907.

[7] Kurt H Jürgen Buschow. *Handbook of magnetic materials*, volume 15. Elsevier, 2003.

[8] Nandish Calchand, Arnaud Hubert, Yann Le Gorrec, and Bernhard Maschke. From canonical hamiltonian to port-hamiltonian modeling: Application to magnetic shape memory alloys actuators. In *ASME 2011 Dynamic Systems and Control Conference and Bath/ASME Symposium on Fluid Power and Motion Control*, pages 17–24. American Society of Mechanical Engineers, 2011.

[9] Herbert B Callen. *THERMODYNAMICS & AN INTRO. TO THERMOSTATISTICS*. Wiley. com, 2006.

[10] Nicolas Chaillet et al. *Microrobotics for micromanipulation*. Wiley. com, 2013.

[11] Frank Claeyssen, N Lhermet, R Le Letty, and P Bouchilloux. Actuators, transducers and motors based on giant magnetostrictive materials. *Journal of Alloys and Compounds*, 258(1):61–73, 1997.

[12] Bernard D Coleman and Morton E Gurtin. Thermodynamics with internal state variables. *The Journal of Chemical Physics*, 47(2):597–613, 2004.

[13] Stephen H Crandall. *Dynamics of mechanical and electromechanical systems*. McGraw-Hill, 1968.

[14] Charles A Desoer and Mathukumalli Vidyasagar. *Feedback systems: input-output properties*, volume 55. SIAM, 2009.

[15] John C Doyle, Bruce A Francis, and Allen R Tannenbaum. *Feedback control theory*. Courier Dover Publications, 2013.

[16] Jean-Yves Gauthier. *Modélisation des Alliages e Memoire de Forme Magnetiques pour la conversion d'energie dans les actionneurs et leur commande*. PhD thesis, Université de Franche-Comte, 2007.

[17] Jean-Yves Gauthier, Arnaud Hubert, Joël Abadie, Christian Lexcellent, Nicolas Chaillet, et al. Multistable actuator based on magnetic shape memory alloy.. *ACTUATOR'2006.*, 1:787–790, 2006.

[18] Jean-Yves Gauthier, Christian Lexcellent, Arnaud Hubert, Joël Abadie, and Nicolas Chaillet. Modeling rearrangement process of martensite platelets in a magnetic shape memory alloy ni2mnga single crystal under magnetic field and (or) stress action. *Journal of intelligent material systems and structures*, 18(3):289–299, 2007.

[19] Jean-Yves Gauthier, Arnaud Hubert, Joël Abadie, Nicolas Chaillet, and Christian Lexcellent. Nonlinear hamiltonian modelling of magnetic shape memory alloy based actuators. *Sensors and Actuators A: Physical*, 141(2):536–547, 2008.

[20] P.J. Gawthrop and G.P. Bevan. Bond-graph modeling. *Control Systems, IEEE*, 27(2):24–45, 2007. ISSN 1066-033X. doi: 10.1109/MCS.2007.338279.

[21] Electroactive Polymer Gels. Electroactive polymer (eap) actuators as artificial muscles: reality, potential, and challenges. 2004.

[22] Michael Goldfarb and Nikola Celanovic. Modeling piezoelectric stack actuators for control of micromanipulation. *Control Systems, IEEE*, 17 (3):69–79, 1997.

[23] Robert B Gorbet, Kirsten A Morris, and David WL Wang. Passivity-based stability and control of hysteresis in smart actuators. *Control Systems Technology, IEEE Transactions on*, 9(1):5–16, 2001.

[24] Donald T Greenwood. *Advanced dynamics*. Cambridge University Press Cambridge, 2003.

[25] David Jeffrey Griffiths. *Introduction to electrodynamics*, volume 3. prentice Hall Upper Saddle River, NJ, 1999.

[26] EA Guillemin. *Introduction to Circuit Theory*. New York: John Wiley and Sons, 1957.

[27] O Heczko, Alexei Sozinov, and Kari Ullakko. Giant field-induced reversible strain in magnetic shape memory nimnga alloy. *Magnetics, IEEE Transactions on*, 36(5):3266–3268, 2000.

[28] Laurent Hirsinger and Christian Lexcellent. Internal variable model for magneto-mechanical behaviour of ferromagnetic shape memory alloys ni-mn-ga. In *Journal de Physique IV (Proceedings)*, volume 112, pages 977–980. EDP sciences, 2003.

[29] Ram V Iyer and Xiaobo Tan. Control of hysteretic systems through inverse compensation. *Control Systems, IEEE*, 29(1):83–99, 2009.

[30] R James and M. Wutting. Magnetostriction of martensite. *Philosophical Magazine*, 2004.

[31] D. Jeltsema and J. M A Scherpen. Multidomain modeling of nonlinear networks and systems. *Control Systems, IEEE*, 29(4):28–59, 2009. ISSN 1066-033X. doi: 10.1109/MCS.2009.932927.

[32] DC Jiles and DL Atherton. Theory of ferromagnetic hysteresis. *Journal of magnetism and magnetic materials*, 61(1):48–60, 1986.

[33] Dean Karnopp. Computer models of hysteresis in mechanical and magnetic components. *Journal of the Franklin Institute*, 316(5):405–415, 1983.

[34] Dean C Karnopp, Donald L Margolis, and Ronald C Rosenberg. *System Dynamics: Modeling, Simulation, and Control of Mechatronic Systems*. Wiley. com, 2012.

[35] Hassan K Khalil and JW Grizzle. *Nonlinear systems*, volume 3. Prentice hall Upper Saddle River, 2002.

[36] B Kiefer and Dimitris C Lagoudas. Modeling the coupled strain and magnetization response of magnetic shape memory alloys under magnetomechanical loading. *Journal of Intelligent Material Systems and Structures*, 20(2):143–170, 2009.

[37] Bjorn Kiefer and Dimitris C Lagoudas. Phenomenological modeling of ferromagnetic shape memory alloys. In *Smart structures and materials*, pages 164–176. International Society for Optics and Photonics, 2004.

[38] Björn Kiefer and Dimitris C Lagoudas. Magnetic field-induced martensitic variant reorientation in magnetic shape memory alloys. *Philosophical Magazine*, 85(33-35):4289–4329, 2005.

[39] ES Kuh and CA Desoer. *Basic circuit theory*. McGraw-Hill Book Company, 1969.

[40] Huibert Kwakernaak and Raphael Sivan. *Linear optimal control systems*, volume 1. Wiley-Interscience New York, 1972.

[41] Dimitris C Lagoudas. *Shape memory alloys: modeling and engineering applications*. Springer, 2008.

[42] Cornelius Lanczos. *The variational principles of mechanics*, volume 4. Courier Dover Publications, 1970.

[43] Lev D Landau and Es Lifshitz. On the theory of the dispersion of magnetic permeability in ferromagnetic bodies. *Phys. Z. Sowjetunion*, 8(153):101–114, 1935.

[44] Richard A Layton. *Principles of Analytical System Dynamics*. Springer, 1998.

[45] AA Likhachev and K Ullakko. Magnetic-field-controlled twin boundaries motion and giant magneto-mechanical effects in ni–mn–ga shape memory alloy. *Physics Letters A*, 275(1):142–151, 2000.

[46] Isaak D Mayergoyz. Mathematical models of hysteresis. *Magnetics, IEEE Transactions on*, 22(5):603–608, 1986.

[47] G Mogylnyy, I Glavatskyy, N Glavatska, O Söderberg, Y Ge, and VK Lindroos. Crystal structure and twinning in martensite of ni< sub> 1.96</sub> mn< sub> 1.18</sub> ga< sub> 0.86</sub> magnetic shape memory alloy. *Scripta materialia*, 48(10):1427–1432, 2003.

[48] Rorbert C O'Handley. Model for strain and magnetization in magnetic shape-memory alloys. *Journal of Applied Physics*, 83(6):3263–3270, 1998.

[49] Romeo Ortega. *Passivity-based control of Euler-Lagrange systems: mechanical, electrical and electromechanical applications*. Springer, 1998.

[50] Romeo Ortega and Eloisa Garcia-Canseco. Interconnection and damping assignment passivity-based control: A survey. *European Journal of Control*, 10(5):432–450, 2004.

[51] Romeo Ortega, Arjan J Van Der Schaft, Iven Mareels, and Bernhard Maschke. Putting energy back in control. *Control Systems, IEEE*, 21 (2):18–33, 2001.

[52] Romeo Ortega, Arjan J Van Der Schaft, Iven Mareels, and Bernhard Maschke. Putting energy back in control. *Control Systems, IEEE*, 21 (2):18–33, 2001.

[53] Romeo Ortega, Arjan Van Der Schaft, Bernhard Maschke, and Gerardo Escobar. Interconnection and damping assignment passivity-based control of port-controlled hamiltonian systems. *Automatica*, 38(4):585–596, 2002.

[54] George F Oster, Alan S Perelson, and Aharon Katchalsky. Network thermodynamics: dynamic modelling of biophysical systems. *Quarterly reviews of Biophysics*, 6(01):1–134, 1973.

[55] GF Oster and CA Desoer. Tellegen's theorem and thermodynamic inequalities. *Journal of theoretical Biology*, 32(2):219–241, 1971.

[56] Henry M Paynter. *Analysis and design of engineering systems*. MIT press, 1961.

[57] Ferenc Preisach. Über die magnetische nachwirkung. *Zeitschrift für physik*, 94(5-6):277–302, 1935.

[58] Hector Ramirez, Bernhard Maschke, and Daniel Sbarbaro. Irreversible port-hamiltonian systems: A general formulation of irreversible processes with application to the cstr. *Chemical Engineering Science*, 89: 223–234, 2013.

[59] Howard Reiss. *Methods of thermodynamics*. Courier Dover Publications, 1965.

[60] Leonardo Riccardi, David Naso, Biagio Turchiano, and Hartmut Janocha. Adaptive modified prandtl-ishlinskii model for compensation of hysteretic nonlinearities in magnetic shape memory actuators. In *Proceedings of the 37th Annual Conference on IEEE Industrial Electronics Society*, pages 56–61, 2011.

[61] Leonardo Riccardi, David Naso, Biagio Turchiano, and Hartmut Janocha. Robust adaptive control of a magnetic shape memory actuator for precise positioning. In *American Control Conference (ACC), 2011*, pages 5400–5405. IEEE, 2011.

[62] Leonardo Riccardi, David Naso, Hartmut Janocha, and Biagio Turchiano. A precise positioning actuator based on feedback-controlled magnetic shape memory alloys. *Mechatronics*, 22(5):568–576, 2012.

[63] Neelesh Nandkumar Sarawate. *Characterization and Modeling of the Ferromagnetic Shape Memory Alloy Ni-Mn-Ga for Sensing and Actuation.* PhD thesis, Ohio State University, 2008.

[64] Arjan Schaft. Port-hamiltonian systems: an introductory survey. 2006.

[65] Arjan van der Schaft. *L2-Gain and Passivity in Nonlinear Control.* Springer-Verlag New York, Inc., 1999.

[66] J.L. Shearer, A.T. Murphy, and H.H. Richardson. *Introduction to system dynamics.* Addison-Wesley series in systems and controls. Addison-Wesley Pub. Co., 1967. URL `http://books.google.fr/books?id=PoBRAAAAMAAJ`.

[67] Sigurd Skogestad and Ian Postlethwaite. *Multivariable feedback control: analysis and design*, volume 2. Wiley New York, 2007.

[68] John C Slater and Nathaniel H Frank. *Electromagnetism.* Courier Dover Publications, 2012.

[69] Jean-Jacques E Slotine, Weiping Li, et al. *Applied nonlinear control*, volume 199. Prentice-Hall Englewood Cliffs, NJ, 1991.

[70] Ralph C Smith. *Smart material systems: Model developments*, volume 32. Siam, 2005.

[71] HMJR Soemers and DM Brouwer. Mechatronics and micro systems. *Mechatronic Systems*, pages 6–8, 2004.

[72] Stefano Stramigioli, Vincent Duindam, and Alessandro Macchelli. *Modeling and Control of Complex Physical Systems: The Port-Hamiltonian Approach/Vincent Duindam, Alessandro Macchelli, Stefano Stramigioli...(Eds.).* Springer, 2009.

[73] Xiaobo Tan and Ram V Iyer. Modeling and control of hysteresis. *IEEE Control Systems Magazine*, 29(1):26–28, 2009.

[74] BDH Tellegen. A general network theorem, with applications. *Philips Research Reports*, 7(4):259–269, 1952.

[75] Kari Ullakko. Magnetically controlled shape memory alloys: a new class of actuator materials. *Journal of materials Engineering and Performance*, 5(3):405–409, 1996.

[76] Mathukumalli Vidyasagar. *Nonlinear systems analysis*, volume 42. Siam, 2002.

[77] Augusto Visintin. Mathematical models of hysteresis. In *Modelling and Optimization of Distributed Parameter Systems Applications to engineering*, pages 71–80. Springer, 1996.

[78] Jiong Wang and Paul Steinmann. A variational approach towards the modeling of magnetic field-induced strains in magnetic shape memory alloys. *Journal of the Mechanics and Physics of Solids*, 60(6):1179–1200, 2012.

[79] Jan C Willems. Dissipative dynamical systems part i: General theory. *Archive for rational mechanics and analysis*, 45(5):321–351, 1972.

[80] Jan C Willems. The behavioral approach to open and interconnected systems. *Control Systems, IEEE*, 27(6):46–99, 2007.

[81] H Woodson and J Melcher. *Electromechanical Dynamics Part 1: Discrete Systems*. John Wiley & Sons, 1968.

[82] Markus Zahn. *Electromagnetic Field Theory: a problem solving approach*. RF Krieger Malabar, 1987.

Résumé :

Les matériaux actifs sont des matériaux qui réagissent quand on leur applique un champ extérieur comme la température, la lumière, un champ magnétique ou un champ électrique. Ces champs changent les propriétés du matériau comme la longueur, la susceptibilité magnétique ou la permittivité électrique. Ces changements peuvent être utilisé pour faire du travail. Quelques exemples sont les matériaux piézoélectriques, qui changent de longueur quand on applique un champ électrique, les alliages à mémoire de forme qui changent leur longueur sous l'action de la température. Un matériau plus recent qu'on appelle les alliages à mémoire de forme magnétique se deforme sous l'action d'un champ magnétique. Dans cette thèse, on utilise ce matériau pour confectionner un actionneur. Pour ce faire, on utilise la thermodynamique des procédés irréversibles pour modéliser le matériau. La thermodynamique s'avère très versatile pour ce type de materiau car il permet de quantifier l'échange et la transformation d'énergie dans le matériau. Aussi, étant donné que le materiau se comporte d'une façon non-linéaire et hysteretique, le cadre énergetique nous permets justement de prendre en compte ces non-linearités. Cette thèse utilise l'approche énergétique notamment les Hamiltonien à ports pour modéliser un actionneur à base d'alliage à memoire de forme. Cette méthode nous permets aussi de concevoir des lois de commande pour contrôler le matériau.

Mots-clés : Modélisation, Hamitonien à ports, Thermodynamique, matériau actif

Abstract:

Active materials are a class of material which react to an external stimulus such as temperature, photons, magnetic field or electric field. These stimuli cause some properties of the material to change usually their length. Some examples are piezoelectric material which change their length under the action of an electric field, Shape Memory alloys which alter their shape on application of heat, and more recently Magnetic Shape Memory Alloys (MSMA) which undergo a deformation on application of a magnetic field. Harnessing this property of MSMAs, we hereby present an actuator using this novel material. We extensively make use of an energy framework, namely the thermodynamics of irreversible processes to model the material. This framework has been proven to be very versatile in modelling energy exchange and transformation as it occurs in the material and also to incorporate hysteresis which arises naturally in such materials. Another advantage of this method is its ability to give us constitutive laws based on simple assumptions. Furthermore, using an energy framework allows us to apply some energy based control. Port Hamiltonian Control is one such method and it is not limited only to linear models. This latter characteristic has proven very useful since MSMAs are very non-linear in nature.

Keywords: Modeling, Hysteresis, Port-Hamiltonian, Thermodynamics, smart materials

SPIM

■ École doctorale SPIM 16 route de Gray F - 25030 Besançon cedex
■ tél. +33 (0)3 81 66 66 02 ■ ed-spim@univ-fcomte.fr ■ www.ed-spim.univ-fcomte.fr

UFC
UNIVERSITÉ DE FRANCHE-COMTÉ